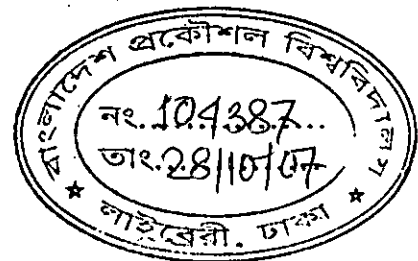
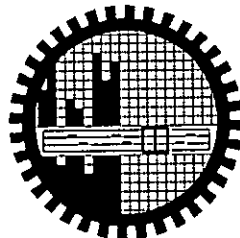


**WIND EFFECT ON SQUARE AND RECTANGULAR, STAGGERED  
CYLINDERS**

By

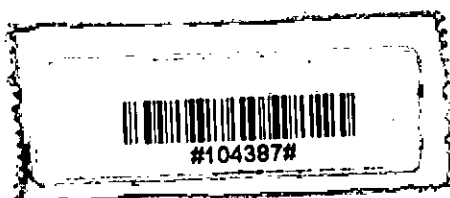
**Mohammad Karar Mahmud Hossain**

In partial fulfillment of the requirements for the degree of  
**MASTER OF SCIENCE IN MECHANICAL ENGINEERING**




**DEPARTMENT OF MECHANICAL ENGINEERING  
BANGLADESH UNIVERSITY OF ENGINEERING & TECHNOLOGY,  
(BUET)  
DHAKA-1000, BANGLADESH**


**September, 2007**

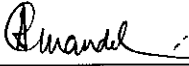


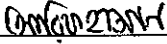
## RECOMMENDATION OF THE BOARD OF EXAMINERS

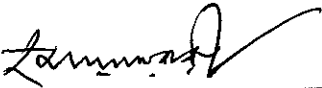
The Board of Examiners hereby recommends to the Department of Mechanical Engineering, Bangladesh University of Engineering and Technology, Dhaka, the acceptance of the thesis, " **WIND EFFECT ON SQUARE AND RECTANGULAR STAGGERED CYLINDERS,**" submitted by Mohammad Karar Mahmud Hossain, Roll No.: 040510054, Session: April-2005, in partial fulfillment of the requirements for the degree of Master of Science in Mechanical Engineering .

  
\_\_\_\_\_  
Dr. Md. Quamrul Islam (Supervisor) Chairman  
Professor  
Department of Mechanical Engineering, BUET,  
Dhaka, Bangladesh.

  
\_\_\_\_\_  
Dr. Md. Maksud Helali (Ex-officio) Member  
Professor & Head  
Department of Mechanical Engineering BUET,  
Dhaka, Bangladesh

  
\_\_\_\_\_  
Dr. Amallesh Chandra Mandal Member  
Professor  
Department of Mechanical Engineering BUET,  
Dhaka, Bangladesh

  
\_\_\_\_\_  
Dr. Md. Arif Hassan Mamun Member  
Assistant Professor  
Department of Mechanical Engineering, BUET,  
Dhaka, Bangladesh

  
\_\_\_\_\_  
Dr. Md. Sadiqul Baree Member(External)  
Professor  
Department of NAME, BUET,  
Dhaka, Bangladesh

## CERTIFICATION OF RESEARCH

This is to certify that the work presented in this thesis is the outcome of the investigation carried out by the author under the supervision of Dr. Md. Quamrul Islam, Professor, Department of Mechanical Engineering, Bangladesh University of Engineering and Technology, (BUET), Dhaka-1000 and that it has not been submitted anywhere for the award of any degree or diploma.

Md. K. M. Hossain

Mohammad Karar Mahmud Hossain  
Author

*Dedicated*  
*To*  
*My Late Father*

## CONTENTS

	Page
<b>TITLE</b>	i
<b>THESIS APPROVAL</b>	ii
<b>DECLARATION</b>	iii
<b>DEDICATION</b>	iv
<b>CONTENTS</b>	v-vii
<b>LIST OF FIGURES</b>	viii-xi
<b>NOMENCLATURE</b>	xii-xiii
<b>ACKNOWLEDGEMENT</b>	xiv
<b>ABSTRACT</b>	xv
<b>CHAPTER-1</b>	
<b>INTRODUCTION</b>	1-4
1.1 Nature of Wind Loading	1
1.2 Motivation for the Study	2
1.3 Aim of the Study	3
1.4 Scope of Thesis	3
<b>CHAPTER-2</b>	
<b>REVIEW OF LITERATURE</b>	5-15
2.1 Literature Concerning Single Body	5
2.2 Literature Concerning multiple Bodies	13
<b>CHAPTER-3</b>	
<b>EXPERIMENTAL SETUP</b>	16-25
3.1 Specification of the Wind Tunnel	16
3.2 Test Section	17
3.3 Constructional Details of Cylinder	18
3.4 Experimental Procedure	19
3.4.1 Single Cylinder	19
3.4.2 Cylinders in Group	20

<b>CHAPTER- 4</b>	
<b>MATHEMATICAL MODEL</b>	26-34
4.1 Pressure Coefficient	26
4.2 Drag and Lift Coefficient	26
4.3 Moment Coefficient	28
4.4 Total Force Coefficient	31
<b>CHAPTER-5</b>	
<b>RESULTS AND DISCUSSIONS</b>	35-90
5.1 Single Cylinder	35
5.1.1 Pressure Distribution	36
5.1.2 Aerodynamic Forces	37
5.2 Group of Cylinders	39
5.2.1 Pressure Distribution on Upstream Cylinder	39
5.2.2 Variation of Drag for Upstream Cylinder	42
5.2.3 Variation of Lift for Upstream Cylinder	43
5.2.4 Variation of Moment Coefficient for Upstream Cylinder	43
5.2.5 Variation of Total Force Coefficient on Upstream Cylinder	44
5.2.6 Pressure Distribution on Downstream Cylinder	44
5.2.7 Variation of Drag for Downstream Cylinder	49
5.2.8 Variation of Lift for Downstream Cylinder	50
5.2.9 Variation of Moment Coefficient for Downstream Cylinder	51
5.2.10 Variation of Total Force Coefficient on Downstream Cylinder	52
5.3 Observation of Pressure Fluctuations	53
5.4 Effect of Reynolds Number	53
5.5 Blockage Corrections	54
<b>CHAPTER-6</b>	
<b>CONCLUSSION AND RECOMMENDATION</b>	91-93
6.1 Conclusions	91

6.2 Recommendations	92
<b>REFERENCES</b>	<b>94-99</b>

## LIST OF FIGURES

Figures		Page
3.1	Schematic diagram of wind tunnel	20
3.2	Sectional view of a specimen rectangular cylinder	21
3.3	The arrangement of tapping points on adjacent sides	21
3.4	Cross section of rectangular cylinders from each set showing position of tapping points	22
3.5	Tunnel test section showing the position of cylinders (one square and two rectangular) in staggered form	23
3.6	Tunnel test section showing the position of cylinders (one rectangular and two square) in staggered form	23
3.7	Velocity distribution along the height of the test section	24
4.1	Section of a cylinder showing pressure tapping points and the forces acting on each strip	31
4.2	Section of a square cylinder showing pressure tapping direction of positive moment and the forces acting along the strips	32
4.3	Section of a rectangular cylinder showing pressure tapping direction of positive moment and the forces acting along the strips	33
5.1	Square cylinder in the flow field showing the vortex street pattern	54
5.2	Rectangular cylinder in flow field showing the vortex street pattern	55
5.3	Effect of angle of attack ( $\alpha$ ) on $C_p$ -distribution at side ratio (H /D) of 1.0 (square)	56
5.4	Effect of angle of attack ( $\alpha$ ) on $C_p$ -distribution at side ratio (H /D) of 1.25 (rectangle)	57
5.5	Variation of drag coefficient ( $C_D$ ) with angle of attack ( $\alpha$ ) for different side ratios (H /D) of rectangular cylinder	58
5.6	Variation of lift coefficient ( $C_L$ ) with angle of attack ( $\alpha$ ) for different side ratios (H /D) of rectangular cylinder	59



5.7	Variation of moment coefficient ( $C_M$ ) with angle of attack ( $\alpha$ ) of rectangular cylinder	60
5.8	Variation of total force coefficient ( $C_F$ ) with angle of attack ( $\alpha$ ) for different side ratios ( $H/D$ ) of rectangular cylinder	61
5.9	Effect of longitudinal spacing ( $L_1$ ) on $C_P$ for upstream square cylinder (F) keeping transverse spacing ( $L_2$ ) constant at 1D	62
5.10	Effect of longitudinal spacing ( $L_1$ ) on $C_P$ for upstream square cylinder (F) keeping transverse spacing ( $L_2$ ) constant at 2D	63
5.11	Effect of longitudinal spacing ( $L_1$ ) on $C_P$ for upstream square cylinder (F) keeping transverse spacing ( $L_2$ ) constant at 4D	64
5.12	Effect of longitudinal spacing ( $L_1$ ) on $C_P$ for upstream rectangular cylinder (F) keeping transverse spacing ( $L_2$ ) constant at 1D	65
5.13	Effect of longitudinal spacing ( $L_1$ ) on $C_P$ for upstream rectangular cylinder (F) keeping transverse spacing ( $L_2$ ) constant at 2D	66
5.14	Effect of longitudinal spacing ( $L_1$ ) on $C_P$ for upstream rectangular cylinder (F) keeping transverse spacing ( $L_2$ ) constant at 4D	67
5.15	Variation of drag coefficient ( $C_D$ ) on upstream square cylinder (F) with longitudinal spacing ( $L_1$ ) for different values of transverse spacing ( $L_2$ )	68
5.16	Variation of drag coefficient ( $C_D$ ) on upstream rectangular cylinder (F) with longitudinal spacing ( $L_1$ ) for different values of transverse spacing ( $L_2$ )	69
5.17	Variation of lift coefficient ( $C_L$ ) on upstream square cylinder (F) with longitudinal spacing ( $L_1$ ) for different values of transverse spacing ( $L_2$ )	70
5.18	Variation of lift coefficient ( $C_L$ ) on upstream rectangular cylinder (F) with longitudinal spacing ( $L_1$ ) for different values of transverse spacing ( $L_2$ )	71
5.19	Variation of moment coefficient ( $C_M$ ) on upstream square cylinder (F) with longitudinal spacing ( $L_1$ ) for different values of transverse spacing ( $L_2$ )	72

5.20	Variation of moment coefficient ( $C_M$ ) on upstream rectangular cylinder (F) with longitudinal spacing ( $L_1$ ) for different values of transverse spacing ( $L_2$ )	73
5.21	Variation of total force coefficient ( $C_F$ ) on upstream square cylinder (F) with longitudinal spacing ( $L_1$ ) for different values of transverse spacing ( $L_2$ )	74
5.22	Variation of total force coefficient ( $C_F$ ) on upstream rectangular cylinder (F) with longitudinal spacing ( $L_1$ ) for different values of transverse spacing ( $L_2$ )	75
5.23	Effect of longitudinal spacing ( $L_1$ ) on $C_P$ for downstream square cylinder (T or B) keeping transverse spacing ( $L_2$ ) constant at 1D	76
5.24	Effect of longitudinal spacing ( $L_1$ ) on $C_P$ for downstream square cylinder (T or B) keeping transverse spacing ( $L_2$ ) constant at 2D	77
5.25	Effect of longitudinal spacing ( $L_1$ ) on $C_P$ for downstream square cylinder (T or B) keeping transverse spacing ( $L_2$ ) constant at 4D	78
5.26	Effect of longitudinal spacing ( $L_1$ ) on $C_P$ for downstream rectangular cylinder (T or B) keeping transverse spacing ( $L_2$ ) constant at 1D	79
5.27	Effect of longitudinal spacing ( $L_1$ ) on $C_P$ for downstream rectangular cylinder (T or B) keeping transverse spacing ( $L_2$ ) constant at 2D	80
5.28	Effect of longitudinal spacing ( $L_1$ ) on $C_P$ for downstream rectangular cylinder (T or B) keeping transverse spacing ( $L_2$ ) constant at 4D	81
5.29	Variation of drag coefficient ( $C_D$ ) on downstream square cylinder (T or B) with longitudinal spacing ( $L_1$ ) for different values of transverse spacing ( $L_2$ )	82
5.30	Variation of drag coefficient ( $C_D$ ) on downstream rectangular cylinder (T or B) with longitudinal spacing ( $L_1$ ) for different values of transverse spacing ( $L_2$ )	83
5.31	Variation of lift coefficient ( $C_L$ ) on downstream square cylinder (T or B) with longitudinal spacing ( $L_1$ ) for different values of transverse spacing ( $L_2$ )	84

5.32	Variation of lift coefficient ( $C_L$ ) on downstream rectangular cylinder (T or B) with longitudinal spacing ( $L_1$ ) for different values of transverse spacing ( $L_2$ )	85
5.33	Variation of moment coefficient ( $C_M$ ) on downstream square cylinder (T or B) with longitudinal spacing ( $L_1$ ) for different values of transverse spacing ( $L_2$ )	86
5.34	Variation of moment coefficient ( $C_M$ ) on downstream rectangular cylinder (T or B) with longitudinal spacing ( $L_1$ ) for different values of transverse spacing ( $L_2$ )	87
5.35	Variation of total force coefficient ( $C_F$ ) on downstream square cylinder (T or B) with longitudinal spacing ( $L_1$ ) for different values of transverse spacing ( $L_2$ )	88
5.36	Variation of total force coefficient ( $C_F$ ) on downstream rectangular cylinder (T or B) with longitudinal spacing ( $L_1$ ) for different values of transverse spacing ( $L_2$ )	89

## NOMENCLATURE

D	Width of cylinder normal to the approach flow
H	Depth of cylinder in the flow direction
A	Frontal area
$\rho$	Density of air
$U_0$	Free stream velocity
$\alpha$	Angle of attack
P	Local static pressure
$P_0$	Free stream static pressure
$\Delta P$	Difference of ambient and local static pressures
$C_p$	Mean pressure co-efficient
$C_L$	Co-efficient of Lift
$C_D$	Co-efficient of Drag
$C_F$	Total force co-efficient
$C_M$	Moment co-efficient
$F_D$	Force due to drag
$F_L$	Force due to lift
M	Moment
$\gamma_w$	Specific weight of manometer liquid
$L_1$	Longitudinal spacing
$L_2$	Transverse spacing
F	Denotes upstream cylinder
T	Denotes top downstream cylinder

- B Denotes bottom downstream cylinder
- h Distance between bottom surface of test section and the point where velocity head is measured
- $H_0$  Tunnel test section height

## ACKNOWLEDGEMENT

The author would like to mention with gratitude Almighty Allah's continual kindness without which no work would reach its goal. The author is highly grateful and obliged to his honorable supervisor, Dr. Md. Quamrul Islam, Professor, Department of Mechanical Engineering, Bangladesh University of Engineering and Technology (BUET), Dhaka, for his continuous guidance, constant support, supervision, inspiration, advice, infinite patience and enthusiastic encouragement throughout this research work.

The author is also grateful to Dr. Md. Maksud Helali, Professor and Head, Department of Mechanical Engineering, BUET, Dhaka, for his moral support, advice, help and permission to use different laboratories of the department at various stages of this work.

The author thanks the members of the Board of Examination namely Professor Dr. Md. Sadiqul Baree, Professor Dr. Amalesh Chandra Mandal and Dr. Md. Arif Hassan Mamun for their contribution in various ways in respect of this thesis.

The author is thankful to Mr. Md Abdul Karim, Superintendent and Chief Instructor, Machine shop, Md Rafiqul Islam, Foreman Instructor, Carpentry shop, Md Nazimuddin, Foreman Instructor, Welding shop, Md. Alauddin Fakir, Senior Lab Instructor cum store keeper, Heat Transfer Lab BUET, for their cordial co-operation and help in assembling different parts and components of the experimental setup. The author is also thankful to Md. Abul kalam Azad, Lab Instructor cum store keeper, Fluid Mechanics Lab, Md. Mizanur Rahman, Lab Instructor, S.M. Lab, Md Hanif, Lab Instrutor, S.M. Lab, Department of Mechanical Engineering, BUET, Dhaka, for their help and co-operation during the experiment.

The author also likes to express his sincere thanks to all other teachers and members of the Mechanical Engineering Department, BUET.

The author also grateful to Jamal Uddin Ahamed, Assistant Professor, CUET, Chittagong, and S.T. Mahmud, Lecturer, IIUC, Dhaka, for their kind cooperation. The author wish to thank specially his friends Sazzad, Shaikat, Enayet, Farid, Shafiq, Rabbu, Sayem, Jewel, Mohan, Tito and innumerable friends for their inspiration and encouragement.

Lastly, the author would like to thank his wife who persistently gave inspiration and encouragement and help many ways to finish this work.

## ABSTRACT

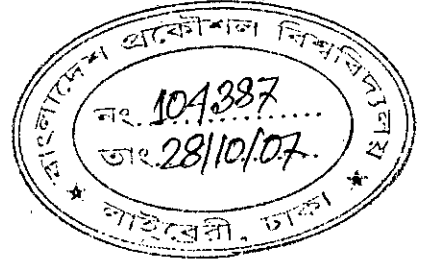
An experimental investigation of the mean pressure distributions around an isolated and a group of square and rectangular cylinders placed in a uniform cross flow is presented here. The cylinders had side ratios of  $H/D=1.0$  (square) and 1.25 (rectangular), where  $D$  is section width normal to flow direction and  $H$  is the section depth along the flow direction. A constant free stream velocity of 13.5m/s was used for this purpose.

Mean pressure distributions around each of the cylinders were measured for angle of attack varying from  $0^\circ$  to  $45^\circ$  in step of  $5^\circ$  in open circuit wind tunnel. In case group of cylinders, one square and two rectangular cylinders of identical dimension were mounted horizontally in the staggered form. The square cylinder was placed centrally in the upstream side and the other two rectangular cylinders were placed symmetrically in the downstream side with respect to tunnel axis. Pressure distributions around the cylinders were measured for the different longitudinal and transverse spacing of the cylinders. Measurements were also taken for one rectangular and two square cylinders in staggered form. Finally, drag coefficients, lift coefficients, moment coefficients and total force coefficients were calculated by numerical integration.

The drag on an isolated cylinder was higher in general than that on the same cylinder while it becomes part of a group. It may be concluded that the group-2 (one rectangular and two square cylinders) attained more suitable condition (minimum drag) for the transverse spacing,  $L_2 = 2D$  than the others.

# CHAPTER -1

## INTRODUCTION



The study of wind loads on buildings and structures was considered as far back as the 17<sup>th</sup> century by Galileo and Newton. Current problems of wind loads on scrapers, chimneys and towers; along with the flow induced vibrations of tubes in heat exchangers, bridges, oil rigs and marine structures, increased the need for detailed investigation of flow patterns and aerodynamics characteristics on bluff bodies. In recent years, the studies of wind load effects have amplified tremendously all around the world. Certain disastrous events, such as the collapse of suspension bridges and damage to towering buildings due to wind effects, have proved that the effects of wind loads should not be taken lightly and consequences of wind loading should be a major criterion for design purposes of new structures and buildings. Extensive research work on isolated bluff bodies, which interfere with each other, has only recently begun being studied. Even though this problem is of considerable significance, there is very little information available concerning the flow over staggered square and rectangular cylinders.

### 1.1 Nature of Wind Loading

Wind loads on buildings and structures as a whole may be treated as the static and dynamic effects of wind action. The static effects refer to the steady (time-average) forces and pressures that tend to give the structure a fixed dislocation. However, the dynamic effect creates an entirely different problem in which the structure end up fluctuating or swing back and forth. A steady wind load on a building is very hard to achieve because of the fluctuating nature of wind loads with its varying wind speeds and directions. The type of wind and the solidity of the structure determine the nature of loading on a building. When a building is very stiff the dynamic response of the structure may be abandoned and only the static loads may be considered, because usually the natural frequency of an extremely stiff building is too high to be excited by wind. In present studies the effect of



static loading is taking into account due to steady wind. It is assumed that since natural winds continuously fluctuates and these fluctuations are so irregular and random that the response of a structure will not differ from that due to a steady wind of the same average speed. Recently, the dynamic response of buildings has been emphasized for study because of the present tendency to build more slender and lighter structures.

## 1.2 Motivation for the Study

Recently, the effects of wind loads are taken into account for designing buildings. The effects of wind on construction and the environmental problems that it might cause are now considered to be one of the most important criteria in the design of tall buildings and structures. Cities are rapidly growing with the importance being placed on creating multi-story buildings to deal with the increasing urban population of Bangladesh. However, in the process of dealing with population demand, the architects and town planners of Bangladesh are not taking into consideration the later need to build tall buildings close together or in more windy sites, which cause wind effects on the building structures. The knowledge of wind loading on a single tall building as well as on a group of tall buildings is essential for good planning and design. The types of wind damage that might occur to buildings and the features of construction which may make building susceptible to damage needs to be carefully investigated in order to prevent future damage. There is very insignificant information available on the effect of wind load on a single tall building because of the interference of neighboring buildings in a group. The nature of wind load differs from a single free standing building to a group of buildings.

With wind tunnel experiments, the problem of predicting the flow around buildings in close proximity can be approached to develop a better understanding of the nature of flows on relatively simple arrangement of bluff bodies. With square and rectangular cylinders ideally representing the general shape of tall buildings, the present investigation of pressure distributions of square and rectangular cylinders was carried out. A study on groups of square and rectangular cylinders combination arranged in the staggered form would be helpful in the analysis of wind effects on groups of buildings. Apart from wind loading problems, a large number of high rise buildings in a specific area can create

environmental problems like unpleasant wind conditions near ground level (creating dust), too high wind load on people, too high wind speed in streets and passages or stagnation of air in certain areas causing air pollution. To find solutions to such problems more detailed research is necessary.

### **1.3 Aim of the Study**

When more than one bluff body is placed in a uniform flow, it is expected that the flow and vortex patterns would be different than the case of a single body because one body would interfere with the other causing the flow patterns to differ depending on the arrangement and spacing of the bodies. The present study does not take into account the complexities of such flows. Rather the study is of a fundamental nature confined to the investigation of aerodynamic forces and pressure distribution on the body. The present study tries to give an understanding about the variation of wind load pattern imposed on a building due to the change in side dimension as well as the influence of near-by buildings.

The prime objectives of the present study are:

(1) To measure the pressure distribution around single square and rectangular cylinders, staggered square and rectangular cylinders, for different aspect ratios (breadth/width).

(2) To determine the wind load for the static pressure distributions and observe the effects of different longitudinal and transverse spacing of the cylinders.

(3) To make comparisons of wind loads for various staggered combinations, spacing and side dimensions of the square and rectangular cylinders.

The results expressed in the form of non-dimensional co-efficient, i.e. pressure, drag, lift, moment and total force co-efficient.

### **1.4 Scope of Thesis**

The present research program covers only the experimental investigation of pressure distributions around bluff bodies of square and rectangular cylinders having side ratios 1.0 and 1.25 respectively. Since the measurements were made on the static rigid models, the

results were expressed in the form of non-dimensional coefficients i.e. pressure coefficients, lift and drag coefficients, total force coefficients, moment coefficients to be useful for general applications. As drag and total forces on buildings are well thought-out as wind loadings, so, these should be as small as possible to design efficiently. Therefore, the coefficients, which are inter-related with drag and total forces, may be used to determine the wind loadings at any wind speed on structures of similar external shapes. The numerous phases of the entire investigation are described in this thesis.

Chapter 2 provides with the brief description of the findings of several researchers in the field of flow over single and multiple bodies. Notable contributions were mainly made by Bearman, P.W. [1], Lee, B.E. [2], Nakamura, Y. [3], Vickery, B.J. [4], Parkinson, G.V. [5], Barriga, A.R. [6] and Robertson, J.M. [7]. Apart from these, findings of several other researchers are also included in this chapter.

In the chapter 3 mainly an account of the experimental arrangement and procedure adopted for the investigation are presented. It includes the description of the wind tunnel, the constructional details of the test section the square and rectangular cylinders used for the study. The experiment was conducted in the wind tunnel for only two dimensional uniform cross flow keeping the velocity and turbulence intensity constant.

In chapter 4 mathematical formulation of different types of non-dimensional parameters i.e. pressure coefficient, drag and lift coefficient, moment coefficient and total force coefficient are presented.

Chapter 5 presents the analyses concerning the results of the experiments are presented in the graphical form. The results of the present work are compared with those of previous works. In few cases, the existing experimental results of different researchers are correlated with the present one.

In chapter 6 the conclusions and results are given, which are drawn from the present investigation. This chapter also includes an outline regarding further research in this field.

## CHAPTER-2

### REVIEW OF LITERATURE

In the last few decades, research work of laboratory simulation, full-scale measurements, numerical calculations, and theoretical predictions for flows over a wide variety of bluff bodies increased due to the increasing importance of bluff body aerodynamics. Researchers from all around the world has greatly contributed to the knowledge of flow over bluff bodies, however, majority of the reported studies only involve the fundamental nature of flow over single body. In most of the research available, it seems that researchers conducted either single cylindrical cylinder, or a square section cylinder over various flow parameters, and not much research is available otherwise. In the sections to follow, brief descriptions of works by researchers Bearman [1], Lee [2], Vickery [4], Nakamura [3], Barriga [6], Castro [8], Roberson [9], Parkinson [5] and many others will be presented.

#### 2.1 Literatures Concerning Single Body

Bearman and Truman [1] investigated the base pressure coefficients, drag coefficients and Strouhal number of rectangular cylinders with one face normal to the flow direction. It was calculated when  $d/h = 0.62$ , where  $d$  is the section depth and  $h$  is the section width normal to the wind direction, the drag coefficient was at maximum (approx 2.94). When a splitter plate is introduced into the wake region, it showed that the increased drag effect completely vanished. These results suggested that the high drag was associated with the regular shedding of vortices. It also showed that if the vortices could be persuaded to form further away from the body, the higher the base pressure would be. It was suggested that for higher values of  $d/h$  ( $>0.6$ ) the vortices were forced to form further downstream because of the influence of the trailing edge corners.

Nakamura, Y. and Yujioitya [10] attempted to study vortex shedding using square prisms, placing them from normal to smooth and using turbulent approaching flows. It was made flow visualization and measured the velocity and pressure for the flow past prisms of

variable length with square section. It was observed that the square prisms shed vortices in one of the two fixed wake planes, which were parallel with the plate sides. The plane of shedding was switched irregularly from one to the other. It was explained in the observation by showing that the vortex shedding from a square prism with  $d/h = 0.5$  and a cube was similar, while for a square prism with  $d/h = 2.0$ , no such vortex shedding was observed.

Davis and Moore [11] conducted a different type of research in which they carried out a numerical study of vortex shedding from rectangular cylinders. It was attempted to present numerical solutions for two-dimensional time dependent flow about rectangles in infinite domains. It was explored the initial and subsequential development of the vortex shedding phenomena for Reynolds number varying from 100 to 2800. The outcome showed the properties of these vortices were strongly dependent on the Reynolds number. Results indicate that the lift, drag and Strouhal number were also influenced by Reynolds number.

Nakamura and Matsukawa [3] used free and forced oscillation methods to experimentally investigate the vortex excitation of rectangular cylinders with a long side normal to the flow in a mode of lateral translation. Results show that the rectangular cylinders had side ratios of 0.2, 0.4 and 0.6. The forced oscillation experiments included measurements of the fluctuating lift-force at amplitude up to 10% of the length of the long side. It was presented the results of the mean base pressure, the fluctuating lift force, and the velocity fluctuation, in the near wake on forced oscillating rectangular cylinders and compared it with the results concerning the rate of growth of oscillation on freely oscillating rectangular cylinders. Nakamura and Matsukawa found that the vortex excitation of a rectangular cylinder was strongly dependent on the side ratio. It was concluded that the main reason for change of the mean base pressure of an oscillating rectangular cylinder with increasing side ratio was closely linked with the vortex excitation characteristics.

Okajima [12] studied the vortex shedding frequencies of various rectangular cylinders by carrying out tests in a wind tunnel and in a water tank. It was showed how Strouhal number varied with width to height ratio of the cylinders for Reynolds number between 70 and  $2 \times 10^4$ . It was found that for a certain range of Reynolds number there existed cylinders with the width to height ratios of 2 and 3, where flow pattern suddenly

changed with an unexpected discontinuity in Strouhal number. It was also found that if the Reynolds number went below this region the flow separated at the leading edges and then reattached on either the upper or lower surfaces of the cylinder during a period of vortex shedding. Again for Reynolds number beyond it, the flow fully detached itself from the cylinder.

Lee [2] studied the effects of turbulence on the surface pressure field of a square prism by presenting the measurements of the mean and fluctuating pressures of a square cylinder placed in a two-dimensional uniform and turbulent flow. It was observed that by adding turbulence to the flow caused the base pressure rise and the drag of the cylinder to fall. It was suggested that this trend was probably due to the increased turbulence intensity, which caused the shear layers to thicken, causing them to be deflected by the downstream corners of the body and resulting in the downstream movement of the vortex formation region. It was also observed that as the intensity of the incident turbulence was increased, the strength of the vortex shedding reduced. Measurement of drag at various angles of attack ( $0^\circ$  to  $45^\circ$ ) showed that with increase in turbulence level the minimum drag occurred at smaller values of angle of attack.

Roberson et al. [13] measured pressure distribution of rectangular rods placed in a cross flow, with the rods slanting at small angles of attack with respect to the wind direction. The effects of the study shows the Reynolds number based on the minimum dimension of the rod was  $4 \times 10^4$  and the turbulence intensity of the cross flow ranged between 1% and 10%. It was concluded that the free-stream turbulence had a significant effect on the pressure distribution about bodies of rectangular cross-section. Further it was also found that with small angle of attack these bodies had a significantly lower pressure on their windward side wall than did the same bodies with zero angle of attack.

To study the pressure distribution of bodies that closely represent building configurations, tests were made on bodies of square cross sections that were placed on the floor of the wind tunnel. It was found that decreasing relative height of the body had an attenuating effect on the negative pressure on the windward sidewall and it also increased the critical angle of attack.

Roberson et al. [9] carried out experiments on circular cylinders, spool shaped bodies, cup-shaped bodies, square rods and rectangular rods to observe the effect of turbulence on the drag of these bodies. For square rods with their axes parallel to the flow direction it was found the  $C_D$  decreased approximately 25% when the turbulence intensity increased from 1% to 10%. In this experiment two rectangular rods were used, in which one had a square cross section and the other had a length (in the free stream direction) to breadth ratio of two ( $L/B = 2$ ). The drag was measured with the axes of the rectangular rods leaning normal to the free stream direction. Observations showed that on the square rod the pressure change with turbulence intensity was same on the sides as well as the rear face. However, on the rectangular rod, it was noted that the change in pressure on the sides was large, but small on the rear face. It was concluded that bodies which have shapes such that reattachment of the flow is not a factor, experience an increase in  $C_D$  with increased turbulence intensity. On the other hand a body for which reattachment or near reattachment of flow occurs with increased turbulence, may experience either a decrease or increase in  $C_D$  with increased turbulence intensity depending upon the shape of the body.

Barriga et al. [6] studied the effects of angle of attack, turbulence intensity and scale on the pressure distribution of single square cylinder placed in a turbulent cross flow. When a square cylinder is positioned in a cross flow with one face normal to the flow direction, only drag force was produced, but in the same flow a negative lift force was developed at small positive angle of attack where the magnitude depended on the turbulence characteristics of the cross flow. It was suggested that the negative lateral force on the square cylinder oriented at a small positive angle of attack was due to the relatively large negative pressure coefficient in the separated zone on the windward sidewall. It was also concluded that the effect of turbulence intensity was to decrease the pressure near the front corner of the windward sidewall and promote flow reattachment near the rear, giving rise to a very significant increase in aerodynamic moment.

Nakamura and Ohya [14] studied the effects of turbulence on the mean flow past square rods. Square rods of different lengths were used to take measurements with their square face normal to the flow to investigate the effects of turbulence intensity and scale the mean flow characteristics. The turbulence intensity varied from 3.5% to 13% and the

length-to-size ratio of  $d/h$  of the rods ranged from 0.1 to 2.0 where  $d$  was the length of the rod. It was found out that there were two main effects that turbulence on the mean flow past a three-dimensional sharp edged bluff body. The first effect is that the small-scale turbulence increased the growth rate of the shear layer, and the second effect is that the large-scale turbulence enhanced the roll up of the shear layer. For a square plate, both small and large-scale turbulence reduced the size of the base cavity. As the length of the square rod was increased beyond the critical (0.6 times the height), the shear-layer-edge direct interaction controlled the near wake, eventually leading to flow reattachment. The effect of small-scale turbulence was to promote the shear layer direct interaction.

Vickery [4] presented in his studies the results of the measurements of the fluctuating lift and drag on a long square cylinder. It was tried to show the correlation between the lift along cylinder and the distribution of fluctuation pressure on a cross-section. It was found that the magnitude of the fluctuating lift was considerably greater than that for a circular cross section and the span wise correlation much stronger. It was also reported that with large scale turbulence in the stream, both the steady and the fluctuating forces were greatly influenced. At small angle of attack (less than  $10^\circ$ ) turbulence caused a reduction in base suction and a decrease in fluctuating lift of about 50%.

Bostock and Mair [15] studied the pressure distributions and forces of rectangular and D-shaped cylinders, placed in two-dimensional flow with the Reynolds number at  $1.9 \times 10^4$ . It was found that for rectangular cylinders a maximum drag co-efficient was obtained when the height  $h$  (normal to the stream) of the section was about 1.5 times the width  $d$ . Reattachments on the sides of the cylinders occurred only for  $h/d$  less than 0.35.

Sakamoto and Arie [16] collected experimental data on the vortex shedding frequency behind a vertical rectangular prism, as well as vertical circular cylinder by having them attached to a plain wall and immersed in a turbulent boundary layer. It was investigated that the effects of the aspect ratio (height/width) of these bodies and the boundary layer characteristics on the vortex shedding frequency. Depending on the aspect ratio measurements revealed that two typed of vortex were formed behind the body. The two types of vortex that were formed were the arch-type vortex and the karman-type vortex.



The arch-type vortex appeared at an aspect ratio less than 2.0 and 2.5 for rectangular and circular cylinders respectively and the karman-type vortex appeared for the aspect ratios greater. The whole experiment was conducted at a turbulence level of 0.2% and free stream velocity of 20m/sec. The aspect ratio varied between 0.5 to 8.0.

Castro and Robins [8] described in their studies the flow around surface mounted cubes of uniform, irrotational, sheared and turbulent flows. The shear flow was simulated by the atmospheric boundary layer which had a height ten times the body dimension. It was presented that the measurements of body surface pressures and mean, and also the fluctuating velocities within the wake region, which reflect the effects of upstream turbulence and shear on the wake flow. The addition of upstream turbulence and shear drastically reduced the size of the cavity zone in the reversed flow region directly behind the body. Unlike in the case of uniform flow, the separating shear layers did not reattach to the body surface. Measurements for a variety of cube size/boundary layer height ratios further revealed that reattachment occurred even for cube heights larger than the boundary layer height. It was found that in the case of uniform flow approaching the cube at 45°, the near wake and pressure field were dominated by strong vortices shed from the top edges of the body.

Laneville et al. [17] included in their research the effects of turbulence on bluff bodies. Square and rectangular prisms were used as their bluff bodies.

Hua [18] made measurements of fluctuating lift and the oscillating amplitudes on square cylinders. It was reported that the wind pressure distributions and the lift on the stationary cylinder are normal to the wind. It was also noted that the lift force was proportional to the square of its amplitude.

Matsumoto [19] has conducted an investigation on the aerodynamic forces acting on an oscillating square prism in a steady flow both experimentally and theoretically. First, a few experiments are performed in order to examine the aerodynamic forces, in the direction of the wind stream and in a plane normal to it, acting on an oscillating square prism. Karman's theory about a thin plate is extended to the case of a square prism and the aerodynamic forces in a plane of the direction of the wind stream are obtained which have

correlate the experimental results fairly well.

Parkinson and Modi [20] describe about the characteristics of the separated flow over bluff two-dimensional bodies that relate to two forms of the aero elastic instability of the bodies, vortex-excited and galloping transverse oscillation. Bodies investigated included cylinders of square, rectangular, circular, elliptical and D-section an idealized structural angle of section.

Hussain and Islam [21] measured coefficient of pressure and coefficient of lift on circular, parabolic and elliptical shell roof in a uniform velocity. The investigation was performed in a small wind tunnel with Reynolds number varying between 1.7 to 350,000 based on model width. The scale of the model was quite high (1:40). The variation of the Reynolds number was obtained by varying the velocity only. As the experiment was carried out in a uniform velocity, the estimated results were higher than it would be in reality.

Keffer [22] investigated the wake produced by the two-dimensional cylinder of diameters 12.7mm, 7.93mm and 4.76mm with straining the flow. The tunnel speed was held constant at 5.48m/sec so that the corresponding Reynolds number based on cylinder diameters were 4630, 2890 and 1740 for cylinder diameters of 12.7mm, 7.93mm and 4.76mm respectively. The mean quantities were measured with a pitot-static tube. Experimentally it was found that the wake width increased with distance along the downstream. The mean velocity distribution of the wake profile was in no way self-preserving.

Gartshore [23] investigated the two-dimensional wake of a square (6.35mm) rod at adverse pressure gradients and at the pressure gradient for exact self-preservation. The velocity ratio was maintained approximately constant and the flow through wake having Reynolds numbers 6300 and 7300 were based on the conditions at the trailing edge.

Pearlstein and Mantle [24] investigated that at low Reynolds numbers ( $Re_c$ ), the flow past axisymmetric and attached. For bluff bodies (e.g. spheres, mindrops and torpedoes) the flow separates as  $Re_c$  increases ultimately transition to unsteady axisymmetric flow becomes unstable with respect to an oscillatory helical instability at  $Re_c = 175.1$ . The critical  $Re_c$  and predicted Strouhal number (dimensionless frequency) agree well with previous

experiments. This work was extended to the case where the body falls or rises freely under the action of gravity. In that case, the rigid body motion can couple to the flow disturbances, leading to a lower critical  $R_c$ .

Pearlstein et al. [25] conducted computational investigations of the stability of the steady (asymmetric) 2-D flow past a rotating cylinder, as well as the time periodic 2-D flow to which it loses its stability as the Reynolds number ( $R_c$ ) is increased. It was shown that the critical  $R_c$  at which the steady flow becomes unstable to 2-D disturbances depends nonmonotonically on the dimensionless rotation rate, and that the frequency of the critical mode that evolves from the Hopf bifurcation has several discontinuities along the stability boundary, corresponding to transitions from one mode to another.

Pris et al. [26] describes many items, one of that is the investigation of galloping oscillation on square cylinders.

Senthooran et al [27] conducted a computational model to predict the pressure fluctuation around bluff bodies. This model was tested to predict the pressure fluctuation on the low-rise experimental building at Texas Tech, for  $60^\circ$  and  $90^\circ$  wind angle of attack. This model predicts the fluctuation quantities with good accuracy. Mean pressure coefficients obtained from the computational model show very good agreement with the experimental results.

Li et al [28] presented in their paper the selected results from the full scale measurements of wind effects on the tallest building in Mainland China during the passage of Typhoon Rananim and 15-hours data of wind speed, wind direction and acceleration responses recorded simultaneously and continuously during the Typhoon were analyzed and discussed in this paper. Wind tunnel experiment is conducted to study wind effects on the Jin Mao Building through force balance model test and full scale measurements are compared wind tunnel test results for verification of wind tunnel test techniques.

Gu and Quan [29] made wind tunnel test on 15 typical tall building models of basic cross-sections aspect ratios from 4 to 9 with high frequency and force balance technique. The effects of terrain condition, aspect ratio and side ratio of cross section and modified corner of the building models on the across-wind forces are investigated in detail. New

formulas of the power spectra of the cross wind dynamic forces, the coefficients of base moment and shear force are derived. The reliability of this formulas is verified through detailed comparisons between the present formulas and those from the literature. The comparison results indicate not only the effect of aerodynamic damping on across-wind dynamic response of the building but also the reliability of the present formulas of the across-wind loads.

Enrico and Riccardelli [30] presented in their paper two applications of spectral proper transformation (SPT) analysis to the fluctuating pressure distributions on a square cylinder and a bridge deck box section.

## 2.2 Literatures Concerning Multiple Bodies

Leutheusser [31] made wind tunnel tests on scale models of typical building configurations. The experiment was conducted using four models, in which each model had different heights and cross sections. It was found out that the static wind loading on each of the building in both free standing condition as well as a member in a group of buildings. It was also realized that wind loading on a building was less severe when it effects a building in a group rather than when it is standing alone.

Hayashi et al. [32] made an experimental investigation into the wake characteristics of a group of flat plates; where two, three or four plates were placed side by side normal to the flow direction. It was found that when the ratio of the split width to the plate width (split ratio) of a row of flat plates was less than about 2; the flows through the gaps were biased either upward or downward in a stable way, leading to multiple flow patterns for a single split ratio value. The plates on the biased side showed high drag and regular vortex shedding, while those on the unbiased side showed the opposite. It was suggested that the origin of biasing was strongly related to the vortex shedding of each plate of a row. The experiment was conducted for Reynolds number of  $(1.3 - 1.9) \times 10^4$ .

Koeing and Roshko [33] investigated the shielding effects of various disks placed co-axially upstream of an axisymmetric flat faced cylinder. In this type of setup, it was observed that a considerable decrease in the drag, for certain combinations of the diameter

and gap ratios. Using the flow visualization technique it was also showed that for optimum shielding, the upstream surface which separated from the disk, reattached smoothly onto the front edge on the downstream cylinder.

Bearman and Wadcock [34] reported that how the flows around two circular cylinders interact as the two bodies are brought close together; when they are displaced in a plane normal to the free stream. Surface pressure measurements at a Reynolds number of  $2.5 \times 10^4$  based on the diameter ( $D$ ) of a single cylinder, showed the presence of a mean repulsive force between the two cylinders. With gaps between  $0.1D$  and  $1D$ , a marked asymmetry in the flow was observed. The two cylinders experienced different drags and base pressure. The base pressure changed from one steady value to another or simply fluctuated between two extremes. It was also showed that how mutual interference influenced the formation of vortex streets from the two cylinders.

Baines [35] described the effects of velocity distribution on wind loads and flow patterns around buildings. It was measured pressure distributions on models of walls and rectangular block structures in a wind tunnel. Tall buildings with square sections have also been included in his study. The tests were conducted both in an artificially produced velocity gradient used to simulate natural conditions, and in a constant velocity field for comparison with standard procedures.

Mandal [36] performed the study effect on the staggered square cylinder. The test was conducted in an open circuit wind tunnel at Reynolds number of 27800 based on the side dimension of the square model. The maximum blockage area was 6.96 percent. Three cylinders were arranged in the staggered form (one in upstream and two in downstream flow) varying the longitudinal and transverse spacings and measurements of pressure coefficients were taken for the upstream and downstream cylinders. Experiments were also carried out for drag coefficients, lift coefficients, total force coefficients and moment coefficients. After all, it is concluded from the results that wind loading on a building is generally less severe when the building forms part of a group than when it is free-standing.

Islam, T. [37] conducted experiments on the wind effect on the rectangular cylinders. The rectangular cylinders had side ratios of  $H/D=1.25, 1.5, 1.75$  and  $2.0$  where  $D$

is the section width normal to flow direction and  $H$  is section depth along the flow direction. The flow had a turbulence intensity of 0.33% and a constant free stream velocity of 18.3 m/sec was used for the purpose. Mean pressure distributions around each of the cylinders was measured for different angle of attack. It was found that the drag on the rectangular cylinder with its axis normal to the approaching flow increased with rise of the value of side ratio up to about 0.6, then decreased with the further increase in the side ratio. It was also observed that the drag on an isolated cylinder was higher in general than that on the same cylinder while it becomes part of a group. The rectangular cylinder with the highest side ratio experienced minimum drag for all conditions of spacings.

## CHAPTER-3

### EXPERIMENTAL SETUP

With the use of subsonic open circuit wind tunnel, various experiments have been performed of wind loads on square and rectangular cylinders. In the present investigation combination of two sets of square and rectangular cylinders were used. To measure the static pressure distribution around the cylinders, which were placed normal to the approaching uniform flow, two inclined multi-manometer banks were used. The following section briefly describes the experimental setup and the procedures of the investigation.

#### 3.1 Specification of the Wind Tunnel

The experimental setup of the present investigation has been shown in the schematic diagram of Figure 3.1. Open circuit subsonic type wind tunnel was used to develop the required flow, and the cylinders were positioned at the exit end of the wind tunnel in the downstream. The tunnel is 5.93 meter long with a test section of 460 x 480 mm cross-section. In order to smooth the flow a honeycomb is fixed near the end of the wind tunnel. There is a bell-shaped converging mouth entry. To generate the wind velocity, two axial flow fans are used, with each of the fans connected to a motor of 2.25 kilowatt and 2900 rpm. There is a butterfly valve to control the wind speed. There is a silencer just after the butterfly valve as shown in the Figure 3.1.

The central longitudinal axis of the wind tunnel is always kept at a constant height of 990 mm from the floor. The axis of the model is also placed in coinciding position with the wind tunnel. The converging mouth entry is then merged into in the wind tunnel so that air can enter smoothly into the tunnel and maintain uniform flow into the duct, keeping it free from any outside disturbances. The flow through the wind tunnel is induced by a two-stage rotating axial flow fan of 18.16 m<sup>3</sup>/s capacity, at the head of 152.4 mm of water and 1475 rpm.

A butterfly valve, which is used to control the flow was actuated by a screw thread

mechanism placed behind the fan. A silencer, which is incorporated with a honeycomb, is fitted at the end of the flow controlling section, which helps reduce the noise of the system. The diverging and converging section of the wind tunnel is 1550 mm long and made of 16 SWG black sheets. The angle of divergence and convergence is  $6^\circ$ , which has been done with a view to minimize expansion, contraction loss, and reduce the possibility of flow separation.

A digital anemometer is used in each of these tests to measure the wind velocity. Results show that the flow velocity was maintained at approximately 13.5 m/s. In the tunnel test section, the measured velocity distribution was uniform almost throughout the upstream side of the models.

### 3.2 Test Section

This test was done at the exit end of the wind tunnel in open air (Figure 3.1). In order to affix the cylinder, a steel frame was manufactured, and installed using nuts and bolts. The top floor of the steel frame had the same level of sides so that the distance between them was same as the distance of the side walls of the wind tunnel exit end. The distance was 485 mm. Both the top and bottom of the test section was kept open, and no cover plates were used. The cylinders were attached to the side walls made of plywood. The cylinder was fastened by bolting it to one of the side walls. The bolt was fixed with the wooden block on one end of the cylinder and through the other end of the cylinder; the plastic tubes were taken out through the wooden block in order to connect them with the inclined manometers. This end was supported in the groove of the side wall of the test section. The cylinder was so positioned and fastened in this way so that the flow direction was parallel to its sides and the front face was perpendicular to the flow direction.

In order to test the group effects, grooves were made on the side walls of the test sections so that multiple cylinders could be used. Three cylinders were placed in staggered form, with one cylinder was placed in the front, and the other two at the rear along the free stream direction. With  $D$  representing the height of the cylinder, the inter space between the front and rear cylinders (in longitudinal direction) varied at  $1D$ ,  $2D$ ,  $4D$ ,  $6D$ , and  $8D$ . The inter space between the rear cylinders (in transverse direction) was varied at  $1D$ ,  $2D$ ,



and 4D. In order to achieve the right spacing, several grooves were made on the side walls of the test section, but the unnecessary grooves were closed during the testing process. The cylinder on one side was fixed by bolting it to a wooden block, while the other end was fixed in grooves with the help of the wooden block. The plastic tubes were taken out from the wooden block through the grooves, and were connected to the inclined manometers. During fixing the cylinders, it was checked carefully whether the sides of the cylinders were parallel to the free stream velocity direction and the front and rear cylinders were arranged in staggered form. Leveling of the cylinder was always checked and balanced by a standard spirit level.

### 3.3 Constructional Details of Cylinder

In the experimental investigation of the four cylinders (two square and two rectangular), there are two sets of cylinders with two identical ones in each set, which were made with Perspex. The constructional details of the cylinders are shown in Figure 3.2. Each of the cylinders was constructed identically. The side dimensions of the cylinders in each set were  $D=51.08$  mm, and  $H=51.08$  mm and  $63.85$  mm.  $4$  mm thick and  $460$  mm long. Perspex plates with the appropriate side dimensions were joined to form the shape of hollow square and rectangular cylinders. One end was closed by inserting a solid wooden block and the other end by inserting another wooden hollow block with  $27$  mm through hole. In order to mount the cylinders, one end was projected  $30$  mm long circular portion and the other end was bolted ( $53$  mm long) by wooden block as shown in Figure 3.2. There was an indicator attached with the bolt as well as adjusted with a circular disc, which was fitted in the sidewall of the test section. This provision was needed to maintain angular orientation of the cylinders.

To measure the pressure distribution of each square and rectangular cylinder, they were tapped on two adjacent sides. It was not possible to accommodate all the tappings in a section perpendicular to the axis of the cylinder because of the space limitations. The tappings were placed in an inclined sectional plane within  $20$  mm from the center of the cylinder, as shown in Figure 3.3. It was assumed that for two-dimensional flow, such tappings would not affect the results. The results show the end tapping points were made at

equal distances from the corners and the interspaces between the consecutive tapping points were kept at equal distance as shown in Figure 3.4. Each tapping was made using 1.71 mm diameter copper tubes and the tapping holes were press fitted with 10mm length copper tubes. The tapping was then connected to the limbs of a multi-manometer using flexible plastic tubes whose diameter was 1.84mm. Water was used as manometric liquid.

### 3.4 Experimental Procedure

The experiment was conducted in two phases. In the first phase, measurements of pressure distribution on cylinders with side ratios  $H/D = 1.0$  and  $1.25$  were taken. Pressure distributions on the cylinders were recorded for angles of attack varying from  $0^\circ$  to  $45^\circ$  in  $5^\circ$  steps. In the second phase, one square and two rectangular cylinders of identical dimension were mounted horizontally in the staggered form. The square cylinder was placed centrally in the upstream side and the other two rectangular cylinders were placed symmetrically in the downstream side with respect to tunnel axis. Pressure distributions around the cylinders were measured for the different longitudinal and transverse spacing of the cylinders. Measurements were also taken for one rectangular and two square cylinders in staggered form. The flow velocity in the test section was kept constant at 13.5 m/s. The Reynolds number based on the side dimension  $D = 51.08\text{mm}$  was  $4.5 \times 10^4$ .

In the experiment, before measuring the pressure distribution, first the mean velocity was measured in a vertical 400mm upstream from the cylinders. This was done by means of a pitot static tube, which was connected to an inclined manometer filled with water. It is clear to from Figure 3.7 that the measured velocity distribution was uniform along the height of test section.

#### 3.4.1 Single Cylinder

The rectangular cylinder with side dimension  $H = 51.08$  mm was mounted in the center of a horizontal plane at a distance of 400 mm downstream from the wind tunnel exit. The 51.08mm side of the cylinder was oriented normal to the flow direction. For angular orientation of the cylinders a graduated circular disc was used. An inclined multi-manometer bank was used to record the mean pressure distribution on the body. An anemometer placed in the middle, approximately 400 mm forward from the center of the cylinder to measure

the free stream velocity.

Pressure tappings were made on the four perpendicular surfaces of the cylinders. Mean pressure distribution was recorded at angle of attack varying from  $0^{\circ}$  to  $45^{\circ}$  with a step of  $5^{\circ}$ . Pressure distributions for each of the cylinder with side dimension  $H = 63.85$  mm were measured in a similar manner.

### 3.4.2 Cylinders in Group

The method in which one square and two rectangular cylinders were placed in staggered form can be seen in Figure 3.5. They were positioned in such way that the 51.08mm side of each of the cylinders was kept normal to the direction of the approaching velocity. Initially, the cylinders were mounted in such a way that the transverse spacing between the downstream cylinders and the longitudinal spacing between the front surface of the downstream cylinders and back surface of the upstream cylinder were  $1D$ . Since the top downstream cylinder (T) and bottom downstream cylinder (B) were symmetrically placed, the pressure distributions were considered on the top cylinder only.

The transverse spacing ( $L_2$ ) for the downstream cylinders were altered to  $1D$ ,  $2D$ ,  $4D$ . For each transverse spacing ( $L_2$ ), the longitudinal spacing ( $L_1$ ) were set at  $1D$ ,  $2D$ ,  $4D$ ,  $6D$  and  $8D$ . Mean pressure distributions were measured for the above, for 15 sets and at zero angle of attack only. Pressures were measured simultaneously for the upstream and downstream cylinders. One rectangular and two square cylinders were placed in staggered form as shown in the Figure 3.6. Pressure distributions for the cylinders were measured in a similar manner.

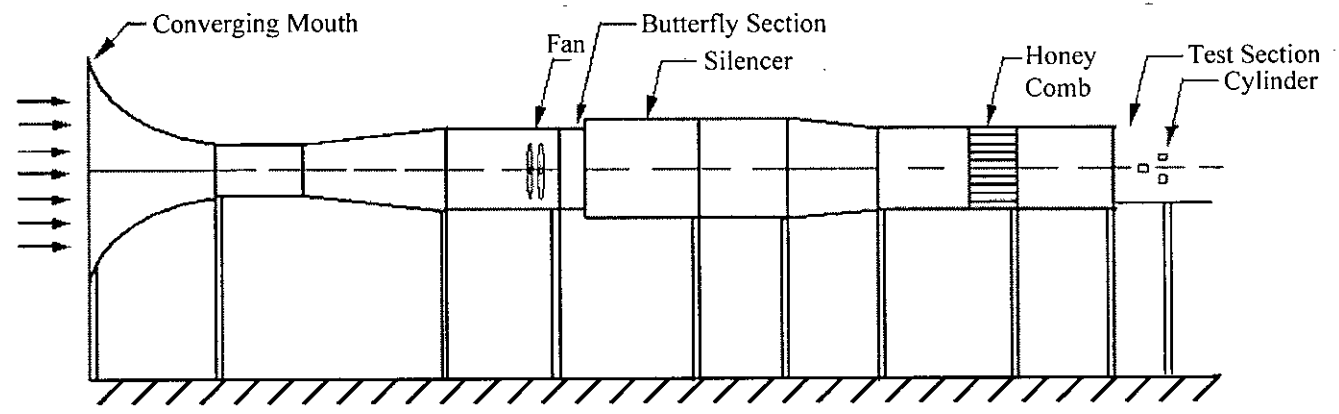


Figure 3.1: Schematic Diagram of Wind Tunnel

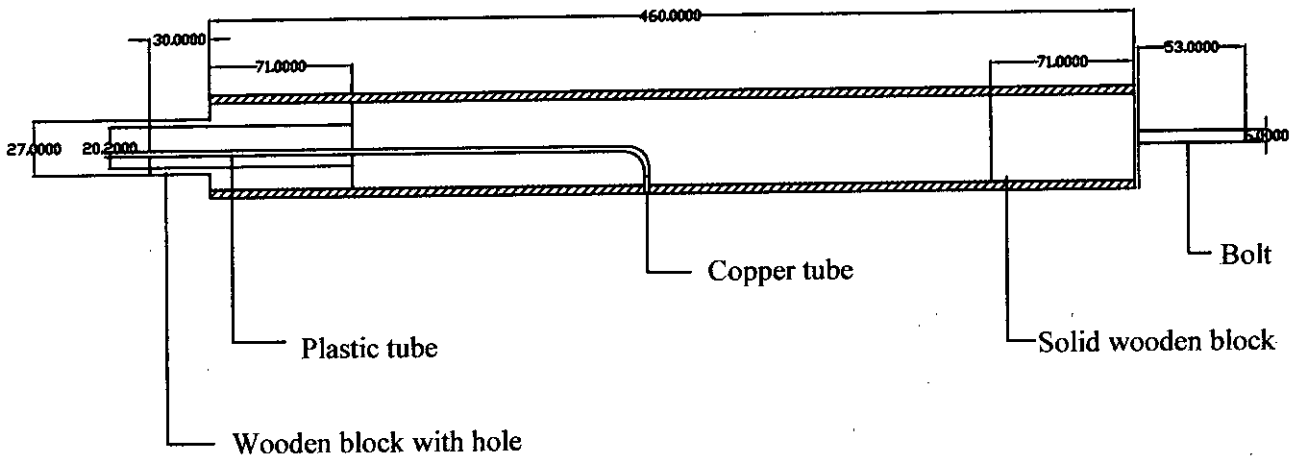


Figure 3.2: Sectional view of a specimen rectangular cylinder.

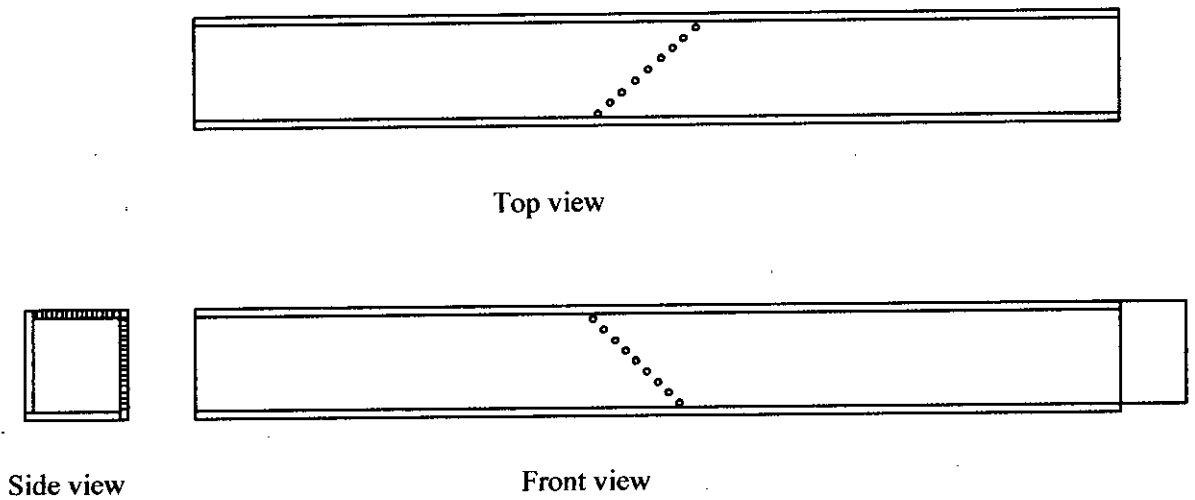


Figure 3.3: The arrangement of tapping points on adjacent sides

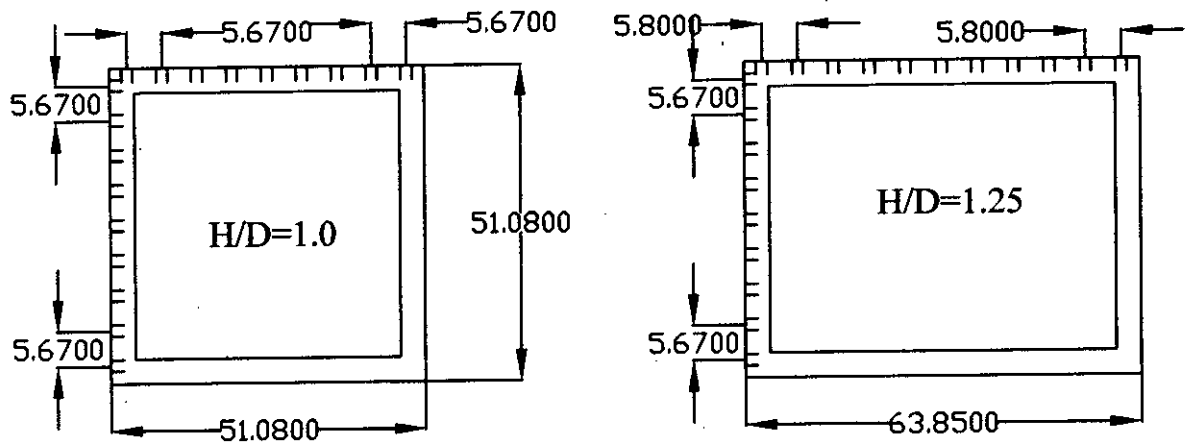
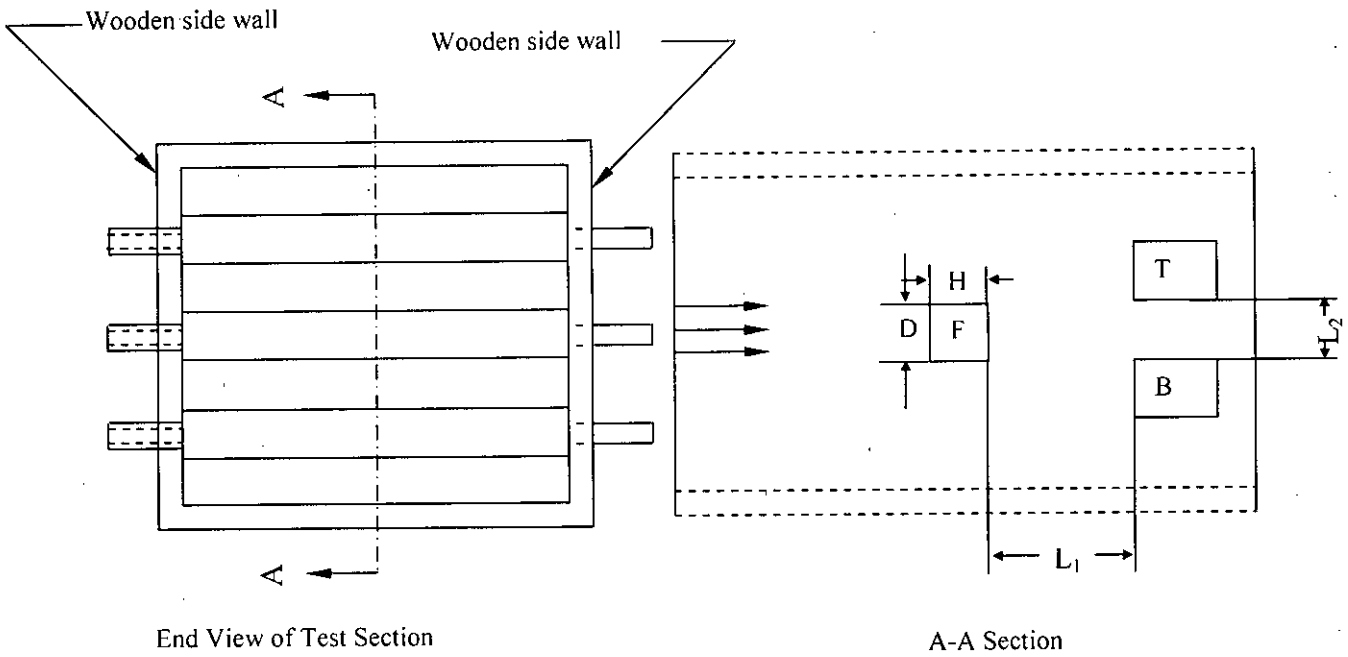
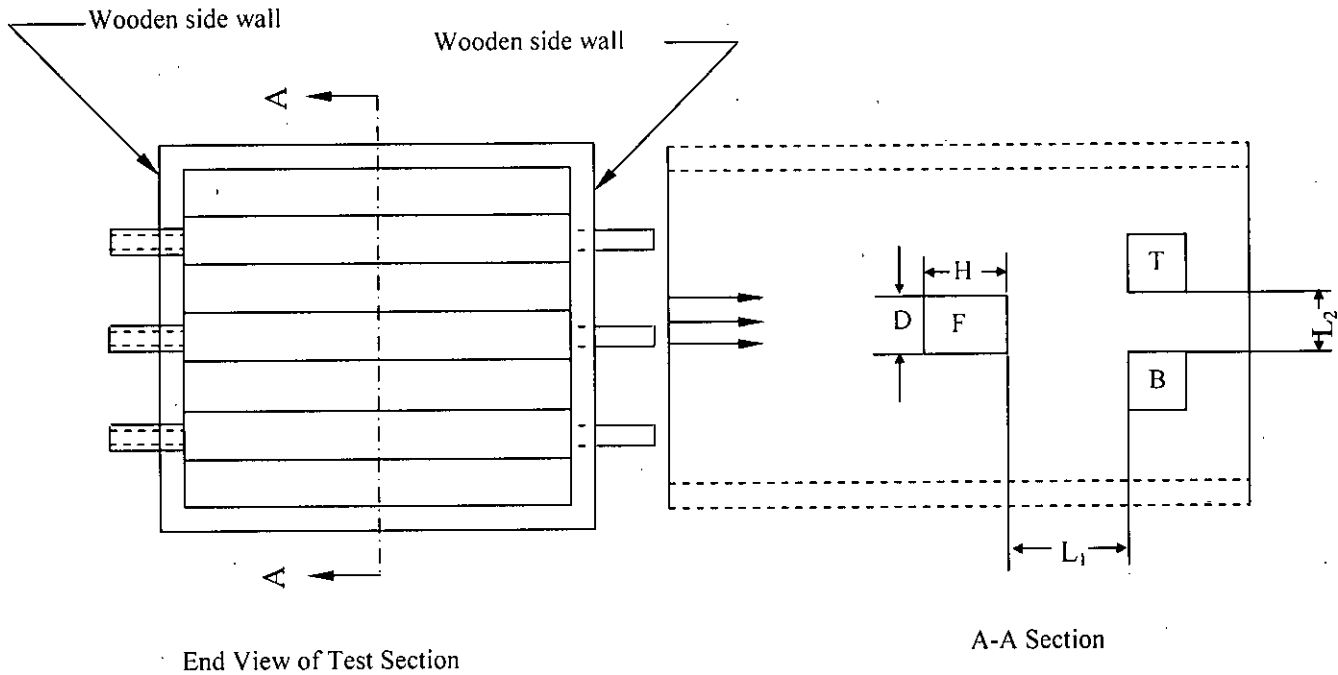


Figure 3.3: Cross-section of rectangular cylinders from each set showing position of tapping points.



**Figure 3.5:** Tunnel test section showing the position of cylinders (one square and two rectangular) in staggered form.



**Figure 3.6:** Tunnel test section showing the position of cylinders (one rectangular and two square) in staggered form.

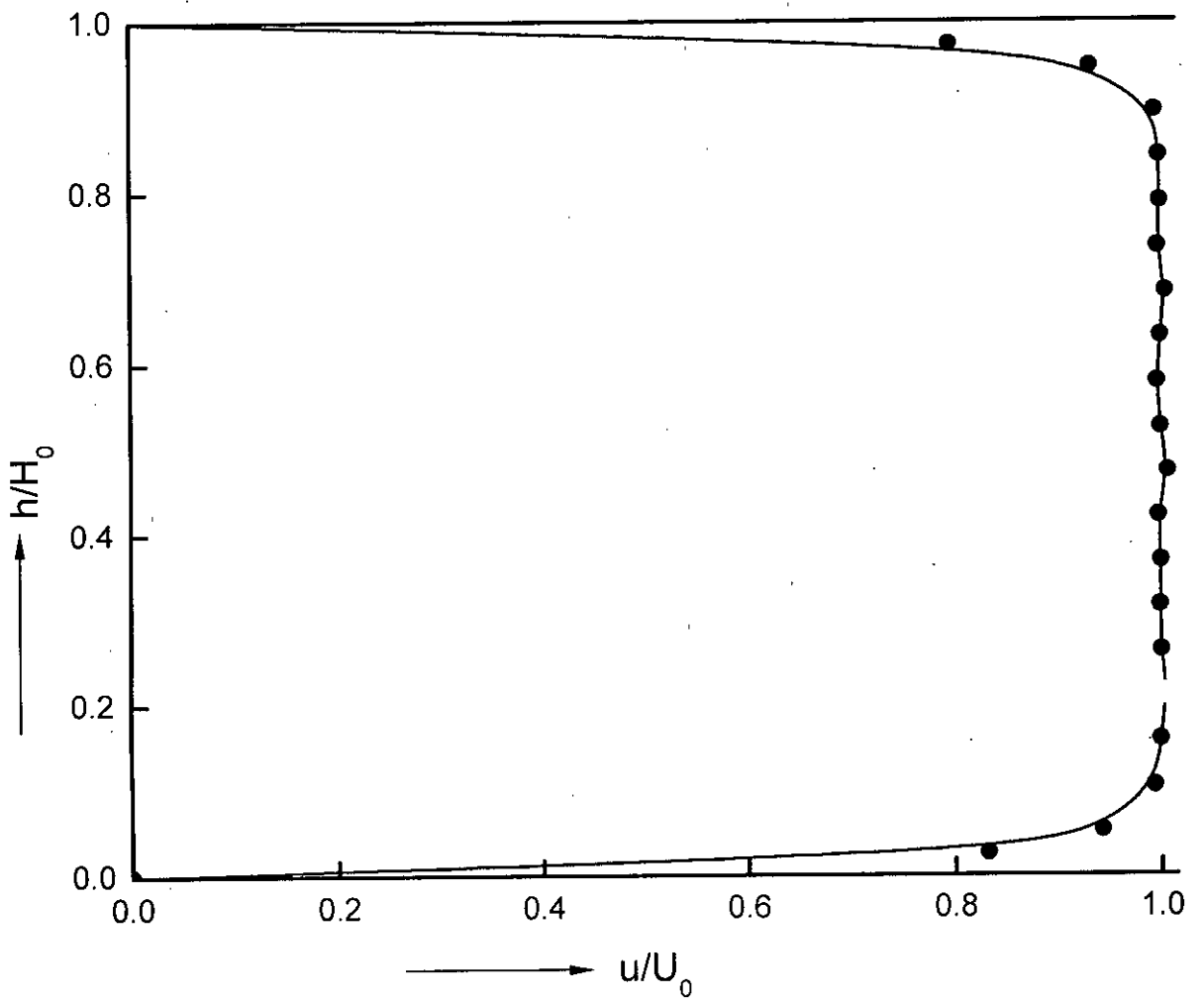


Figure 3.7: Velocity distribution along the height of the test section.



## CHAPTER-4

### MATHEMATICAL MODEL

The local surface pressures on the cylinders were measured relative to the free upstream static pressure prevailing in the test section of the wind tunnel. All the data are hereby presented in terms of non-dimensional coefficients. The equations of coefficients of lift, drag and moment are derived briefly as shown below.

#### 4.1 Pressure Co-efficient

Pressure co-efficient is defined as, 
$$C_p = \frac{P - P_0}{1/2 \rho U_0^2} \quad (4.1)$$

#### 4.2 Drag and Lift Coefficients

Drag co-efficient is defined as, 
$$C_D = \frac{F_D}{1/2 \rho A U_0^2} \quad (4.2)$$

Lift co-efficient is defined as, 
$$C_L = \frac{F_L}{1/2 \rho A U_0^2} \quad (4.3)$$

Now, the equation (4.2) and (4.3) are simplified by applying numerical integration method to the suitable form to be used directly to obtain the values of coefficients.

The section of the cylinder shown in the Figure 4.1 is divided horizontally (along x-axis) into nine strips of equal width  $\Delta l$ . Similarly, it is divided vertically (along y-axis) into  $n$  equal strips, where  $n$  is the number of tapping points on the bottom surface of the cylinders of different side ratios. There are pressure-tapping points at the mid-point of each strip. Because of two-dimensional uniform flow, pressure distributions have been assumed to be same at every section along the cylinder. A certain length  $l$  is considered over which the pressure distribution is same at every section. So, area under each strip becomes  $\Delta l \times l$ .

Let  $\Delta P_{1h}, \Delta P_{2h}, \Delta P_{3h}, \Delta P_{4h}, \dots, \Delta P_{9h}$ , and  $\Delta P_{1v}, \Delta P_{2v}, \Delta P_{3v}, \Delta P_{4v}, \dots, \Delta P_{nv}$  are respectively the pressure differences in millimeter of manometer liquid between the opposite surfaces of each strip along the horizontal and vertical directions. Adding the all forces acting along the strips and taking the components,

$$F_D = \left( \frac{\Delta P_{1h} \times \gamma_w \times \Delta l \times l}{1000} + \frac{\Delta P_{2h} \times \gamma_w \times \Delta l \times l}{1000} + \frac{\Delta P_{3h} \times \gamma_w \times \Delta l \times l}{1000} + \frac{\Delta P_{4h} \times \gamma_w \times \Delta l \times l}{1000} + \dots + \frac{\Delta P_{9h} \times \gamma_w \times \Delta l \times l}{1000} \right) \cos \alpha + \left( \frac{\Delta P_{1v} \times \gamma_w \times \Delta l \times l}{1000} + \frac{\Delta P_{2v} \times \gamma_w \times \Delta l \times l}{1000} + \frac{\Delta P_{3v} \times \gamma_w \times \Delta l \times l}{1000} + \frac{\Delta P_{4v} \times \gamma_w \times \Delta l \times l}{1000} + \dots + \frac{\Delta P_{nv} \times \gamma_w \times \Delta l \times l}{1000} \right) \sin \alpha \quad (4.4)$$

$$F_L = \left( \frac{\Delta P_{1h} \times \gamma_w \times \Delta l \times l}{1000} + \frac{\Delta P_{2h} \times \gamma_w \times \Delta l \times l}{1000} + \frac{\Delta P_{3h} \times \gamma_w \times \Delta l \times l}{1000} + \frac{\Delta P_{4h} \times \gamma_w \times \Delta l \times l}{1000} + \dots + \frac{\Delta P_{9h} \times \gamma_w \times \Delta l \times l}{1000} \right) \sin \alpha + \left( \frac{\Delta P_{1v} \times \gamma_w \times \Delta l \times l}{1000} + \frac{\Delta P_{2v} \times \gamma_w \times \Delta l \times l}{1000} + \frac{\Delta P_{3v} \times \gamma_w \times \Delta l \times l}{1000} + \frac{\Delta P_{4v} \times \gamma_w \times \Delta l \times l}{1000} + \dots + \frac{\Delta P_{nv} \times \gamma_w \times \Delta l \times l}{1000} \right) \cos \alpha \quad (4.5)$$

Equation (4.4) becomes,

$$F_D = \frac{\gamma_w \times \Delta l \times l}{1000} \left[ (\Delta P_{1h} + \Delta P_{2h} + \Delta P_{3h} + \Delta P_{4h} + \dots + \Delta P_{9h}) \cos \alpha + (\Delta P_{1v} + \Delta P_{2v} + \Delta P_{3v} + \Delta P_{4v} + \dots + \Delta P_{nv}) \sin \alpha \right]$$

$$\text{Or, } F_D = \frac{\gamma_w \times \Delta l \times l}{1000} \left[ \Delta P_h \cos \alpha + \Delta P_v \sin \alpha \right] \quad (4.6)$$

Where,  $\Delta P_h = \Delta P_{1h} + \Delta P_{2h} + \Delta P_{3h} + \dots + \Delta P_{9h}$

and  $\Delta P_v = \Delta P_{1v} + \Delta P_{2v} + \Delta P_{3v} + \dots + \Delta P_{nv}$

Equation (4.6) may be written in the form,

$$F_D = \frac{\gamma_w \times \Delta l \times l}{1000} \left[ \Delta P_D \right] \quad (4.7)$$

Where,  $\Delta P_D = \Delta P_h \cos \alpha + \Delta P_v \sin \alpha$

Similarly, equation (4.5) is reduced to the form

$$F_L = \frac{\gamma_w \times \Delta l \times l}{1000} \left[ \Delta P_L \right] \quad (4.8)$$



Where,  $\Delta P_L = \Delta P_h \sin\alpha + \Delta P_v \cos\alpha$

From equations (4.2) and (4.7)

$$C_D = \frac{\gamma_w \times \Delta l \times l \times \Delta P_D}{1000 \times 1/2 \times \rho \times A \times U_0^2} \quad \text{since, } A = 9 \times \Delta l \times l$$

$$\text{Or, } C_D = \frac{\gamma_w \Delta P_D}{4500 \rho U_0^2} \quad (4.9)$$

Similarly, from equations (4.3) and (4.8)

$$C_L = \frac{\gamma_w \times \Delta l \times l \times \Delta P_L}{1000 \times 1/2 \times \rho \times A_1 \times U_0^2} \quad \text{since, } A_1 = n \times \Delta l \times l$$

$$C_L = \frac{\gamma_w \Delta P_L}{500 n \rho U_0^2} \quad (4.10)$$

At zero angle of incidence, i.e. when  $\alpha = 0^\circ$ , lift and drag coefficients are reduced to the forms,

$$C_D = \frac{\gamma_w \Delta P_h}{4500 \rho U_0^2} \quad (4.11)$$

$$C_L = \frac{\gamma_w \Delta P_v}{500 n \rho U_0^2} \quad (4.12)$$

Using the equation (4.9), (4.10), (4.11) and (4.12) the values of lift and drag coefficients are obtained directly.

### 4.3 Moment Co-efficient

In the present analysis the moment co-efficient may be defined as,

$$C_M = \frac{M}{1/2 \rho A U_0^2 D} \quad (4.13)$$

Equation (4.13) is simplified to the form to be used directly to find moment co-efficient by applying numerical integration method.

The section of square cylinder shown in Figure 4.2 has been divided into nine strips of equal width  $\Delta l$ , both horizontally and vertically. The positions of pressure tapping points are at the middle of the strips. A certain length  $l$  is considered over which the pressure distribution is same at every section. The moment about clockwise direction is considered positive. The equation of moment is obtained as

$$\begin{aligned}
 M &= \left( \frac{\Delta P_{1v} \gamma_w}{1000} \times 4 \times \Delta l + \frac{\Delta P_{2v} \gamma_w}{1000} \times 3 \times \Delta l + \frac{\Delta P_{3v} \gamma_w}{1000} \times 2 \times \Delta l + \frac{\Delta P_{4v} \gamma_w}{1000} \times \Delta l \right) l \times \Delta l \\
 &\quad - \left( \frac{\Delta P_{6v} \gamma_w}{1000} \times \Delta l + \frac{\Delta P_{7v} \gamma_w}{1000} \times 2 \times \Delta l + \frac{\Delta P_{8v} \gamma_w}{1000} \times 3 \times \Delta l + \frac{\Delta P_{9v} \gamma_w}{1000} \times 4 \times \Delta l \right) l \times \Delta l \\
 &\quad + \left( \frac{\Delta P_{1h} \gamma_w}{1000} \times 4 \times \Delta l + \frac{\Delta P_{2h} \gamma_w}{1000} \times 3 \times \Delta l + \frac{\Delta P_{3h} \gamma_w}{1000} \times 2 \times \Delta l + \frac{\Delta P_{4h} \gamma_w}{1000} \times \Delta l \right) l \times \Delta l \\
 &\quad - \left( \frac{\Delta P_{6h} \gamma_w}{1000} \times \Delta l + \frac{\Delta P_{7h} \gamma_w}{1000} \times 2 \times \Delta l + \frac{\Delta P_{8h} \gamma_w}{1000} \times 3 \times \Delta l + \frac{\Delta P_{9h} \gamma_w}{1000} \times 4 \times \Delta l \right) l \times \Delta l \\
 M &= \frac{(\Delta l)^2 \times l \times \gamma_w}{1000} [(4\Delta P_{1v} + 3\Delta P_{2v} + 2\Delta P_{3v} + \Delta P_{4v}) - (\Delta P_{6v} + 2\Delta P_{7v} + 3\Delta P_{8v} + 4\Delta P_{9v}) \\
 &\quad + (4\Delta P_{1h} + 3\Delta P_{2h} + 2\Delta P_{3h} + \Delta P_{4h}) - (\Delta P_{6h} + 2\Delta P_{7h} + 3\Delta P_{8h} + 4\Delta P_{9h})] \\
 &= \frac{(\Delta l)^2 \times l \times \gamma_w}{1000} [Z] \tag{4.14}
 \end{aligned}$$

where,

$$\begin{aligned}
 Z &= (4\Delta P_{1v} + 3\Delta P_{2v} + 2\Delta P_{3v} + \Delta P_{4v}) - (\Delta P_{6v} + 2\Delta P_{7v} + 3\Delta P_{8v} + 4\Delta P_{9v}) \\
 &\quad + (4\Delta P_{1h} + 3\Delta P_{2h} + 2\Delta P_{3h} + \Delta P_{4h}) - (\Delta P_{6h} + 2\Delta P_{7h} + 3\Delta P_{8h} + 4\Delta P_{9h})
 \end{aligned}$$

Now, from equations (4.13) and (4.14)

$$C_M = \frac{(\Delta l)^2 \times l \times \gamma_w \times Z}{1000 \times \frac{1}{2} \rho U_0^2 AD} \tag{4.15}$$

Since,  $D = 9\Delta l$  and  $A = 9 \times \Delta l \times l$ , so equation (4.15) reduces to

$$C_M = \frac{Z \gamma_w}{40500 \rho U_0^2} \tag{4.16}$$

Using equation (4.16), the values of moment coefficients are obtained for square cylinder.

The section of rectangular cylinder shown in the Figure 4.3 is divided horizontally (along x-axis) into nine strips of equal width  $\Delta l$ . Similarly it is divided vertically (along y-axis) into eleven strips of equal width  $\Delta l_1$  which is very close to  $\Delta l$  i.e.  $\Delta l_1 \approx \Delta l$ . The positions of pressure tapping points are at the middle of the strips. A certain length  $l$  is considered over which the pressure distribution is same at every section. The moment about clockwise direction is considered positive. The equation of moment is obtained as

$$\begin{aligned}
 M = & \left( \frac{\Delta P_{1v} \gamma_w}{1000} \times 5 \times \Delta l + \frac{\Delta P_{2v} \gamma_w}{1000} \times 4 \times \Delta l + \frac{\Delta P_{3v} \gamma_w}{1000} \times 3 \times \Delta l + \frac{\Delta P_{4v} \gamma_w}{1000} \times 2 \times \Delta l + \frac{\Delta P_{5v} \gamma_w}{1000} \times \Delta l \right) l \times \Delta l \\
 & - \left( \frac{\Delta P_{7v} \gamma_w}{1000} \times \Delta l + \frac{\Delta P_{8v} \gamma_w}{1000} \times 2 \times \Delta l + \frac{\Delta P_{9v} \gamma_w}{1000} \times 3 \times \Delta l + \frac{\Delta P_{10v} \gamma_w}{1000} \times 4 \times \Delta l + \frac{\Delta P_{11v} \gamma_w}{1000} \times 5 \times \Delta l \right) l \times \Delta l \\
 & + \left( \frac{\Delta P_{1h} \gamma_w}{1000} \times 4 \times \Delta l + \frac{\Delta P_{2h} \gamma_w}{1000} \times 3 \times \Delta l + \frac{\Delta P_{3h} \gamma_w}{1000} \times 2 \times \Delta l + \frac{\Delta P_{4h} \gamma_w}{1000} \times \Delta l \right) l \times \Delta l \\
 & - \left( \frac{\Delta P_{6h} \gamma_w}{1000} \times \Delta l + \frac{\Delta P_{7h} \gamma_w}{1000} \times 2 \times \Delta l + \frac{\Delta P_{8h} \gamma_w}{1000} \times 3 \times \Delta l + \frac{\Delta P_{9h} \gamma_w}{1000} \times 4 \times \Delta l \right) l \times \Delta l \\
 M = & \frac{(\Delta l)^2 \times l \times \gamma_w}{1000} [(5\Delta P_{1v} + 4\Delta P_{2v} + 3\Delta P_{3v} + 2\Delta P_{4v} + \Delta P_{5v}) - (\Delta P_{7v} + 2\Delta P_{8v} + 3\Delta P_{9v} + 4\Delta P_{10v} + 5\Delta P_{11v}) \\
 & + (4\Delta P_{1h} + 3\Delta P_{2h} + 2\Delta P_{3h} + \Delta P_{4h}) - (\Delta P_{6h} + 2\Delta P_{7h} + 3\Delta P_{8h} + 4\Delta P_{9h})] \\
 = & \frac{(\Delta l)^2 \times l \times \gamma_w}{1000} [Z] \tag{4.17}
 \end{aligned}$$

where,

$$\begin{aligned}
 Z = & (5\Delta P_{1v} + 4\Delta P_{2v} + 3\Delta P_{3v} + 2\Delta P_{4v} + \Delta P_{5v}) - (\Delta P_{7v} + 2\Delta P_{8v} + 3\Delta P_{9v} + 4\Delta P_{10v} + 5\Delta P_{11v}) \\
 & + (4\Delta P_{1h} + 3\Delta P_{2h} + 2\Delta P_{3h} + \Delta P_{4h}) - (\Delta P_{6h} + 2\Delta P_{7h} + 3\Delta P_{8h} + 4\Delta P_{9h})
 \end{aligned}$$

Now, from equations (4.13) and (4.17)

$$C_M = \frac{(\Delta l)^2 \times l \times \gamma_w \times Z}{1000 \times \frac{1}{2} \rho U_0^2 AD} \quad (4.18)$$

Since,  $D = 9\Delta l$  and  $A = 11 \times \Delta l \times l$ , so equation (4.18) reduces to

$$C_M = \frac{Z \gamma_w}{49500 \rho U_0^2} \quad (4.19)$$

Using equation (4.19), the values of moment coefficients are obtained for rectangular cylinder.

#### 4.4 Total Force Co-efficient

Total force co-efficient can be defined as,  $C_F = \sqrt{C_D^2 + C_L^2}$  (4.20)

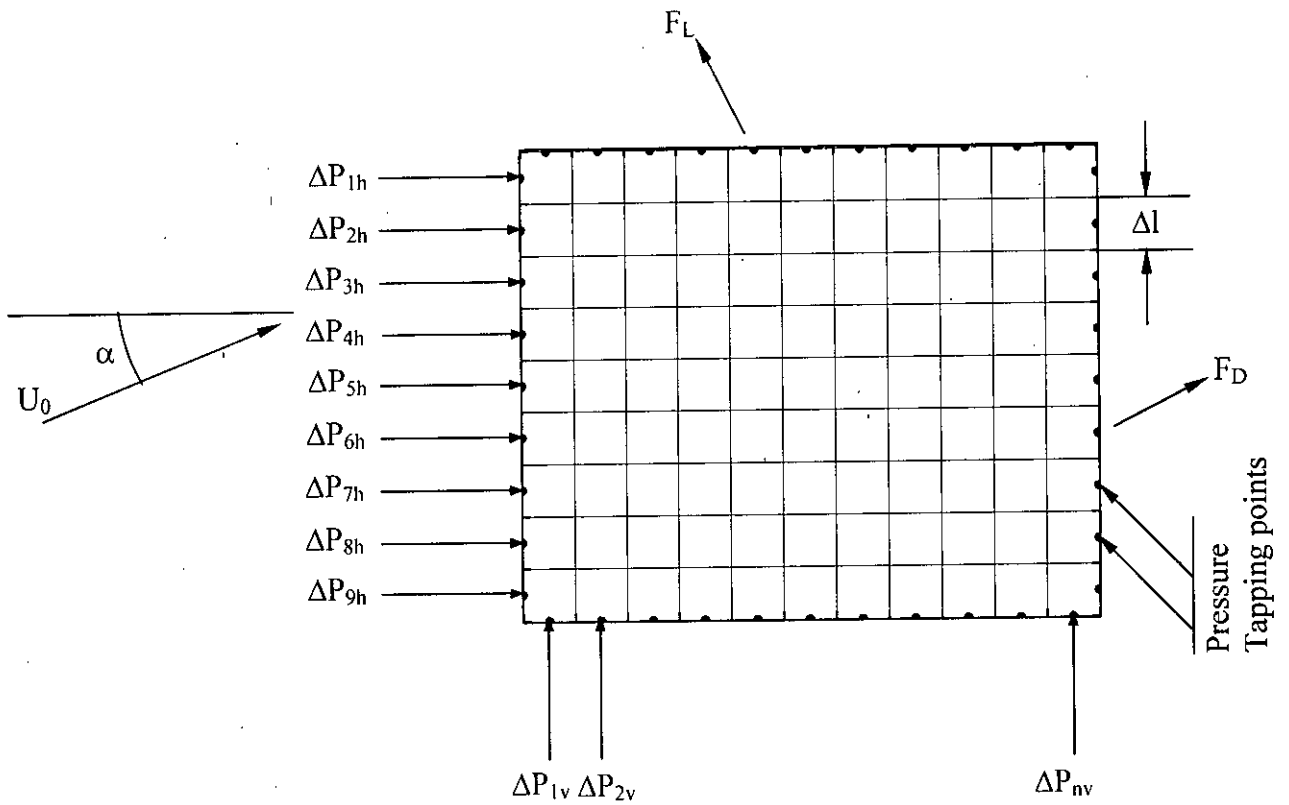


**Figure 4.1:** Section of a cylinder showing pressure tapping points and the forces acting on each strip.

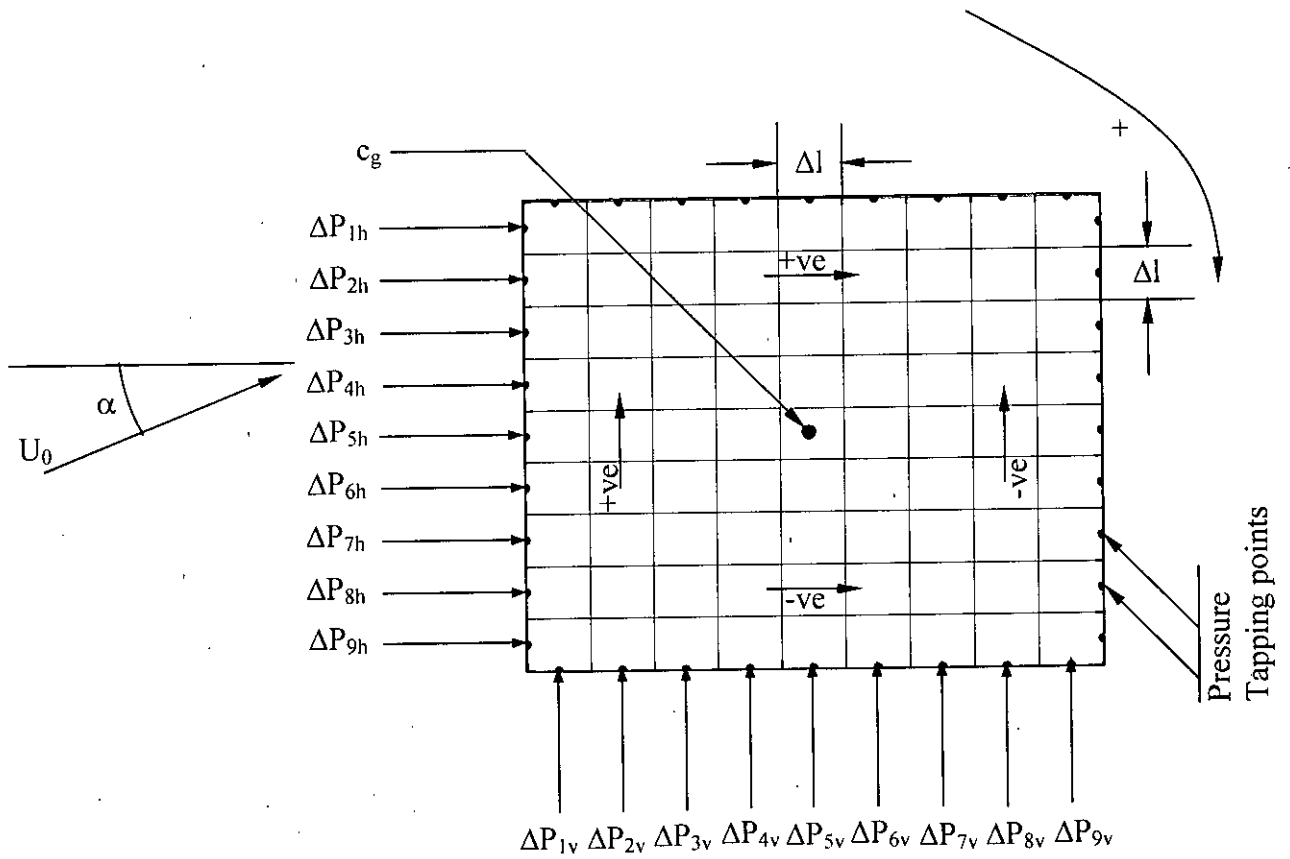


**Figure 4.2:** Section of a square cylinder showing pressure-tapping direction of positive moment and the forces acting along the strips.



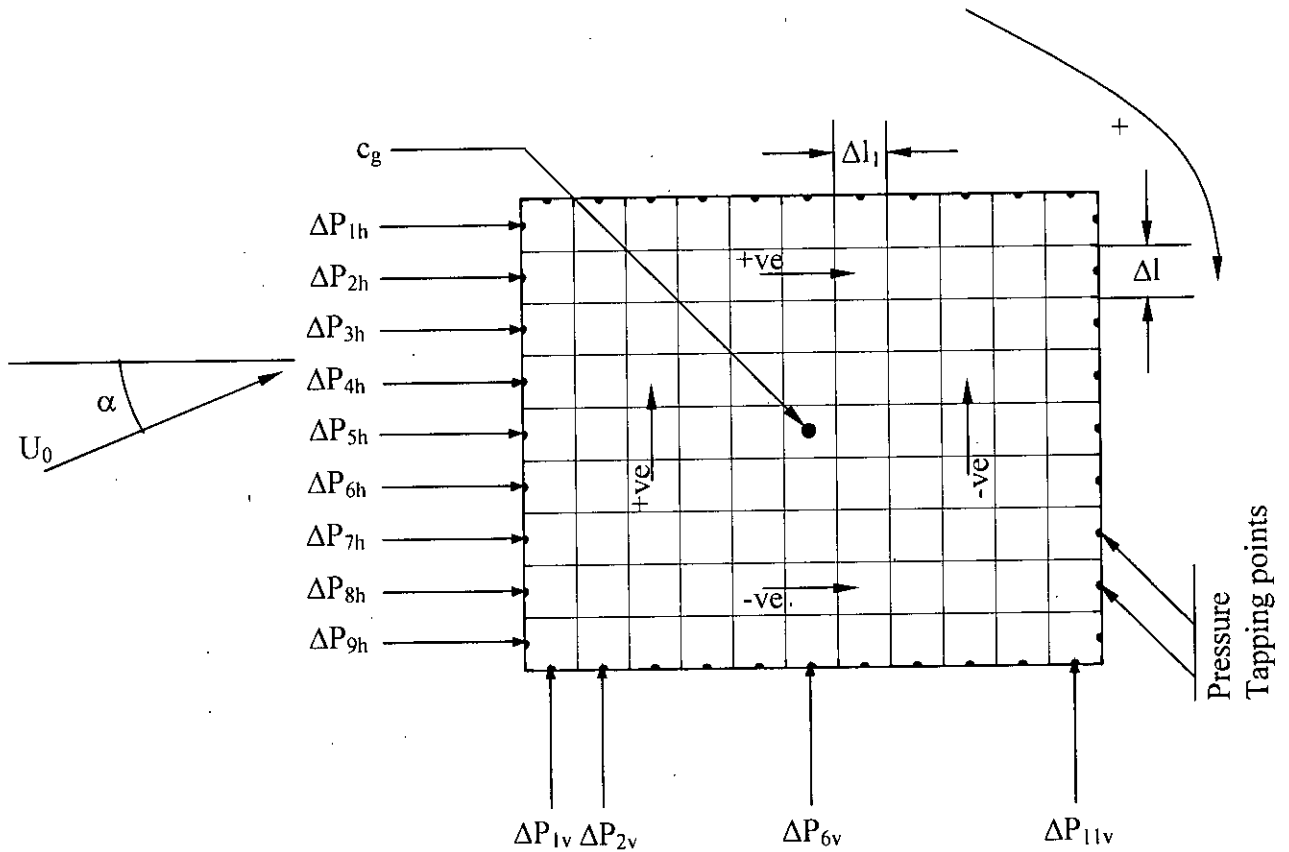


**Figure 4.3:** Section of a rectangular cylinder showing pressure-tapping direction of positive moment and the forces acting along the strips.

## **CHAPTER-5**

### **RESULTS AND DISCUSSION**

In this chapter the results of the experimental investigation in regard to distribution of static pressure coefficient on the square and rectangular cylinders have been discussed and analyzed. First of all the distribution of static pressure coefficient on single cylinder (for both square and rectangular) at varying angles of attack is considered. Then the distribution of static pressure coefficient on the cylinders in a group is taken. At zero angle of attack the results of the coefficient of the pressure distribution on a group of cylinders for different longitudinal and transverse spacing are discussed. Then the drag coefficients, lift coefficients, moment coefficients and total force coefficients have been calculated from measured static pressure, for both the single cylinder and the cylinders in groups. The results of the present research works have been compared with the existing research works.

#### **5.1 Single Cylinder**

In the following sub-section mean pressure coefficients distribution and variations of the aerodynamic forces on a single cylinder at varying angle of attack from  $0^{\circ}$  to  $45^{\circ}$  with a step of  $5^{\circ}$  are discussed. The effects of variable side ratios are also considered for this study.

It would be relevant to show the approximate flow pattern around a square and rectangular cylinders before discussing the results of the experimental investigation. The nature of the flow pattern around a square and rectangular prism at zero angle of attack are shown in Figures 5.1(a) and 5.2(a) respectively. These figures reveal that the separation points are fixed at the leading edges and the shear layers originating from the leading corners curve outwards and from the familiar vortex street in the wake is formed close behind the body. The nature of formation of vortex shedding may also be observed from the same figures. The pressure developed on the back surface depends on the distance of vortices. While the distance of vortices from the body is longer, the backpressure is higher and vice versa. For this reason pressure increases at the rear surface of the model in small range of angle of attack but decreases in the higher range of angle of attack. The nature of

the flow pattern around a square and rectangular cylinders at  $45^\circ$  angle of attack are shown in Figures 5.1(b) and 5.2(b) respectively.

### 5.1.1 Pressure Distribution

The effect of angle of attack on mean pressure coefficients around the cylinders of side ratios of  $H/D=1.0$  (square) and 1.25 (rectangle) are shown in Figures 5.3 and 5.4 respectively. From these figures it is clear that the  $C_p$ -distribution is a function of angle of attack  $\alpha$ . The test results are obtained for two dimensional uniform flow. The turbulence intensity and scale were not measured. The turbulence intensity in the test section is believed to be 0.4% as supplied by the manufacturer of the tunnel. The  $C_p$ -distributions on the front surface of the cylinder with side ratio of 1.0 (Figure 5.3) reveal that a stagnation point is established at the mid point for angle of attack of  $0^\circ$ . This stagnation point is shifted towards the bottom corner of the surface with increasing in angle of attack.

The  $C_p$ -distributions on the bottom surface of the cylinder at  $\alpha = 0^\circ$  is almost uniform throughout the surface. As the angle of attack  $\alpha$  is increased the pressure gradually falls near the front corner and rises near the rear corner on the bottom surface in comparison to that at angle of attack of  $0^\circ$ . This tendency is observed up to the angle of attack of  $15^\circ$ . The increase of pressure in the rear corner indicates the appearance of reattachment. The Figure 5.3 reveals that as the angle attack is increased further, the location of the highest pressure at each angle gradually shifts towards the front corner with increasing magnitude. At  $\alpha = 45^\circ$ , the  $C_p$ -distribution on the front and bottom surfaces are almost identical which is understandable.

On the top surface, variation of  $C_p$ -distributions with angle of attack is small and for each angle of attack  $C_p$ -distribution is almost uniform throughout the surface. At  $\alpha=0^\circ$  this distribution is same as that on the bottom surface which is obvious. As the angle of attack increases from  $0^\circ$  to  $15^\circ$  the value of  $C_p$  increases but decreases in negligibly small amount when  $\alpha$  goes from  $15^\circ$  to  $45^\circ$  as the Figure 5.3 reveals. Now observing the  $C_p$ -distributions on the back surface it is seen that the values of  $C_p$  are found to increase up to  $10^\circ$  and with onward increases of  $\alpha$ , these values decrease up to  $\alpha=45^\circ$ . One may observe that the pressure distributions on the back surface reveals a similar trend.

In the case of sharp edged body like a rectangular cylinder, the separation points are fixed at the leading edges and thus the shear layers originating at the front corner curve outward and there appear the formation of familiar vortex shedding in the wake region behind the body. The free shear layers are basically unstable and roll up to form discrete vortices. The growing vortices draw in fluid from the base region and it is suggested that it is this continual entrainment process that sustain the low back pressure. In fact the magnitude of the back pressure is determined almost solely by the manner in which the shear layers leave the body and roll up to form discrete vortices. Thus a low base pressure is associated with vortex formation close to the body while a high base pressure (less negative value) is caused by vortex formation further away. The rise in pressure with increase of angle of attack in the lower range at the back surface of the rectangular body as Figure 5.3 shows, happens due to vortex formation at larger distance from the back side and the fall in pressure with further increase of angle of attack occurs due to the vortex formation at smaller distance from the back surface.

The nature of the  $C_p$ -distribution curves, which are presented in the Figure 5.4, is similar to that of the Figure 5.3. The patterns of the curves shown in Figure 5.4 may be explained in the similar manner as in the case of the Figure 5.3.

To cross check the results of the experiment,  $C_p$ -distribution of the present study (for side ratio,  $H/D=1.0$ ) is compared with that of Mandal [36] at  $\alpha=0^\circ$  for uniform flow with turbulence intensity of 0.4%. It is observed that the results are in close agreement verifying the general characteristic of the results.

To cross check the results of the experiment,  $C_p$ -distribution of the present study (for side ratio,  $H/D=1.25$ ) is compared with that of Islam [37] at  $\alpha=0^\circ$  for uniform flow with turbulence intensity of 0.4%. It is observed that the results are in close agreement verifying the general characteristic of the results.

### 5.1.2 Aerodynamic force

The variation of drag co-efficient ( $C_D$ ) for side ratios  $H/D = 1.0$  and  $1.25$  with angle of attack from  $0^\circ$  to  $45^\circ$  is shown in the Figure 5.5. It can be seen from this figure that for all side ratios the general trend of drag variation occur in such a way that with the increase

of angle of attack the drag coefficient falls and becomes minimum in the region of angle of attack  $8^{\circ}$  to  $12^{\circ}$  and subsequently with further increase of angle of attack its value rises sharply up to the angle of attack of  $45^{\circ}$ . Furthermore, it can be seen from this figure that there occur remarkable variation of the drag coefficients for the different side ratios of the cylinders. It is already mentioned that as the angle of attack increases the vortex formation occurs at larger distance thereby creating higher back pressure, which is mainly the cause of lower drag with increased value of angle of attack. For further increase of angle of attack vortex formation appear closer to the back surface of the body making the back pressure lower which is mainly the reason of higher drag for increased value of angle of attack in the higher range. In the lower range of angle of attack, as the side ratio of the cylinder increases, reattachment of the shear layer occurs towards the rear corner which probably forces the vortices to form further downstream thereby creating higher back pressure and consequently lower drag as Figure 5.5 shows.

Comparison is also made in Figure 5.5 with the experimental results presented by Mandal [38] for a square section cylinder placed in a uniform flow with a turbulence intensity of 0.4%. It is seen that the drag coefficient follow the same pattern and are reasonably close with acceptable range. The variation of drag coefficient of rectangular cylinder of side ratio  $H/D = 1.25$  with angle of attack in this study is also compared with that presented by Islam [37] and it is seen that the present results agrees well with the existing results. But the values are higher than that of the Islam [37] because the turbulence intensity is higher than that of Islam [37].

The variation of lift coefficient ( $C_L$ ) with angle of attack for different side ratios ( $H/D$ ) is shown in the Figure 5.6. The general trend in the variation of lift is similar to that of drag with angle of attack. The variation of lift coefficient with angle of attack is compared with that of Mandal [38] and it is seen that they are almost same up to certain angle of attack but at higher angle of attack, small difference is observed. The variation of lift coefficient presented by Islam [37] for side ratio 1.25 shown in this figure also follows a similar trend. The high negative lift at small angle of attack is associated with the formation of large enclosed separation bubble on the bottom surface of the cylinder, which caused higher local suction than those on the top surface. As mentioned earlier the reattachment

point on the bottom surface shifts towards the front corner with increase in the angle of attack thereby reducing the size of the separation bubble. This results in rise of lift coefficient for further increase in angle of attack. However, no appreciable change in lift occurs with increase in angle of attack more than  $25^\circ$  for all the cylinders.

The variation of moment coefficient ( $C_M$ ) with angle of attack for different side ratios ( $H/D$ ) is presented in Figure 5.7. The figure reveals that at about angle of attack  $\alpha = 20^\circ$ , moment coefficient is minimum i.e. maximum moment occurs in the anticlockwise direction. At this angle maximum twisting effect is developed on the cylinder. The pressure distributions on the top surface remain almost uniform, but reattachment occurs at the rear part of the bottom surface, which is the reason of this high value of moment.

The variation of total force coefficients ( $C_F$ ) with angle of attack for different side ratios including that presented by Mandal [38] for a square section cylinder and Islam [37] for a rectangular cylinder of side ratio 1.25 is shown in Figure 5.8. It is observed from the figure that in small and high range of angle of attack  $\alpha$ , it is almost same as drag coefficient, because the influence of lift coefficient is negligibly small. But in the middle range of  $\alpha$ , the difference in values is prominent due to the fact that the contradictory effect of the lift coefficients is high. The trend of the curves in this figure may be explained from the Figures 5.5 and 5.6.

## 5.2 Group of cylinders:

In this section the distribution of mean pressure coefficients and variation of the aerodynamic forces on the cylinders in a group arranged in staggered form at  $0^\circ$  angle of attack are discussed. Two groups have been formed and each group contends three cylinders. Group-1 consists of one square cylinder at upstream side and two rectangular cylinders at downstream side. Whereas, group-2 consists of one rectangular cylinder at upstream side and two square cylinders at downstream side.

### 5.2.1 Pressure Distribution on Upstream Cylinder

The pressure distribution around the upstream square cylinder ( $F$ ) for different longitudinal spacing ( $L_1$ ) with constant transverse spacing i.e.  $L_2=1D$  is shown in Figure

5.9. It is found from the figure that for all  $L_1$ , pressure distributions on the top and bottom surfaces are symmetrical. It can also be concluded from this figure that at  $L_1=8D$ , the pressures on the top, bottom and back surfaces are close to those of the single cylinder. But for a given location, when the longitudinal spacing ( $L_1$ ) decreases, pressure coefficient ( $C_p$ ) increases i.e. negative value of  $C_p$  decrease upto the spacing  $L_1=1D$ . The pressure distribution on the front surface for all the longitudinal spacing  $L_1$ , remain almost same as that of the single cylinder. Due to the proximity of the downstream cylinders interference takes place and hence the flow becomes turbulent. This leads to the exchange of momentum between the fluid particles as a result of which rapid pressure recovery occurs on the top, bottom and back surfaces of the upstream cylinder. While the distance increases, this effect is minimized and at large distance ( $L_1=8D$ ), it becomes very small. The pressure distributions at this distance becomes near to those of the single cylinder.

Figure 5.10 shows the pressure distribution around the upstream square cylinder for varying longitudinal spacing ( $L_1$ ) with constant transverse spacing i.e.  $L_2=2D$ . It can be concluded that, almost the same nature of curves are found as those for transverse spacing,  $L_2=1D$  with exception that, the pressure at  $L_1=1D$  is lower than that at  $L_1=2D$ , instead of being higher. When  $L_2=2D$ , the downstream cylinders probably fall outside of the influence zone of wake created by the upstream cylinder for  $L_1=1D$  whereas, they fall within the influence zone at  $L_1=2D$  and hence, pressure at  $L_1=1D$  is lower than that at  $L_1=2D$ .

Figure 5.11 shows the pressure distribution around the upstream square cylinder for different longitudinal spacing ( $L_1$ ) keeping transverse spacing constant i.e.  $L_2=4D$ , it can be noticed that a little variation in pressure distribution for different longitudinal spacing ( $L_1$ ) is occurred but the nature of the curves are similar to those in Figure 5.10.

The pressure distribution around the upstream rectangular cylinder for different longitudinal spacing ( $L_1$ ) with constant transverse spacing i.e.  $L_2=1D$  is shown in Figure 5.12. It is seen in the figure that for all  $L_1$ , pressure distributions on the top and bottom surfaces are symmetrical. It can also be concluded from the figure that at  $L_1=8D$ , the pressure on the top, bottom and back surface are lower than that of the single cylinder. But at a given location, when the longitudinal spacing ( $L_1$ ) decreases, pressure coefficient

increases (i.e. negative value decrease) upto the spacing  $L_1=1D$ . The pressure distribution on the front surface for different spacing  $L_1$ , remains almost same as that of the single cylinder. It is due to the influence produced by the downstream cylinders for which the flow become significantly turbulent; the values of fluctuating transverse velocity components increase appreciably thereby high momentum and mass transfer, as the pressure recovery occurs on the surfaces (top, back and bottom) of the upstream cylinder. As the distance increases, this effect is minimized and at large distance ( $L_1=8D$ ), it becomes very small.

Figure 5.13 shows the pressure distribution around the upstream rectangular cylinder for different longitudinal spacing ( $L_1$ ) with constant transverse spacing i.e.  $L_2=2D$ . It can be noticed in the figure that almost the same nature of curves are found as those for transverse spacing  $L_2=1D$  with exception that, the pressure on the bottom surface at  $L_1=1D$  is slightly lower than that at  $L_1=2D$ , instead of being higher. With transverse spacing of  $L_2=2D$ , the downstream cylinders perhaps interfere very less with the wake created by the upstream cylinder when  $L_1=1D$  whereas, the interference is remarkably higher thereby making higher pressure recovery while further increase of  $L_1$  the interference gradually diminishes. It may also notice that the pressure distribution on the bottom surface is little more than those of top surface and at  $L_1=8D$  the pressure distribution is remarkably higher than that of single cylinder.

The pressure distribution around the upstream rectangular cylinder for different longitudinal spacing ( $L_1$ ) with constant transverse spacing i.e.  $L_2 = 4D$  is shown in Figure 5.14. The figure reveals that at  $L_1=8D$ , the pressure on the top, bottom and back surface are closer to that of the single cylinder. When the longitudinal spacing ( $L_1$ ) decreases, pressure coefficient increases (i.e. negative value decrease) upto the spacing  $L_1=2D$  but at  $L_1 = 1D$  the pressure coefficient is close to that of at  $L_1 = 8D$ . It is observed from the pressure distribution curves on the top and bottom surfaces that except at  $L_2=1D$ , there appear considerable interference in the flow.



### 5.2.2 Variation of Drag for Upstream Cylinder

The variation of drag coefficient ( $C_D$ ) on upstream square cylinder (F) with different longitudinal spacing ( $L_1$ ) corresponding to different values of transverse spacing is shown in Figure 5.15. The figure reveals that, for variation of spacing ( $L_1$ ) from 4D to 8D, the drag coefficients remain almost constant for transverse spacing  $L_2 = 2D$  and 4D but it highly increases for  $L_2 = 1D$ . Minimum drag coefficient is observed at  $L_1=1D$  for spacing  $L_2=2D$ , which is the most favorable position. For small values of  $L_1$  (below 4D), the drag coefficients are small for both transverse spacing  $L_2=1D$  and 2D, which is obvious, because the Figures 5.9 and 5.10 reveal that pressure distribution on the front face do not vary, whereas, pressure distribution on the back surface in the range of small spacing  $L_1$  is significantly high. But for spacing  $L_2=4D$ , though the pressure distribution on the front surface is similar to that of for spacing  $L_2=1D$  or 2D, the back pressure is not high enough, as shown in the Figure 5.11, so the drag coefficient does not remain small. However, for all values of  $L_1$ , the drag developed on the upstream cylinder is always less than that on the single cylinder at angle of attack,  $\alpha = 0^\circ$ .

Variation of drag coefficient ( $C_D$ ) on the upstream rectangular cylinder (F) with different longitudinal spacing ( $L_1$ ) corresponding to different values of transverse spacing ( $L_2$ ) is shown in Figure 5.16. It is observed that the nature of the curves for variation of longitudinal spacing ( $L_1$ ) with  $L_2=1D$  and 2D are similar. The figure reveals that, as longitudinal spacing increases, the drag coefficients increases for transverse spacing  $L_2 = 1D, 2D$  and 4D, but there is an exception for  $L_2 = 4D$  at  $L_1 = 8D$ . Minimum drag coefficient is observed for  $L_2 = 2D$  at  $L_1 = 1D$ , which is the most favorable position. For small values of  $L_1$ , the drag coefficient is small for both transverse spacing i.e.  $L_2=1D$  and 2D, which is obvious, because the Figures 5.12 and 5.13 reveal that pressure distribution on the front face does not vary, whereas pressure distribution on the back surface in the small values of  $L_1$  is significantly high. But for spacing  $L_2=4D$ , though the pressure distribution on the front surface is similar to that of spacing  $L_2=1D$  or 2D, back pressure is not high enough, as shown in the Figure 5.14, so the drag coefficient does not remain small. However, for all

values of  $L_1$ , the drag developed on the upstream cylinder is always less than that on the single cylinder at angle of attack,  $\alpha = 0^\circ$ .

### 5.2.3 Variation of Lift for Upstream Cylinders:

The variation of the lift coefficient ( $C_L$ ) on upstream square cylinder (F) with different longitudinal spacing ( $L_1$ ) for different values of transverse spacing ( $L_2$ ) is shown in Figure 5.17. The figure reveals that for transverse spacing  $L_2=1D$ , positive lift coefficient was developed for all values of  $L_1$  except at  $L_1 = 4D$  which can be explained from Figure 5.9. At  $L_1 = 4D$ , the values of lift coefficient for different  $L_2$  are almost same. The figure also reveals that for higher range of transverse spacing (for  $L_2 = 2D$  and  $4D$ ) the values of lift coefficient remains almost zero, which is similar to that of the single cylinder at angle of attack,  $\alpha = 0^\circ$  i.e. no lift is developed.

The variation of the lift coefficient ( $C_L$ ) on upstream rectangular cylinder (F) with different longitudinal spacing ( $L_1$ ) for different values of transverse spacing ( $L_2$ ) is shown in Figure 5.18. The figure reveals that for transverse spacing  $L_2=2D$ , the values of the lift coefficient increase with the increase of longitudinal spacing,  $L_1$ . At  $L_1 = 4D$  the values of lift coefficient for different transverse spacing become close. The figure also reveals that for transverse spacing  $L_2 = 1D$  and  $4D$  at higher range of longitudinal spacing the values of lift coefficient remain almost zero, which is similar to that of the single cylinder at angle of attack,  $\alpha = 0^\circ$  i.e. no lift is developed.

### 5.2.4 Variation of Moment Coefficient for Upstream Cylinder

The variation of moment coefficient ( $C_M$ ) on upstream square cylinder (F) with different longitudinal spacing ( $L_1$ ) for different values of transverse spacing ( $L_2$ ) is shown in Figure 5.19. The figure reveals that for all longitudinal spacing ( $L_1$ ) with different transverse spacing ( $L_2$ ), the moment coefficients are nearly zero which is similar to that of single cylinder at angle of attack,  $\alpha = 0^\circ$ .

The variation of moment coefficient ( $C_M$ ) on upstream rectangular cylinder (F) with different longitudinal spacing ( $L_1$ ) for different values of transverse spacing ( $L_2$ ) is shown

in Figure 5.20. The figure reveals that for all longitudinal spacing ( $L_1$ ) with different transverse spacing ( $L_2$ ), the moment coefficient remains almost zero.

### 5.2.5 Variation of Total Force Coefficient on Upstream Cylinder

The Figure 5.21 shows the variation of total force coefficient ( $C_F$ ) on upstream square cylinder (F) with longitudinal spacing ( $L_1$ ) for different values of transverse spacing ( $L_2$ ). The figure reveals that for different transverse spacing ( $L_2$ ), the total force coefficient for all longitudinal spacing ( $L_1$ ) is less than that of the single cylinder, at  $\alpha = 0^\circ$ . It also shows that more suitable condition (minimum total force) is attained for all  $L_1$  at  $L_2 = 2D$ .

The Figure 5.22 shows the variation of total force coefficient ( $C_F$ ) on upstream rectangular cylinder (F) with longitudinal spacing ( $L_1$ ) for different values of transverse spacing ( $L_2$ ). The figure reveals that for different transverse spacing ( $L_2$ ), the total force coefficient for all the longitudinal spacing  $L_1 = 1D$  to  $6D$  is less than that of the single cylinder, at  $\alpha = 0^\circ$ . It also shows that more suitable condition (minimum total force) is attained for  $L_1 = 1D$  to  $6D$  at  $L_2 = 2D$ .

### 5.2.6 Pressure Distribution on Downstream Cylinder

The pressure distribution around the downstream square cylinder (T or B) with different longitudinal spacing ( $L_1$ ) keeping transverse spacing constant ( $L_2 = 1D$ ) is shown in Figure 5.23. It is observed from the figure that, when the longitudinal spacing is low i.e.  $L_1 = 1D, 2D$  and  $4D$  the pressure distributions on the front surface are negative, but for high longitudinal spacing i.e.  $L_1 = 6D$  and  $8D$ , the pressure distributions become positive and hence, pressure distribution for  $L_1 = 8D$  is higher than that of the other longitudinal spacings. Even though at  $L_1 = 8D$ , the pressure distribution is lower than that of the single cylinder. There is a wake region in front of the front surface of the downstream cylinder produced by the upstream rectangular cylinder. When the  $L_1$  is low, relatively larger wakes take place. The flow on this face never becomes potential whereas it is potential for the single cylinder. The velocity on the front face of the single cylinder is higher than that of the front face of the downstream cylinder, because the mean velocity in the wake is less

than the free stream velocity. For this reason, the pressure distribution on the front face is quite different than those produced on the front face of the single cylinder, at  $\alpha = 0^\circ$ .

On the back surface of this cylinder the pressure distribution curves are almost uniform throughout the surface and do not vary a lot for different longitudinal spacing ( $L_1$ ). Again, these pressures are higher i.e. less negative, than those of single cylinder on the subsequent surface. This is may be due to high turbulence this nature of pressure distribution occurred.

On the top surface, it is noticed that while the upstream rectangular cylinder is close to downstream square cylinder i.e.  $L_1 = 1D$ , the pressure distribution is almost uniform throughout the surface and the values are much higher than those for the single cylinder, which is due to the turbulence nature of flow. At longitudinal spacing  $L_1 = 2D$  and  $4D$ , separation on the front corner and pressure recovery at the rear part of this face is observed. At longitudinal spacing  $L_1 = 6D$  and  $8D$ , the pressure distribution curve are nearly close together; separation tendency at the front corner and reattaching tendency at the rear part of this face appear. But on the bottom surface, the appearance of pressure curve is quite different. At small longitudinal spacing i.e.  $L_1 = 1D$ , pressure recovery is extremely high near the front corner, whereas towards the rear corner again separation tendency is observed. At  $L_1 = 2D$  and  $4D$  similar distribution occurs with a small variation. At  $L_1 = 6D$  and  $8D$ , the pressure distribution curves nearly overlap towards the rear corner; near the front corner separation and towards the rear corner, reattachment is seen to be developed.

The pressure distribution around the downstream square cylinder (T or B) with different longitudinal spacing ( $L_1$ ) and constant transverse spacing i.e.  $L_2=2D$  is shown in Figure 5.24. No negative pressure observed on the front surface as in the previous case. The figure reveals that the value of  $C_p$  is higher at small longitudinal spacings ( $L_1 = 1D, 2D$ ) and lower at large longitudinal spacings ( $L_1 = 4D, 6D$  and  $8D$ ). This is logical because at small  $L_1$ , the downstream cylinders are almost outside of the influence of wake region produced by the upstream rectangular cylinder. While the longitudinal spacing ( $L_1$ ) is large, the front surface is affected by wakes but because of higher spacing ( $L_1$ ), the influence is small. At small longitudinal spacings i.e.  $L_1 = 1D$  and  $2D$ , the pressure distribution curves

are closer to that of the single cylinder. Whereas, the pressure distribution curves on the back surface are seen to be very close together. The values of pressure are higher than that of single cylinder because of turbulent nature of flow. It is clear from the Figures 5.23 and 5.24 that the value of pressures are more than those for transverse spacing  $L_2 = 1D$ . Because the turbulence intensity is higher than that for transverse spacing  $L_2 = 1D$ .

On the top surface at longitudinal spacing  $L_1 = 1D$  and  $2D$ , the curves are very close to each other and are reasonably uniform in nature throughout the whole surface along the flow direction. The values of pressure are more than those for  $L_2 = 1D$ , which are due to high turbulence. At longitudinal spacing  $L_1 = 4D, 6D$  and  $8D$  the pressure distribution curves are similar with a very small change in values having high separation near the front corner and pressure recovery towards the rear corner. It is seen on the bottom surface the nature of the curves of  $C_p$ -distribution at  $L_1 = 1D$  and  $2D$ , are almost same but they differ in values, having high suction on the front side and pressure recovery on the rear side of this face. At Longitudinal spacing  $L_1 = 4D, 6D$  and  $8D$ , the nature of  $C_p$ -distribution curves are similar having separation near the front corner and reattachment near the rear corner of this face.

The pressure distribution around the downstream square cylinder (T or B) with longitudinal spacing ( $L_1$ ) for constant transverse spacing i.e.  $L_2=4D$  is shown in Figure 5.25. The figure reveals that the pressure distribution curves on the front surface are very close to that of single cylinder for all the longitudinal spacings ( $L_1$ ). Because the face is almost out of the influence of wakes produced by upstream rectangular cylinder. The pressure distribution curves on the back surface for various spacings ( $L_1$ ) are closer to that for single cylinder for the same reason. It is found that, on the top surface the influence is small; pressure distribution curves for all the longitudinal spacing  $L_1$ , remain not far off from that of the single cylinder. It is also found that on the bottom surface the shape of the curves of  $C_p$ -distribution at  $L_1 = 1D$  and  $2D$ , are same i.e. almost uniform throughout the surface but they differ much in values from that of single cylinder. At  $L_1 = 4D, 6D$  and  $8D$ , the nature of  $C_p$ -distribution curves are similar having separation near the front corner and reattachment appears near the rear corner of this face.

Figure 5.26 shows the pressure distribution around the downstream rectangular cylinder (T or B) with varying longitudinal spacing ( $L_1$ ) with constant transverse spacing i.e.  $L_2=1D$ . It is observed from the figure that when the longitudinal spacing is low i.e.  $L_1 = 1D$  and  $2D$  the pressure distributions on the front surface are negative, but for high longitudinal spacing i.e.  $L_1 = 4D, 6D$  and  $8D$ , the pressure distributions become positive and hence pressure distribution for  $L_1 = 8D$  is higher than that of the other longitudinal spacings. Even though at  $L_1 = 8D$ , the pressure distribution is lower than that of the single cylinder. There is a wake region in front of the front surface of the downstream cylinder produced by the upstream square cylinder. While the value of  $L_1$  is low, relatively larger wakes take place. The flow on this face never becomes potential whereas it is potential for the single cylinder. The velocity on the front face of the single cylinder is greater than that of the front face of the downstream cylinder, because the mean velocity in the wake is less than the free stream velocity. For this reason, the pressure distribution on the front face is quite different than those produced on the front face of the single cylinder, at  $\alpha = 0^\circ$ .

On the back surface of this cylinder the pressure distribution curves are almost uniform throughout the surface and do not vary a lot for different longitudinal spacing ( $L_1$ ). Again these pressures are higher i.e. less negative, than those of single cylinder on the subsequent surface. This is may be due to high turbulence this nature of pressure distribution occurred.

On the top surface, it is noticed that while the upstream square cylinder is close to downstream rectangular cylinder i.e.  $L_1 = 1D$ , the pressure distribution is almost uniform throughout the surface and the values are much higher than those for the single cylinder, which is due to the turbulence nature of flow. At longitudinal spacing  $L_1 = 2D$  separation on the front corner and pressure recovery at the rear part of this face is observed. At longitudinal spacings  $L_1 = 4D, 6D$  and  $8D$ , the pressure distribution curves are nearly close together; separation tendency at the front corner and reattaching tendency at the rear part of this face appear. But on the bottom surface, the appearance of pressure curve is quite different. At small range of longitudinal spacing i.e.  $L_1 = 1D$  and  $2D$ , pressure recovery is extremely high near the front corner, whereas towards the rear corner again separation tendency is observed. At  $L_1 = 4D, 6D$  and  $8D$ , the pressure distribution curves nearly

overlap towards the rear corner; near the front corner separation and towards the rear corner, reattachment is seen to be developed.

Figure 5.27 shows the pressure distribution around the downstream rectangular cylinder (T or B) for varying longitudinal spacing ( $L_1$ ) with constant transverse spacing i.e.  $L_2=2D$ . No negative pressure observed on the front surface as in the previous case. The figure reveals that the value of  $C_p$  is higher at small longitudinal spacings ( $L_1 = 1D, 2D$ ) and lower at large longitudinal spacings ( $L_1 = 4D, 6D$  and  $8D$ ). This is logical because at small  $L_1$ , the downstream cylinders are almost outside of the influence of wake region produced by the upstream square cylinder. While the longitudinal spacing ( $L_1$ ) is large, the front surface is affected by wakes but because of higher spacing ( $L_1$ ), the influence is small. At small longitudinal spacings i.e.  $L_1 = 1D$  and  $2D$ , the pressure distribution curves are closer to that of the single cylinder. The pressures distribution curves on the back surface are seen to be very close together. The values of pressure are higher than that of single cylinder because of turbulent nature of flow. It is clear from the Figures 5.26 and 5.27 that the values of pressure are more than those for transverse spacing  $L_2 = 1D$ . Because the turbulence intensity of transverse spacing ( $L_2 = 2D$ ) is higher than that for  $L_2 = 1D$ .

On the top surface at longitudinal spacing  $L_1 = 1D$  and  $2D$ , the curves are very close to each other and are reasonably uniform in nature throughout the whole surface along the flow direction. The values of pressure are more than those for  $L_2 = 1D$ , which are due to high turbulence. At longitudinal spacing  $L_1 = 4D, 6D$  and  $8D$  the pressure distribution curves are similar with a very small change in values having high separation near the front corner and pressure recovery towards the rear corner. It is found on the bottom surface the nature of the curves of  $C_p$ -distribution at  $L_1 = 1D$  and  $2D$ , are almost same but they differ in values, having high suction on the front side and pressure recovery on the rear side of this face. At Longitudinal spacing  $L_1 = 4D, 6D$  and  $8D$ , the nature of  $C_p$ -distribution curves are similar having separation near the front corner and reattachment near the rear corner of this face.

The pressure distribution around the downstream rectangular cylinder (T or B) for different longitudinal spacing ( $L_1$ ) with constant transverse spacing i.e.  $L_2=4D$  is shown in

Figure 5.28. This figure reveals that the pressure distribution curves on the front surface are very close to that of single cylinder for all the longitudinal spacings ( $L_1$ ). Because the face is lie almost outside of the influence of wakes produced by upstream square cylinder. The pressure distribution curves on the back surface for various spacings ( $L_1$ ) are closer to that of single cylinder for the same reason. It is found that, on the top surface the influence is small; pressure distribution curves for all the longitudinal spacing  $L_1$ , remain not far off from that of the single cylinder. It is also found that on the bottom surface the shape of the curves of  $C_p$ -distribution at  $L_1 = 1D$  and  $2D$ , are same i.e. almost uniform throughout the surface but the values are much lower than that of single cylinder. At  $L_1 = 4D, 6D$  and  $8D$ , the nature of  $C_p$ -distribution curves are similar having separation near the front corner and reattachment appears near the rear corner of this face.

### 5.2.7 Variation of Drag for Downstream Cylinder

The variation of drag coefficient ( $C_D$ ) on the downstream square cylinder (T or B) with different longitudinal spacing ( $L_1$ ) corresponding to different values of transverse spacing is shown in Figure 5.29. The figure reveals that for transverse spacing  $L_2 = 1D$ , the drag is high at large longitudinal spacing ( $L_1 = 4D, 6D$  and  $8D$ ) and low at small longitudinal spacing ( $L_1 = 1D$  and  $2D$ ). It can be explained from Figure 5.23 which shows that the pressure curves on the back surface are close together and uniform at all longitudinal spacings ( $L_1$ ); whereas, on the front surface, there are negative pressure distribution at small values of  $L_1$  and positive pressure distributions in the range of large  $L_1$ . For this reason low drag at small  $L_1$  and high drag on large  $L_1$  are developed. The figure also reveals that for transverse spacing  $L_2 = 2D$ , the reverse phenomenon occurs i.e. low drag at large  $L_1$  and high drag at small  $L_1$  (below  $4D$ ) are developed. The reason of such behavior of drag can be explained from Figure 5.24, which shows that the pressure distribution on the back surface is nearly same and uniform whereas, pressure distribution on the front surface in the range of small spacing  $L_1$  is significantly high and it gradually decreases with the increase of spacing  $L_1$ . The curve for transverse spacing  $L_2 = 4D$  can be explained from Figure 5.25 in similar manner.



The variation of drag coefficient ( $C_D$ ) on the downstream rectangular cylinder (T or B) with different longitudinal spacing ( $L_1$ ) corresponding to different values of transverse spacing is shown in Figure 5.30. The figure reveals that for transverse spacing  $L_2 = 1D$ , the drag is high at large longitudinal spacing ( $L_1 = 4D, 6D$  and  $8D$ ) and low at small longitudinal spacing ( $L_1 = 1D$  and  $2D$ ). It can be explained from Figure 5.26 that the pressure curves on the back surface are close together and uniform at all longitudinal spacings ( $L_1$ ); whereas, on the front surface, there are negative pressure distribution at small values of  $L_1$  and positive pressure distributions in the range of large  $L_1$ . For this reason low drag at small  $L_1$  and high drag at large  $L_1$  are developed. The figure also reveals that for transverse spacing  $L_2 = 2D$ , the reverse phenomenon occurs i.e. low drag at large  $L_1$  and high drag at small  $L_1$  (below  $4D$ ) are developed. The reason of such behavior of drag can be explained from Figure 5.27, which shows that the pressure distribution on the back surface are nearly same and uniform whereas, pressure distribution on the front surface in the range of small spacing  $L_1$  is significantly high and it gradually decreases with the increase of spacing  $L_1$ . The figure also reveals that for transverse spacing  $L_2 = 4D$ , low drag at large  $L_1$  and high drag at small  $L_1$  (below  $4D$ ) are developed. It can be explained from Figure 5.27, which shows that the pressure distribution on the back surface are very close together and uniform whereas, pressure distribution on the front surface in the range of small spacing  $L_1$  is significantly high and it gradually decreases with the increase of longitudinal spacing  $L_1$ .

### 5.2.7 Variation of Lift for Downstream Cylinder

The variation of lift coefficient ( $C_L$ ) on downstream square cylinder (T or B) with different longitudinal spacing ( $L_1$ ) corresponding to different values of transverse spacing is shown in Figure 5.31. The figure reveals that for transverse spacing  $L_2 = 1D$ , the value of lift coefficient ( $C_L$ ) is almost constant at all longitudinal spacings ( $L_1$ ). It is found that at transverse spacing  $L_2 = 2D$  and at large range of spacing i.e.  $L_1 = 4D, 6D$  and  $8D$ , low negative lift is developed and at small range of spacing i.e.  $L_1 = 1D$  and  $2D$ , a high negative lift is developed, because in the range of small  $L_1$ , as in the Figure 5.24 reveals, high suction effect is produced on bottom surface whereas the pressures on top surface are not sufficiently low. It is also found that for spacing  $L_2 = 4D$ , at small spacing ( $L_1 = 1D$  and  $2D$ )

negative lift is developed whereas, in the range of large spacing ( $L_1$ ), positive lift is developed with zero lift at certain spacing ( $L_1 = 4D$ ); the cause of which can be explained from the Figure 5.25, where it is observed that in the range of small spacing  $L_1$ , higher negative pressures are developed on the bottom surface than on the top whereas at large spacing ( $L_1$ ); reverse phenomenon occurs. It may be mentioned here that for single square cylinder at angle of attack i.e.  $\alpha = 0^\circ$ , no lift is developed whereas, it is found in the staggered form.

The variation of lift coefficient ( $C_L$ ) on downstream rectangular cylinder (T or B) with different longitudinal spacing ( $L_1$ ) corresponding to different values of transverse spacing is shown in Figure 5.32. The figure reveals that for transverse spacing  $L_2 = 1D$ , the value of lift coefficient ( $C_L$ ) is almost constant at all longitudinal spacings ( $L_1$ ). It is found that, at transverse spacing  $L_2 = 2D$  and at large longitudinal spacing ( $L_1$ ) a high positive lift is developed and at small range of  $L_1 = 1D$ , a high negative lift is developed. Because in the range of small  $L_1$ , as in the Figure 5.27 reveals, high suction effect is produced on bottom surface whereas, the pressures on top surface are not sufficiently low. It is also found that for spacing  $L_2 = 4D$ , at all the longitudinal spacing ( $L_1$ ) negative lift is developed. The reason of such behavior can be explained from the Figure 5.28, where it is observed that at all the longitudinal spacings  $L_1$ , higher negative pressures are developed on the bottom surface than on the top. It may be mentioned here that for single square cylinder at angle of attack i.e.  $\alpha = 0^\circ$ , no lift is developed whereas, it is found in the staggered form.

### 5.2.8 Variation of Moment Coefficient for Downstream Cylinder

The variation of moment coefficient ( $C_M$ ) on downstream square cylinder (T or B) with different longitudinal spacing ( $L_1$ ) corresponding to different transverse spacing ( $L_2$ ) is represented in Figure 5.33. The figure reveals that at large longitudinal spacings  $L_1$  ( $4D$  to  $8D$ ) for transverse spacings  $L_2 = 1D$  and  $2D$ , the moment coefficients are nearly zero, but at  $L_1 = 1D$  the moments are negative and at  $L_1 = 2D$ , positive moment for spacing  $L_2 = 1D$  and negative moment for spacing  $L_2 = 2D$ , are produced having higher magnitude for the former, the cause which may be explained from the Figures 5.23 and 5.24. Figure 5.23 presents that pressure distribution on the back surface at spacing  $L_1 = 2D$  is uniform but the

pressure on the top surface, shows lower pressures near the front corner than near the rear corner; the pressure on the bottom surface, shows higher pressures near the front corner than near the rear corner and on the front face the pressure near the top corner are than those near the bottom corner, as a result high positive movement is developed. In the same manner it may be explained for transverse spacing  $L_2 = 2D$  from figure 5.24. For spacing  $L_2 = 4D$ , moment coefficients are very low at small spacings ( $L_1$ ) and high in magnitude at large spacings ( $L_1$ ), the causes of which are explained from Figure 5.25.

The variation of moment coefficient ( $C_M$ ) on downstream rectangular cylinder (T or B) with different longitudinal spacing ( $L_1$ ) corresponding to different transverse spacing ( $L_2$ ) is shown in Figure 5.34. The figure reveals that at all the longitudinal spacings ( $L_1$ ) and for transverse spacing  $L_2 = 1D$ , positive moment is developed. It can be explained from Figure 5.26 which shows that pressure distributions on the top and back surfaces at spacings  $L_1 = 1D$  are uniform but the pressure on the bottom surface, shows higher pressures near the front corner than near the rear corner and on the front face the higher pressures near the top corner than near the bottom corner, as a result high positive movement is developed. It is found that for  $L_2 = 2D$  and at  $L_1 = 1D$  to  $4D$  negative moment is developed whereas, at  $L_1 = 6D$  and  $8D$  positive moment is developed, which can be explained from figure 5.27 in a similar manner. It is also found that for spacing  $L_2 = 4D$ , moment coefficients are very low at small spacings ( $L_1$ ) and high in magnitude at large spacings ( $L_1$ ), the causes of which are explained from Figure 5.28.

### 5.2.9 Variation of Total Force Coefficient on Downstream Cylinder

The variation of total force coefficient ( $C_F$ ) on downstream square cylinder (T or B) with different longitudinal spacing ( $L_1$ ) corresponding to different values of transverse spacing ( $L_2$ ) is shown in Figure 5.35. It may concluded from the figure that for the transverse spacings  $L_2 = 1D$  and  $2D$ , the total force coefficient for all the longitudinal spacing ( $L_1$ ) is less than that of the single cylinder, at  $\alpha = 0^\circ$ . For  $L_2 = 4D$  has the only one suitable condition (minimum total force) which is at large spacing  $L_1 = 8D$ . It shows that more suitable condition (minimum total force) is attained for spacing  $L_2 = 2D$  than the others.

The variation of total force coefficient ( $C_F$ ) on downstream rectangular cylinder (T or B) with different longitudinal spacing ( $L_1$ ) corresponding to different values of transverse spacing ( $L_2$ ) is shown in Figure 5.36. It may be concluded from the figure that for the transverse spacings  $L_2 = 1D$  and  $2D$ , the total force coefficient for all the longitudinal spacing ( $L_1$ ) is less than that of the single cylinder, at  $\alpha = 0^\circ$ . For  $L_2 = 4D$  has no suitable condition i.e. the total force coefficient is higher than that of the single cylinder for all the longitudinal spacing. It shows that more suitable condition (minimum total force) is attained for spacing  $L_2 = 1D$  than the others.

### 5.3 Observation of Pressure Fluctuations

The Pressure data were recorded at steady state condition. During recording of the Pressure data, fluctuation of liquid in the manometer limbs was always observed due to separated flow and interference of the flows (in staggered form). This fluctuation was very low for the test on a single cylinder at an angle of attack,  $\alpha = 0^\circ$ . Whereas, in the higher range of angle of attack fluctuation of pressure slightly increased, specially on the bottom surface; but the difference between the maximum and minimum liquid column observed in the manometer limb never exceeded  $\pm 5\text{mm}$ . When three cylinders were considered, fluctuations increased appreciably on the downstream cylinder and the maximum fluctuation observed was of the order of  $\pm 3.4\text{mm}$ . However, for this test, always mean pressure was recorded with careful observation.

### 5.4 Effect of Reynolds Number

The effect of Reynolds number is very small for all the structure except the rounded cross-section. At very low values of Reynolds number it has been shown by test carried over a wide range of Reynolds number that the flow pattern around sharp-edged body is significantly independent to the Reynolds number. This is due to the positions of the flow separations are fixed by the sharp edges bluff bodies. Davis [11] showed that for Reynolds number less than 1000 the flow around rectangular cylinders was strongly dependent on Reynolds number. In case of very low Reynolds number flow reattachment takes a place immediately after separation from the front corner and finally it separates at the trail edges.

While increase of Reynolds number, flow separation takes place at the leading edges and hence, flow pattern becomes independent of Reynolds number. However, in case of reattachment appearing for the change of angle of attack and the side ratio of rectangular cylinder, the effect of Reynolds number may not be ignored.

### 5.5 Blockage Corrections

Non-dimensional coefficients were subject to error due to the blockage effects mainly resulting from 'solid blocking' and 'wake blocking' while determined by wind tunnel tests. The flow area of the wind tunnel test section reduces due to the presence of a body and thereby increases the velocity of air as it flows around the body. This increase of velocity due to the presence of the body is called solid blocking. The wake behind a body has a mean velocity lower than the free stream. According to the law of continuity, the velocity outside the wake must be higher than free stream so that a constant volume of fluid may pass through the tunnel test section. According to Bernoulli's principle the higher velocity in the main stream has lower static pressure. Therefore, since the static pressure within the wake is governed by that of the steady airstream immediately adjacent to the boundary of the wake, the static pressure at the back surface of the body tends to be less than it would be if the airstream were as in the full-scale case [39]. Due to this wake blocking and solid blocking, blockage corrections are required to obtain accurate values of non-dimensional coefficients. The total solid and wake blockage corrections are summed to get the total blockage corrections. According to Pope and Harper [40] the total blockage corrections to  $C_p$  would be approximately of the order of half times the blockage percentage.

In the present study, no blockage corrections were made because the test was conducted at the outlet of the wind tunnel and no cover plates were used in the test section.

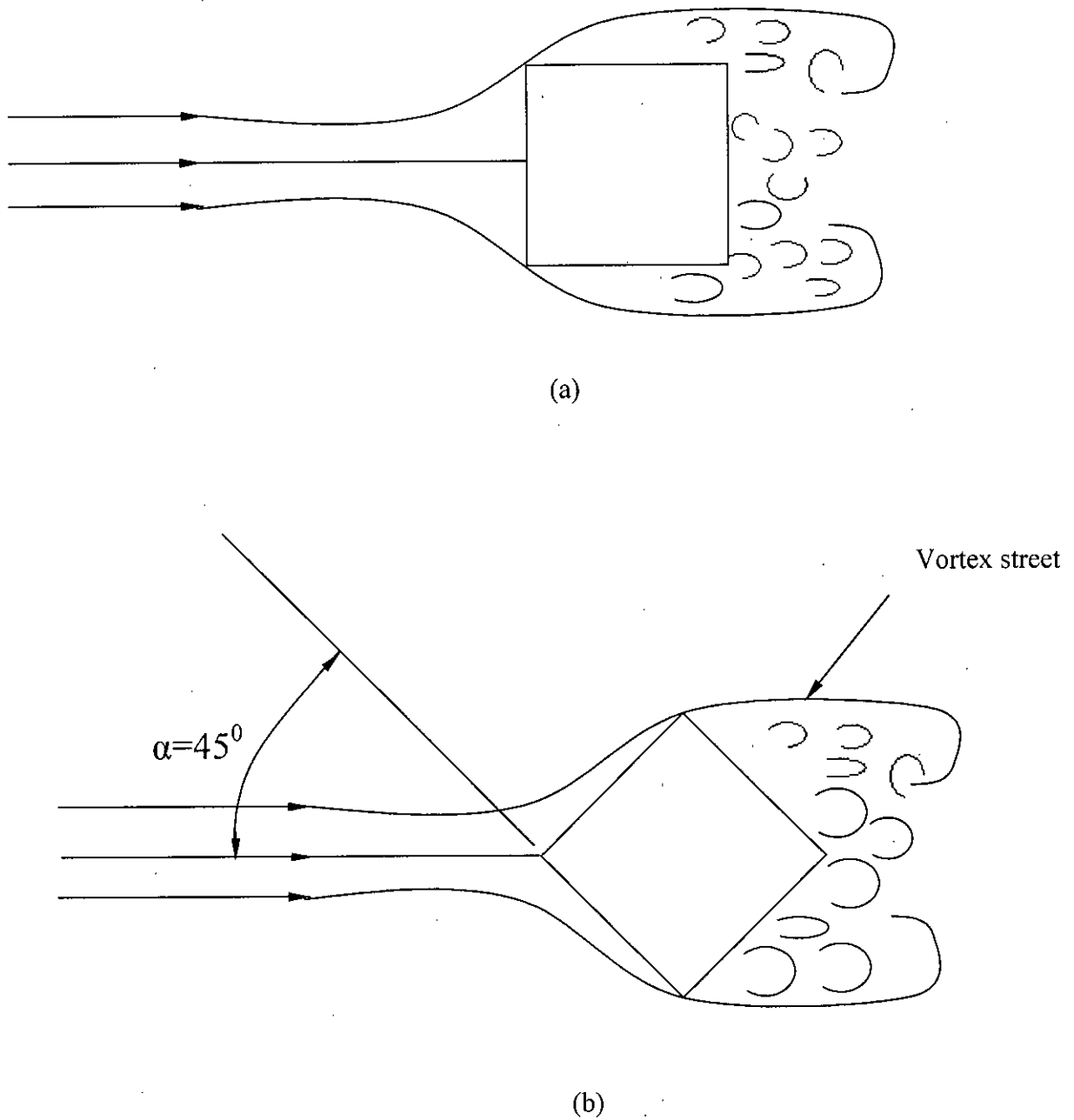
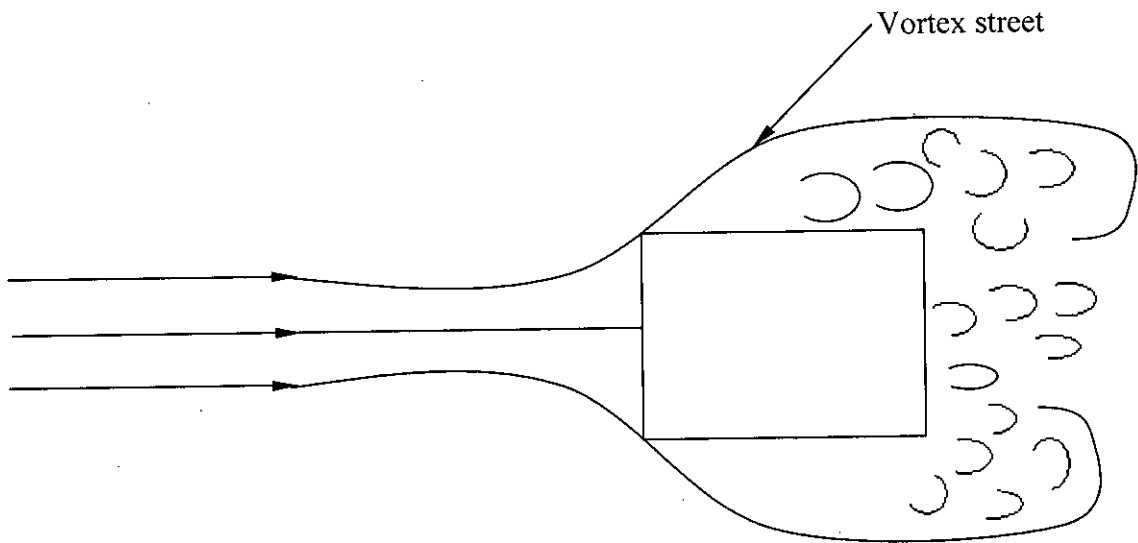
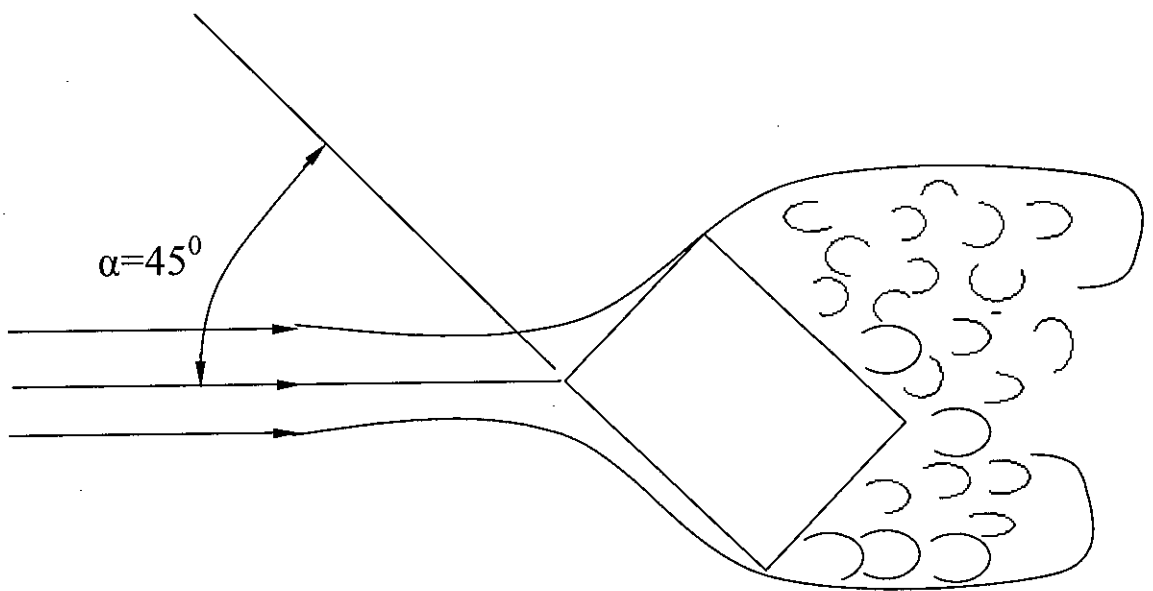


**Figure 5.1:** Square cylinder in the flow field showing the vortex street pattern.



(a)



(b)

**Figure 5.2:** Rectangular cylinder in flow field showing the vortex street pattern.

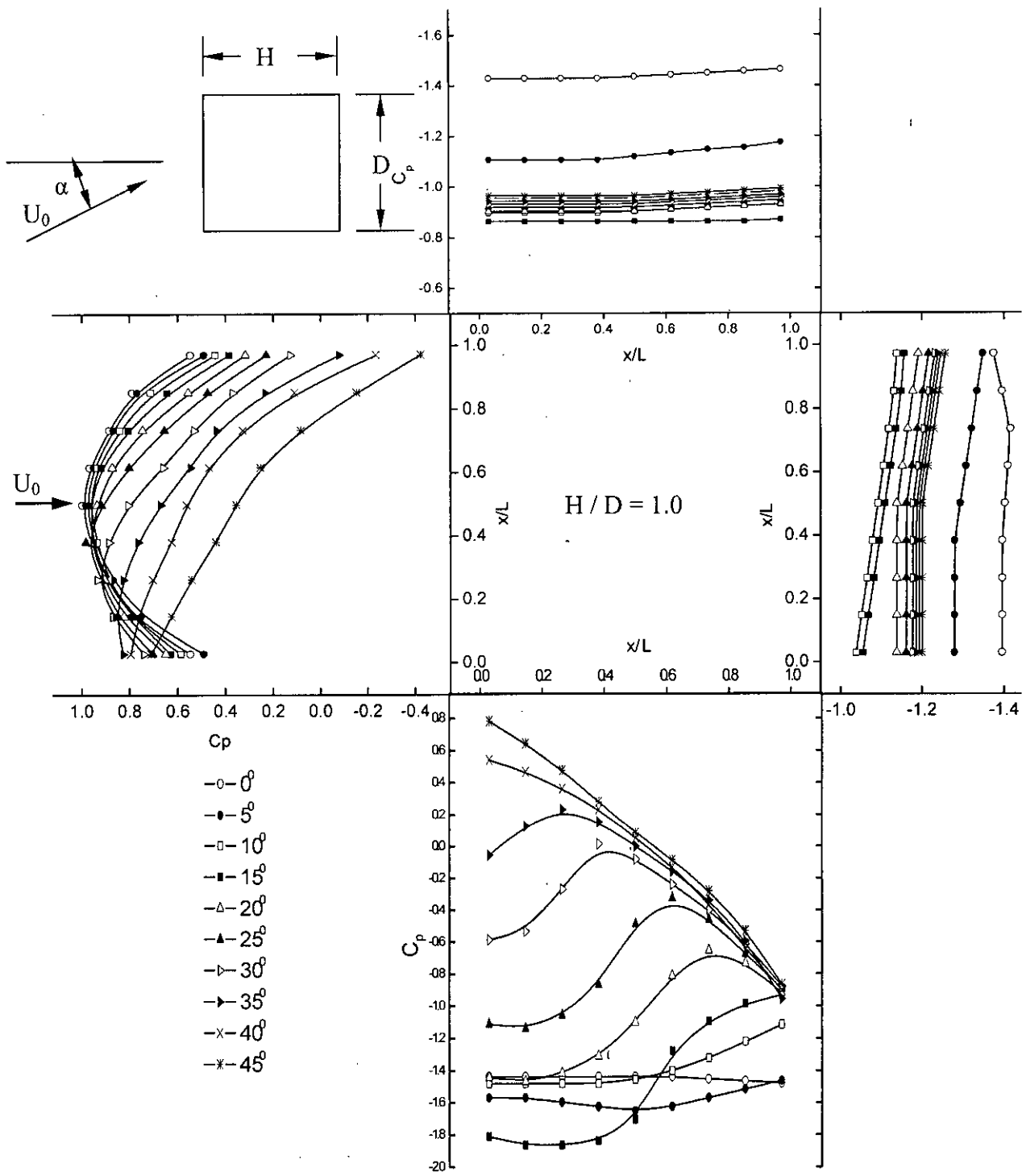


Figure 5.3: Effect of angle of attack ( $\alpha$ ) on  $C_p$ -distribution at side ratio ( $H/D$ ) of 1.0 (square)



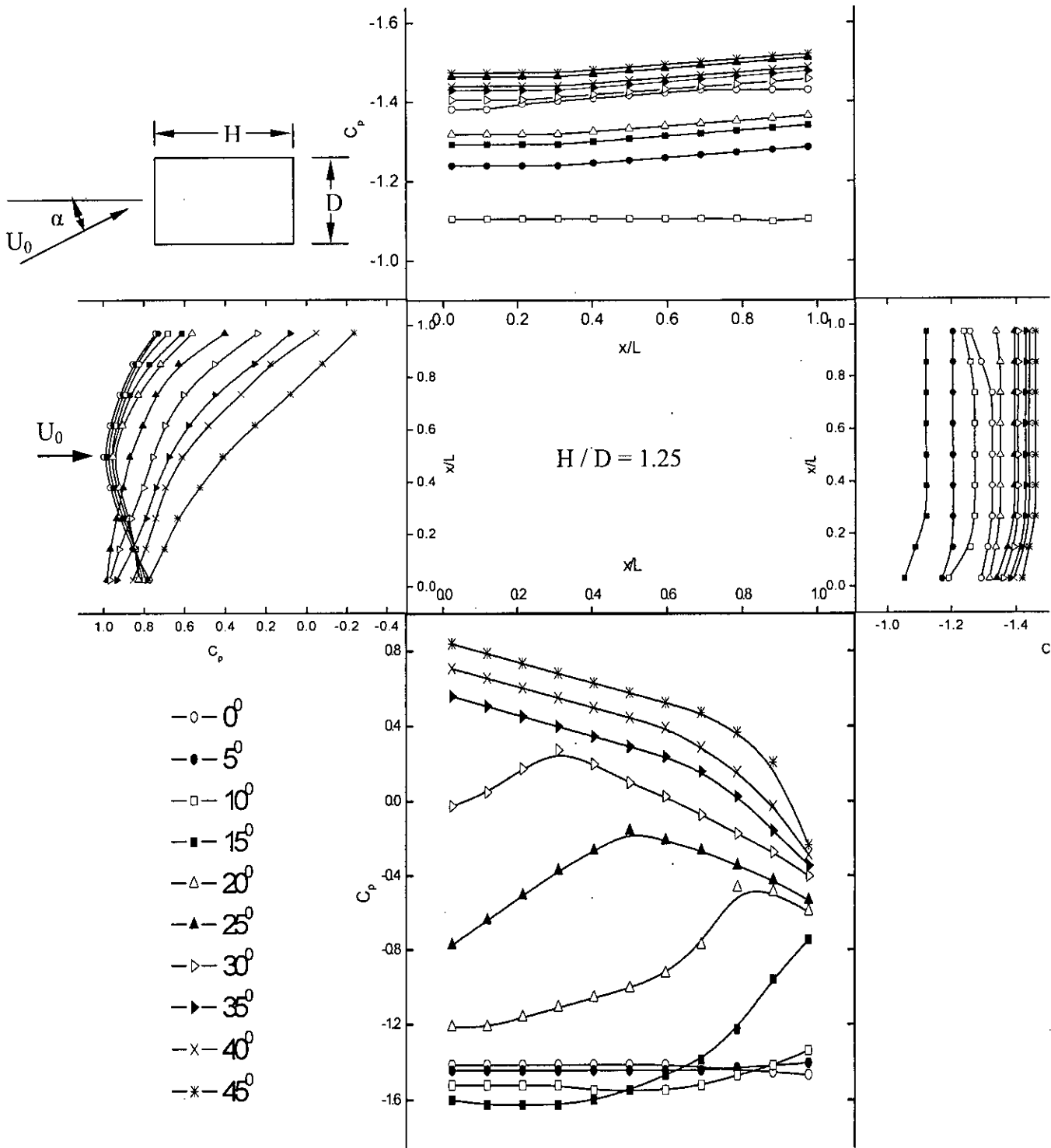
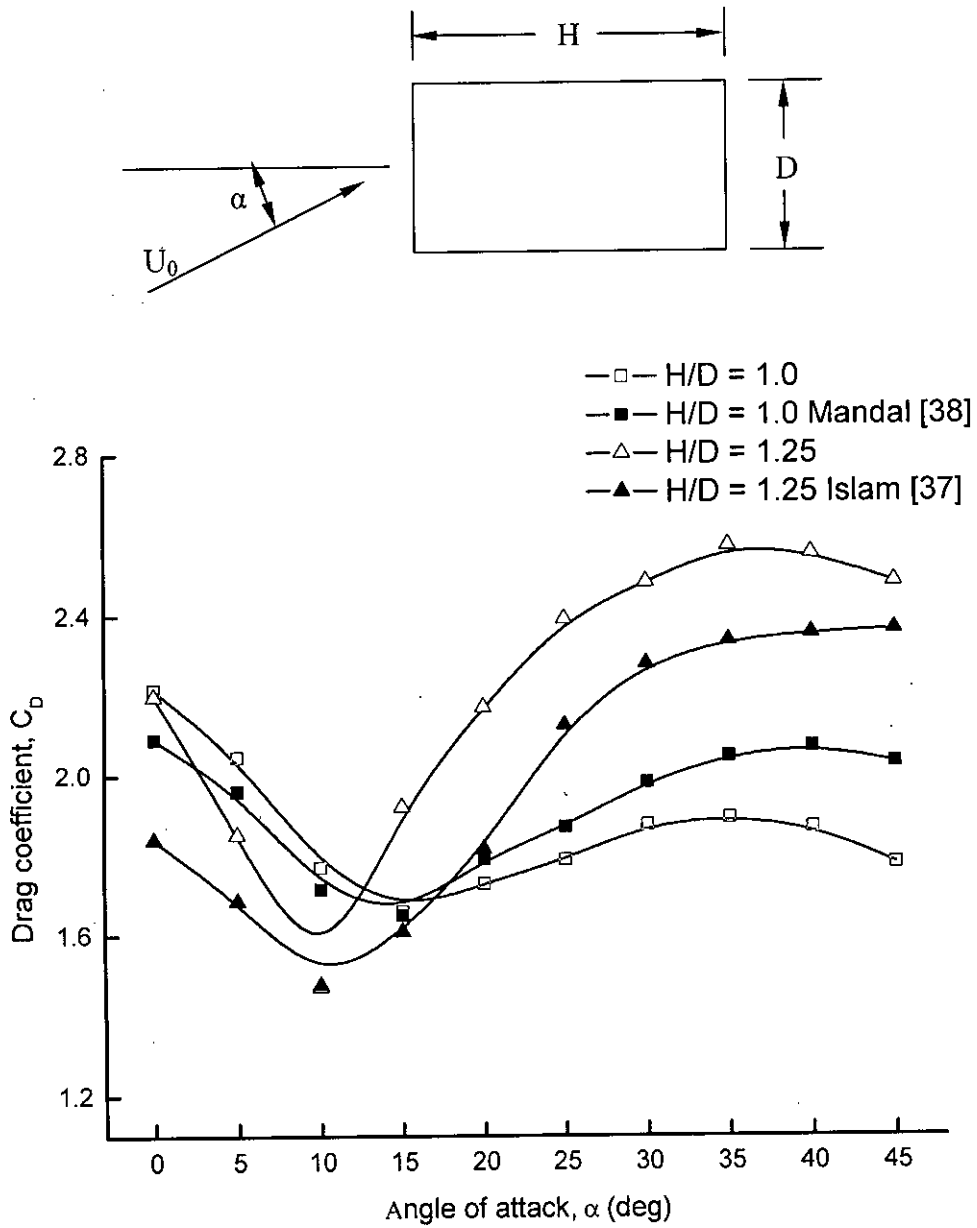
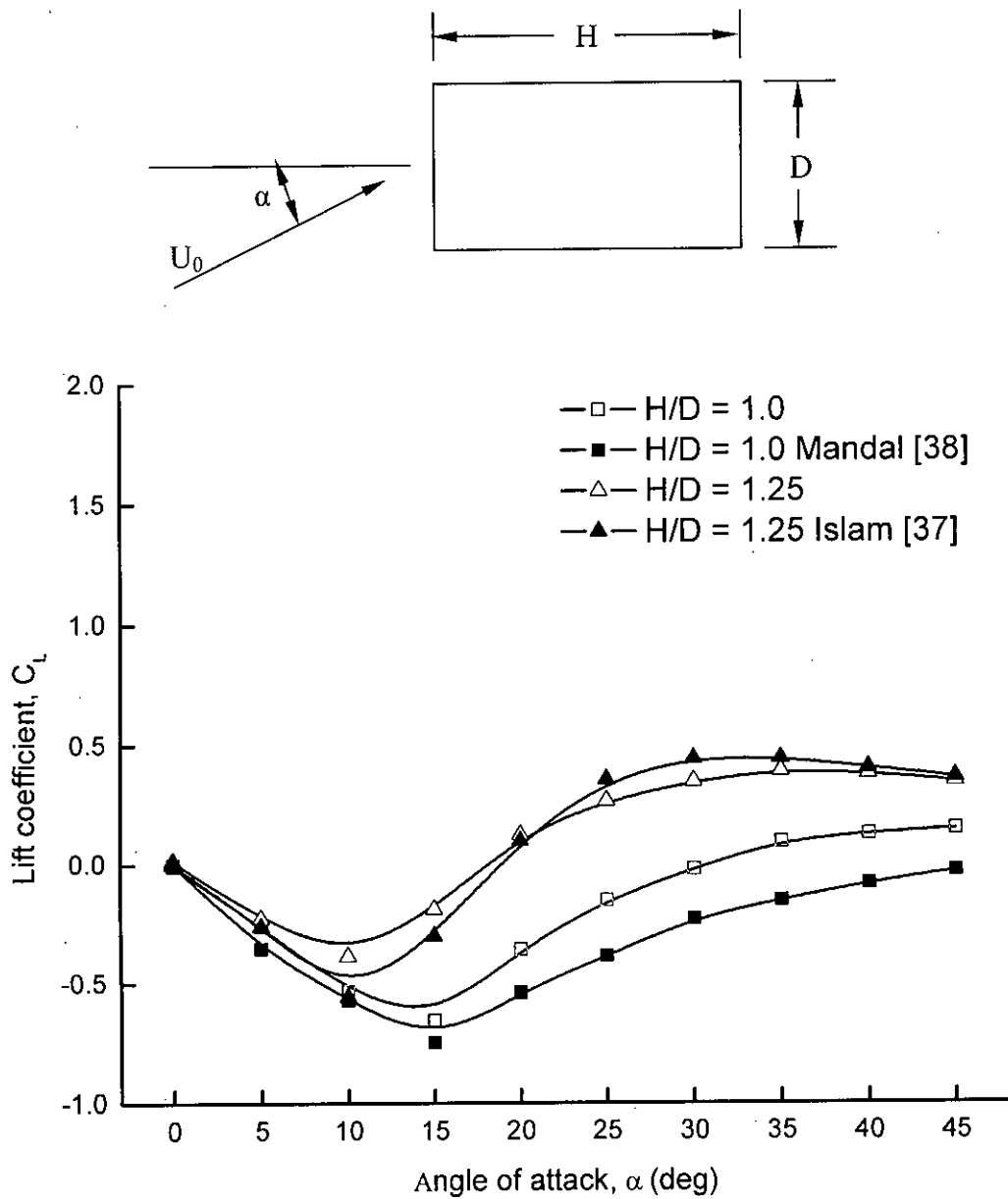


Figure 5.4: Effect of angle of attack ( $\alpha$ ) on  $C_p$ -distribution at side ratio ( $H/D$ ) of 1.25 (rectangle).



**Figure 5.5:** Variation of drag coefficient ( $C_D$ ) with angle of attack ( $\alpha$ ) for different side ratios ( $H/D$ ) of rectangular cylinder.



**Figure 5.6:** Variation of lift coefficient ( $C_L$ ) with angle of attack ( $\alpha$ ) for different side ratios ( $H/D$ ) of rectangular cylinder.

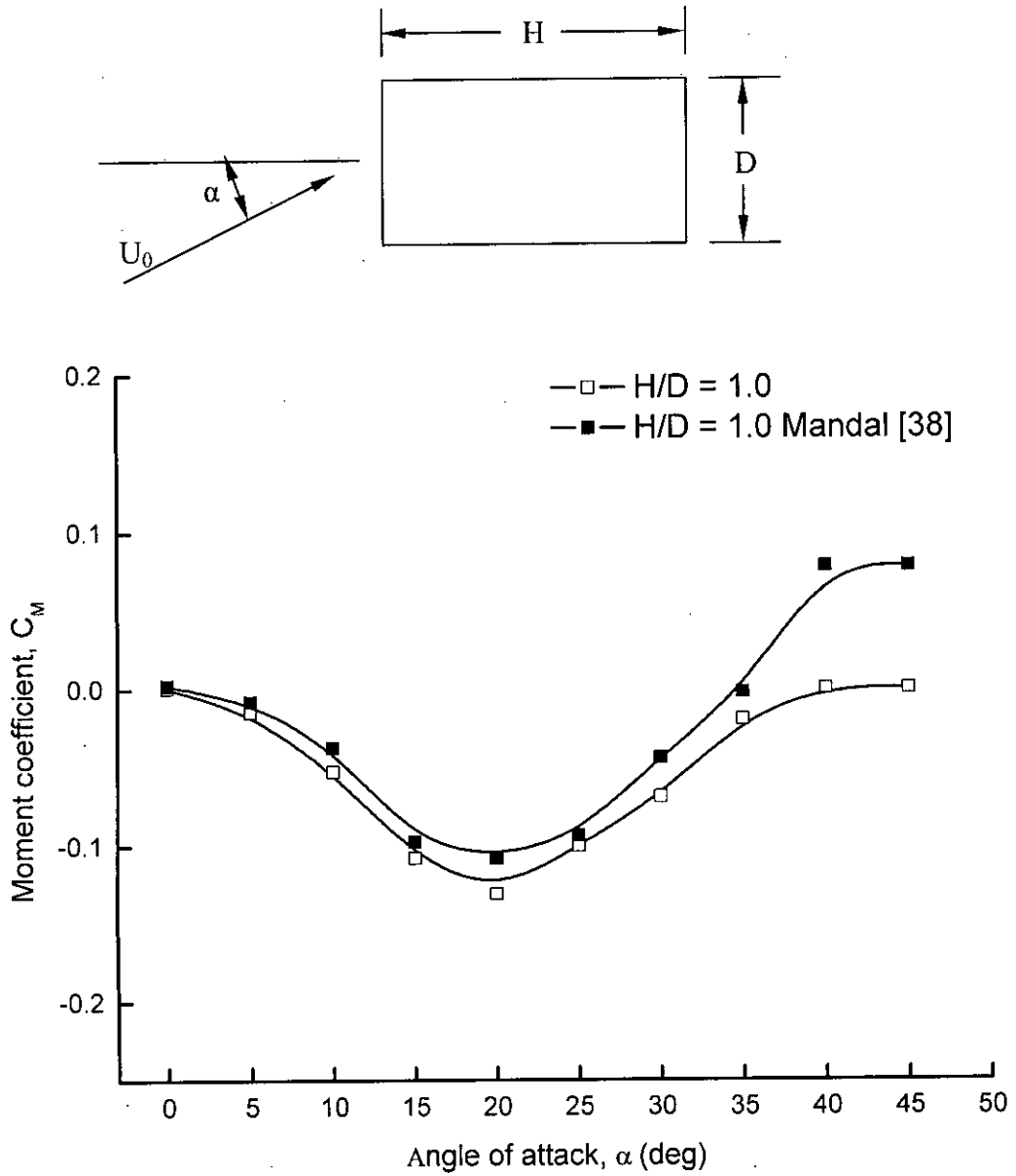


**Figure 5.7:** Variation of moment coefficient ( $C_M$ ) with angle of attack ( $\alpha$ ) of rectangular cylinder.

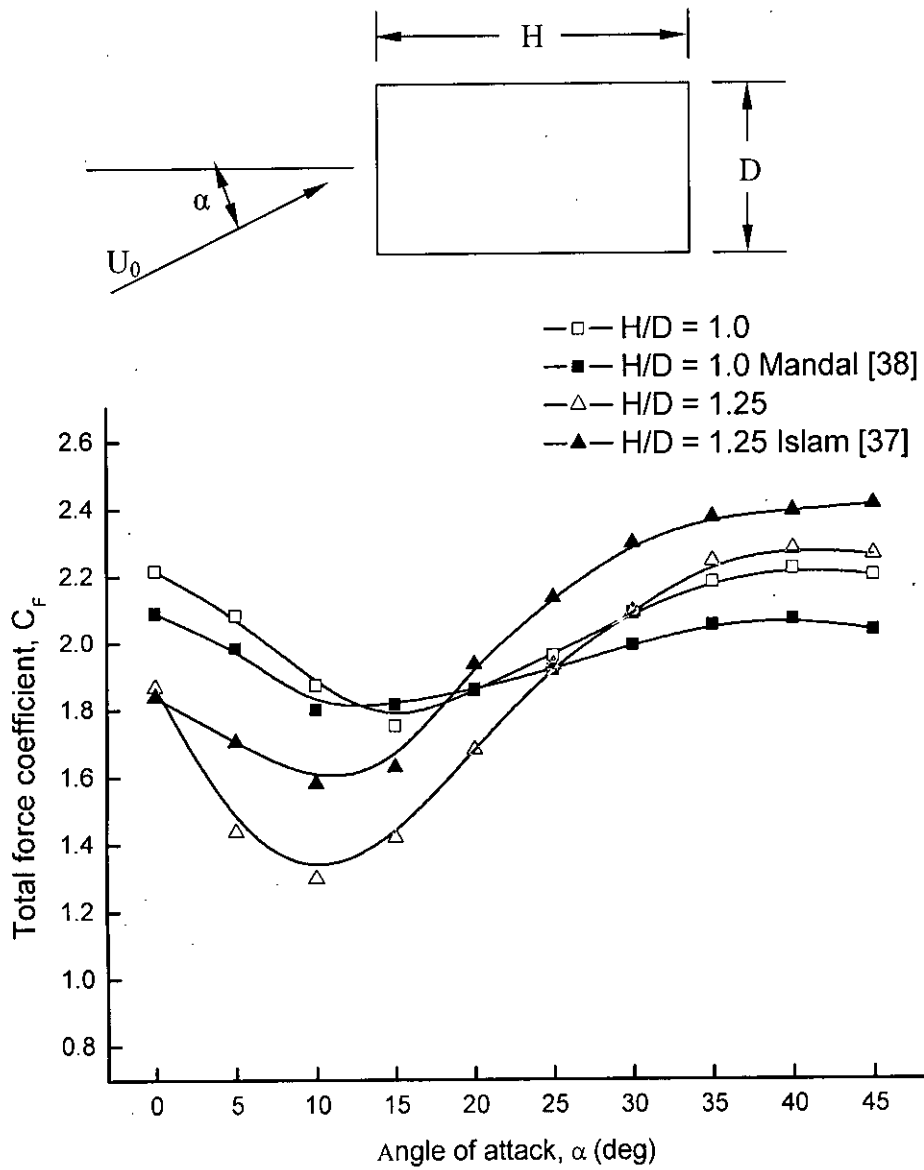


**Figure 5.8:** Variation of total force coefficient ( $C_F$ ) with angle of attack ( $\alpha$ ) for different side ratios ( $H/D$ ) of rectangular cylinder.

104387

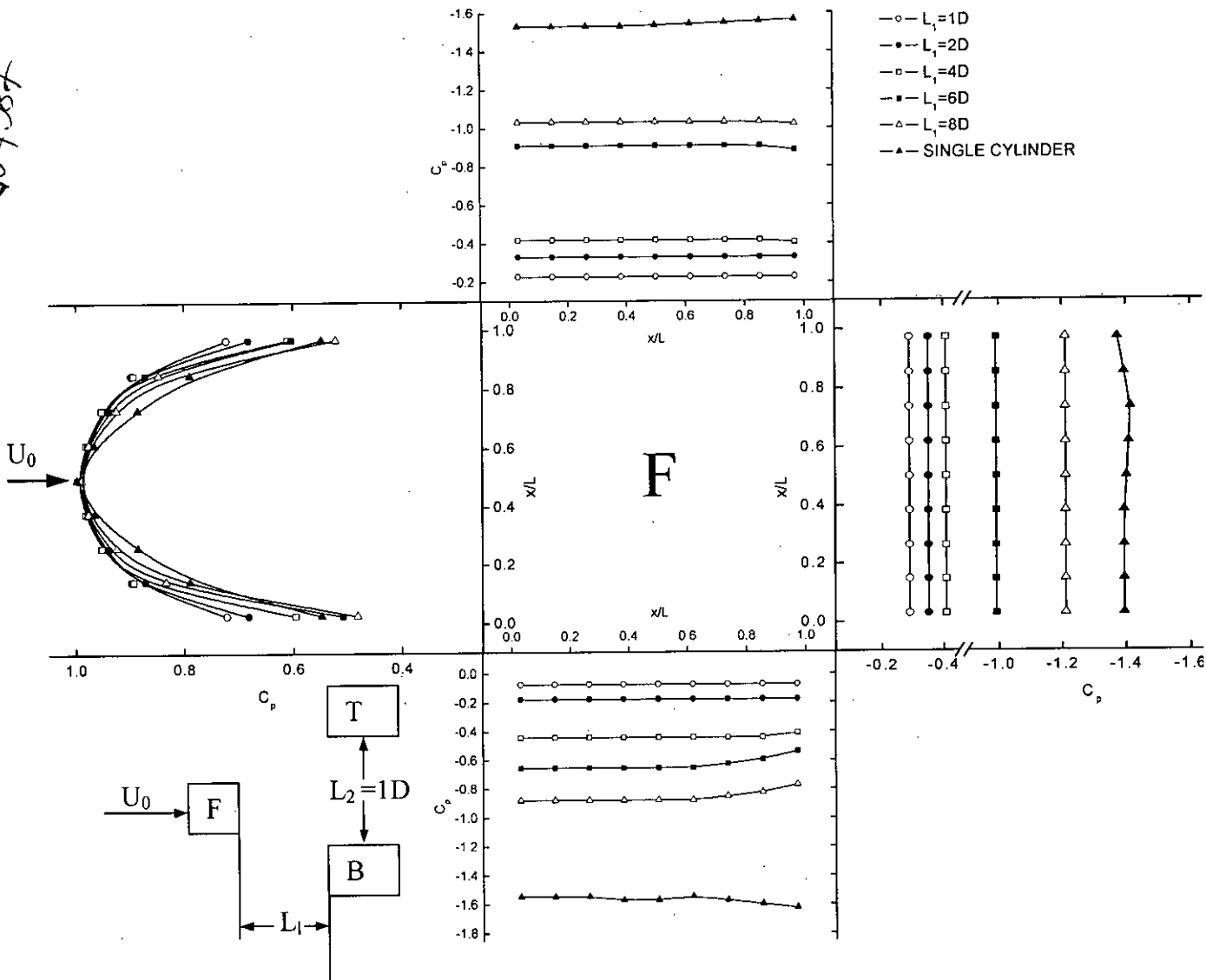


Figure 5.9: Effect of longitudinal spacing ( $L_1$ ) on  $C_p$  for upstream square cylinder (F) keeping transverse spacing ( $L_2$ ) constant at  $1D$ .

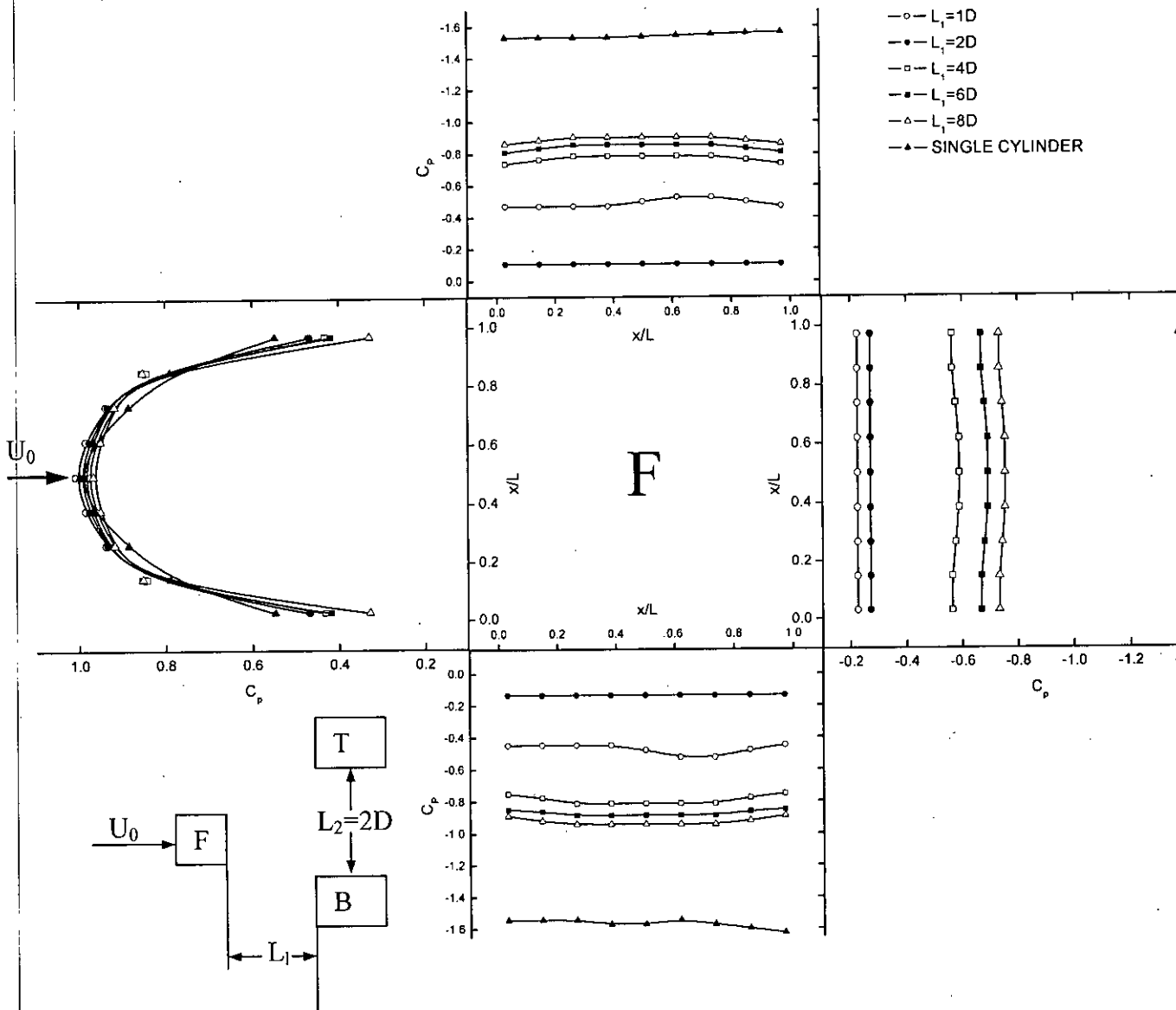
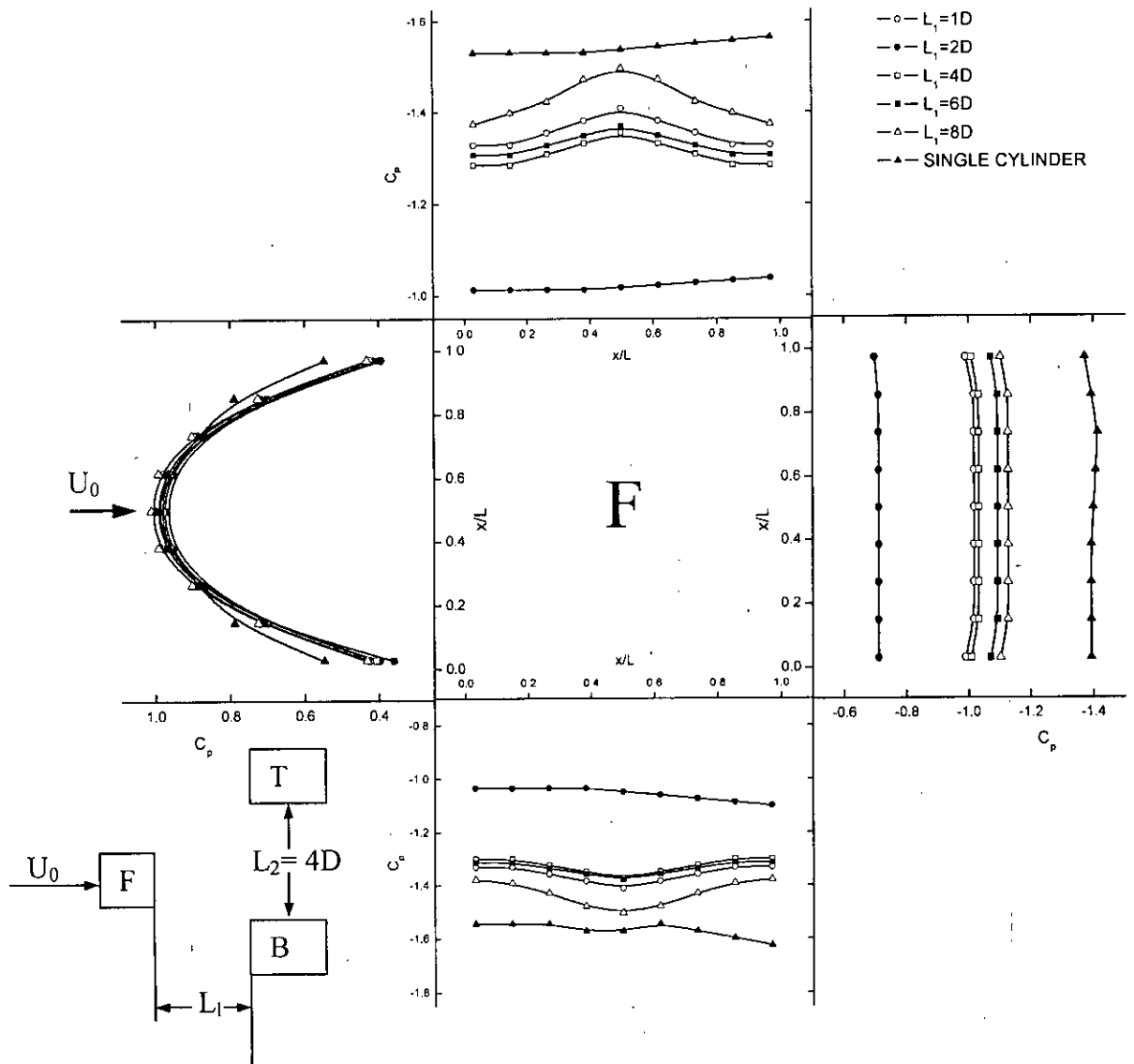


Figure 5.10: Effect of longitudinal spacing ( $L_1$ ) on  $C_p$  for upstream square cylinder (F) keeping transverse spacing ( $L_2$ ) constant at  $2D$ .



**Figure 5.11:** Effect of longitudinal spacing ( $L_1$ ) on  $C_p$  for upstream square cylinder (F) keeping transverse spacing ( $L_2$ ) constant at  $4D$ .



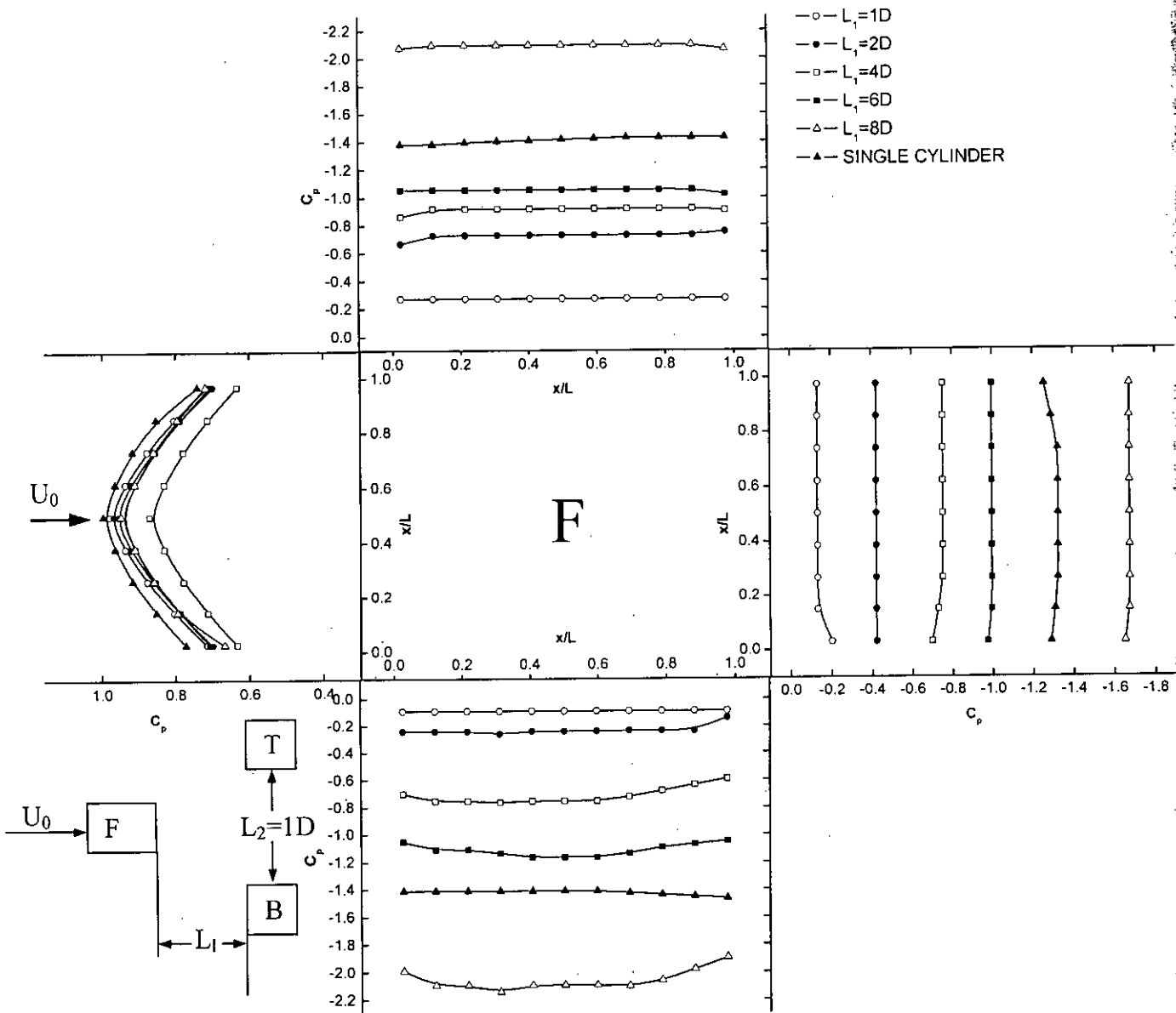


Figure 5.12: Effect of longitudinal spacing ( $L_1$ ) on  $C_p$  for upstream rectangular cylinder (F) keeping transverse spacing ( $L_2$ ) constant at  $1D$ .

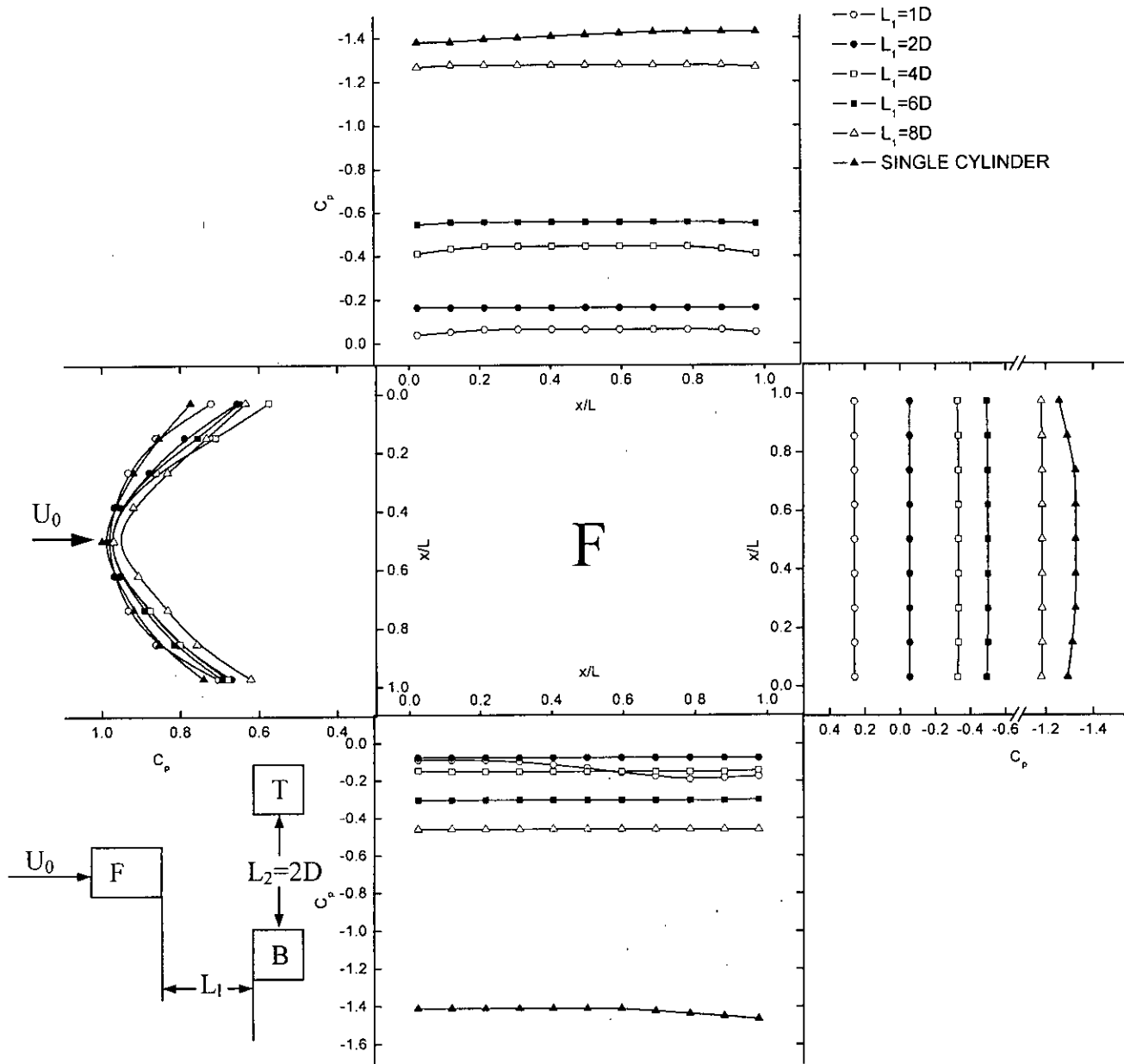


Figure 5.13: Effect of longitudinal spacing ( $L_1$ ) on  $C_p$  for upstream rectangular cylinder (F) keeping transverse spacing ( $L_2$ ) constant at  $2D$ .

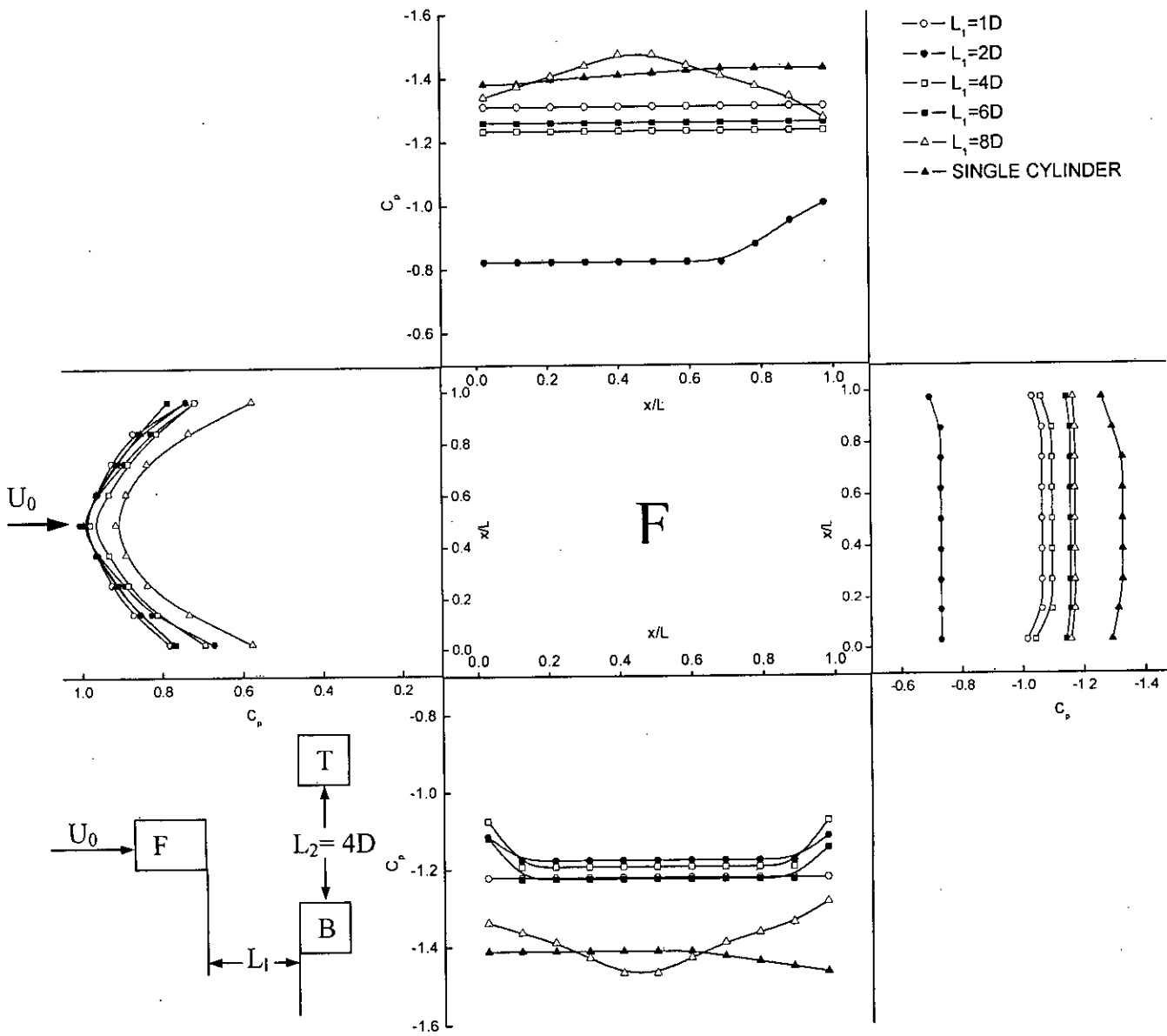
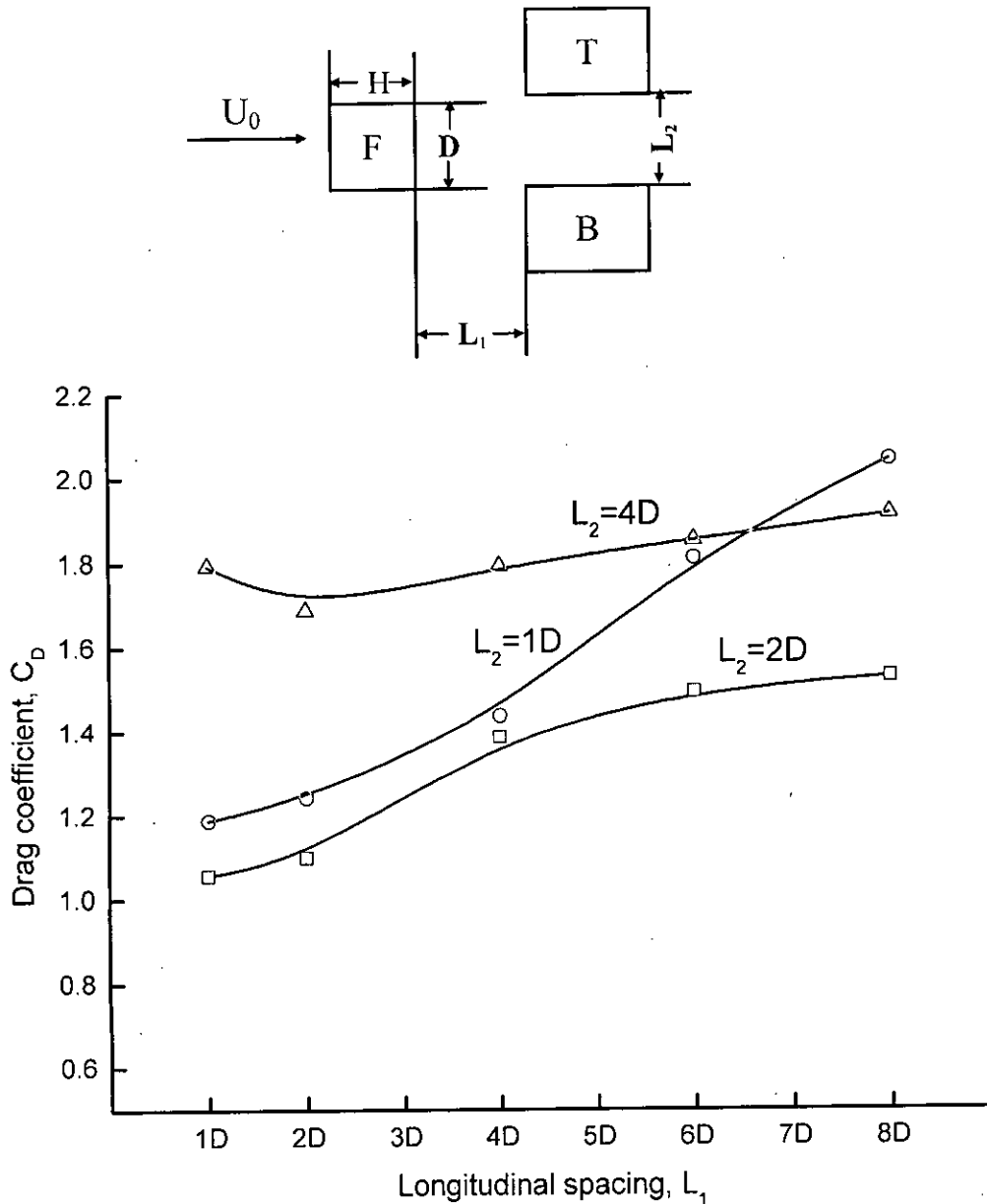


Figure 5.14: Effect of longitudinal spacing ( $L_1$ ) on  $C_p$  for upstream rectangular cylinder (F) keeping transverse spacing ( $L_2$ ) constant at  $4D$ .



**Figure 5.15:** Variation of drag coefficients ( $C_D$ ) on upstream square cylinder (F) with longitudinal spacing ( $L_1$ ) for different values of transverse spacing ( $L_2$ ).

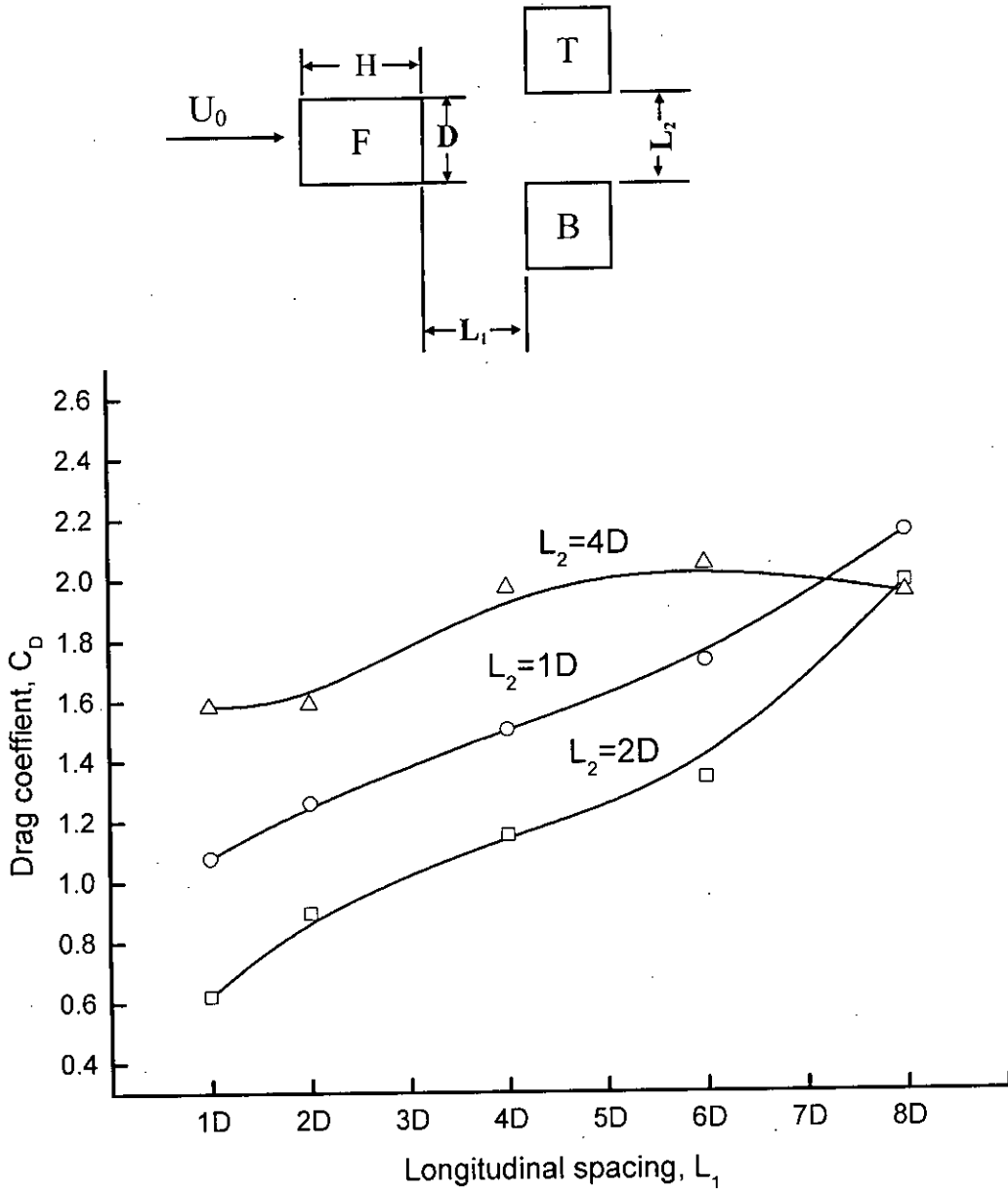
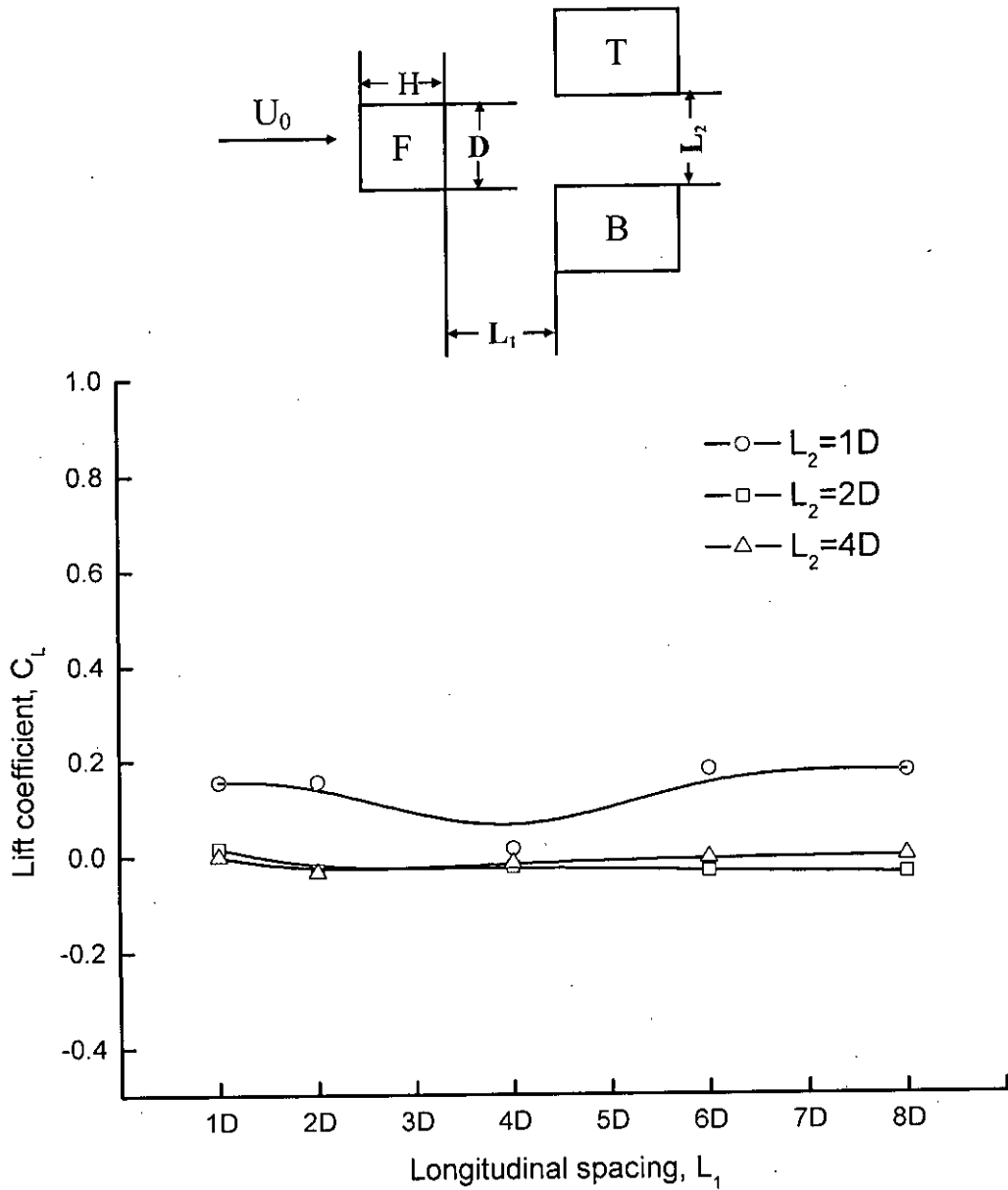
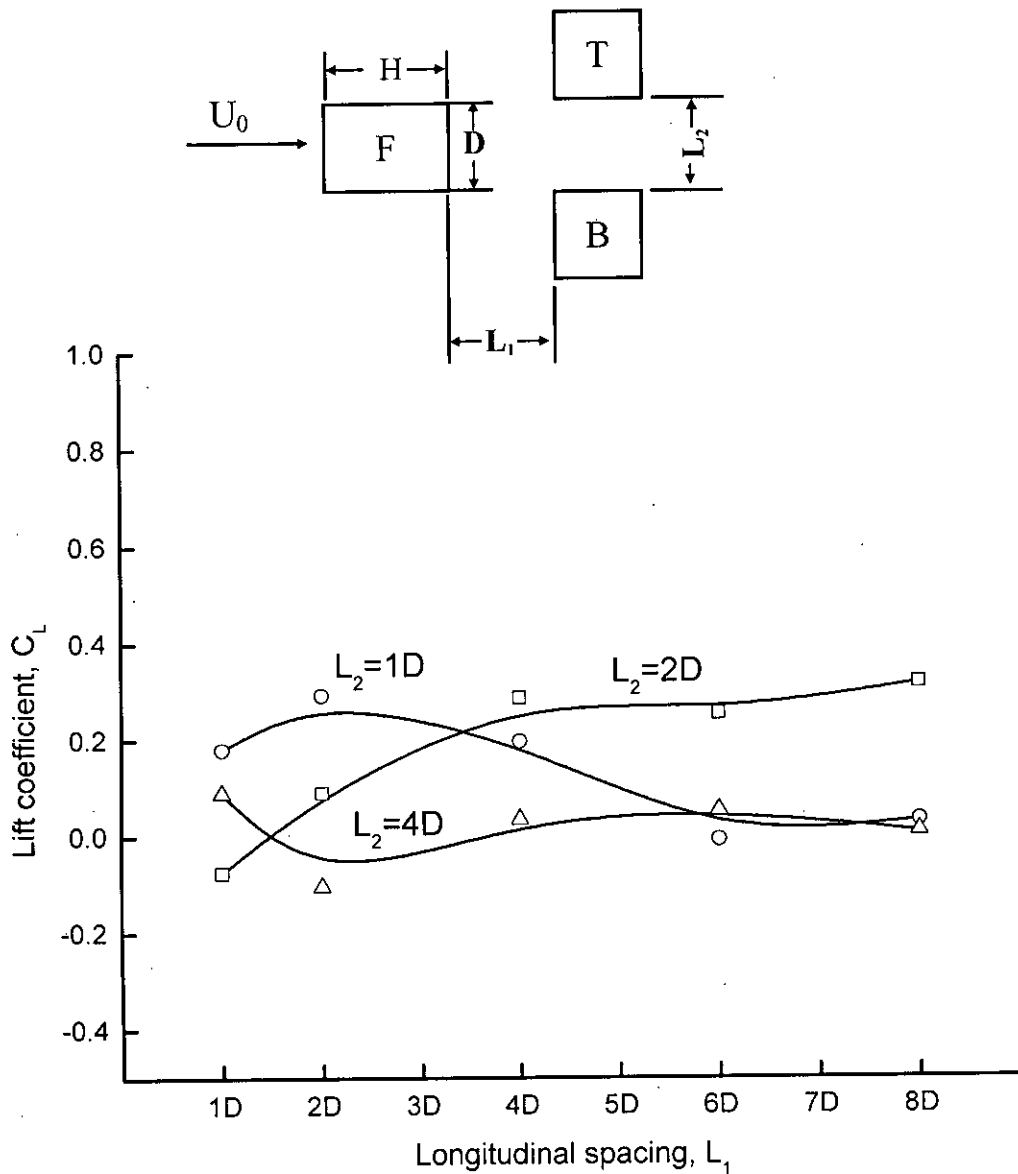


Figure 5.16: Variation of drag coefficients ( $C_D$ ) on upstream rectangular cylinder (F) with longitudinal spacing ( $L_1$ ) for different values of transverse spacing ( $L_2$ ).



**Figure 5.17:** Variation of lift coefficients ( $C_L$ ) on upstream square cylinder (F) with longitudinal spacing ( $L_1$ ) for different values of transverse spacing ( $L_2$ ).



**Figure 5.18:** Variation of lift coefficients ( $C_L$ ) on upstream rectangular cylinder (F) with longitudinal spacing ( $L_1$ ) for different values of transverse spacing ( $L_2$ ).

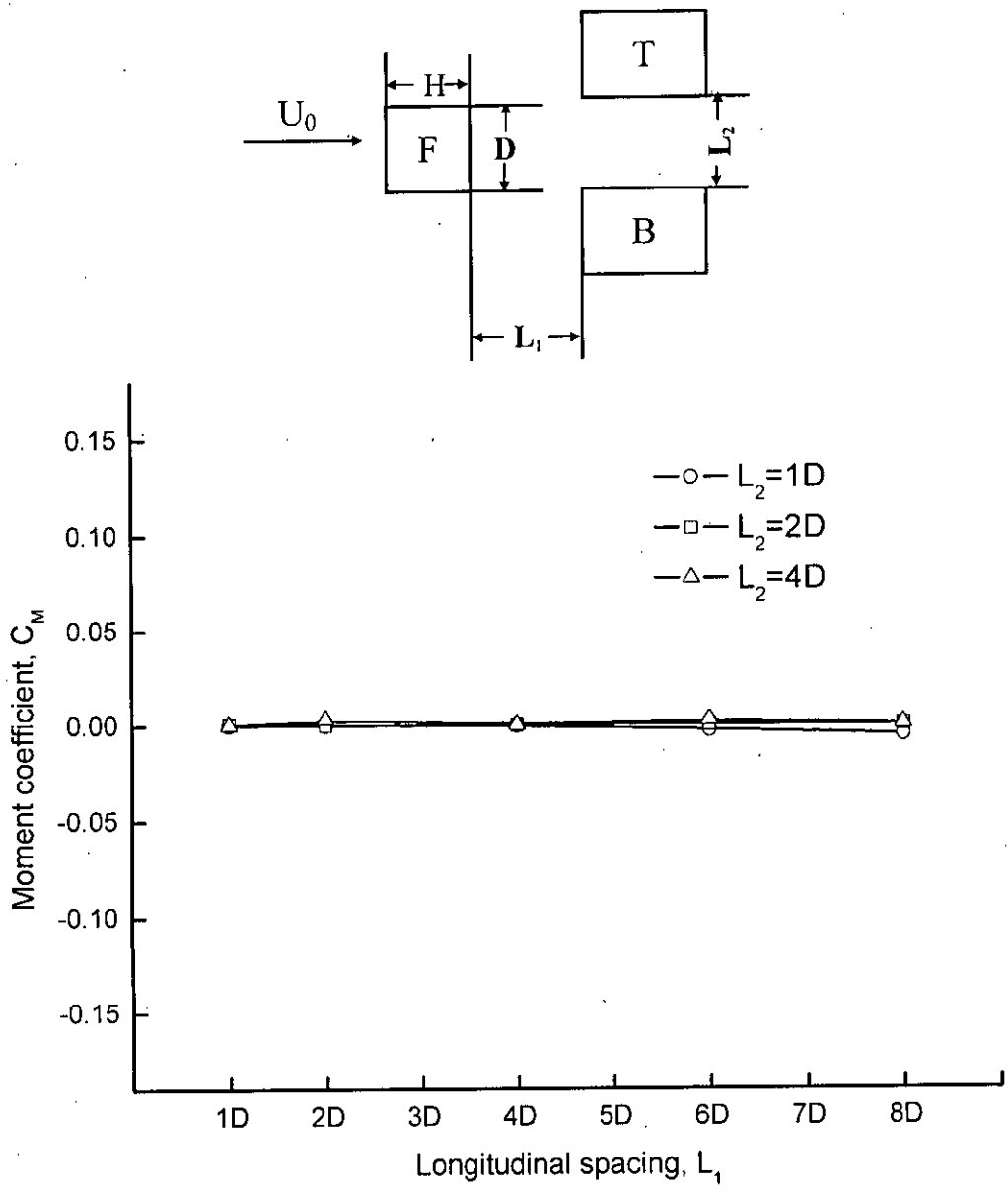


**Figure 5.19:** Variation of moment coefficients ( $C_M$ ) on upstream square cylinders (F) with longitudinal spacing ( $L_1$ ) for different values of transverse spacing ( $L_2$ ).



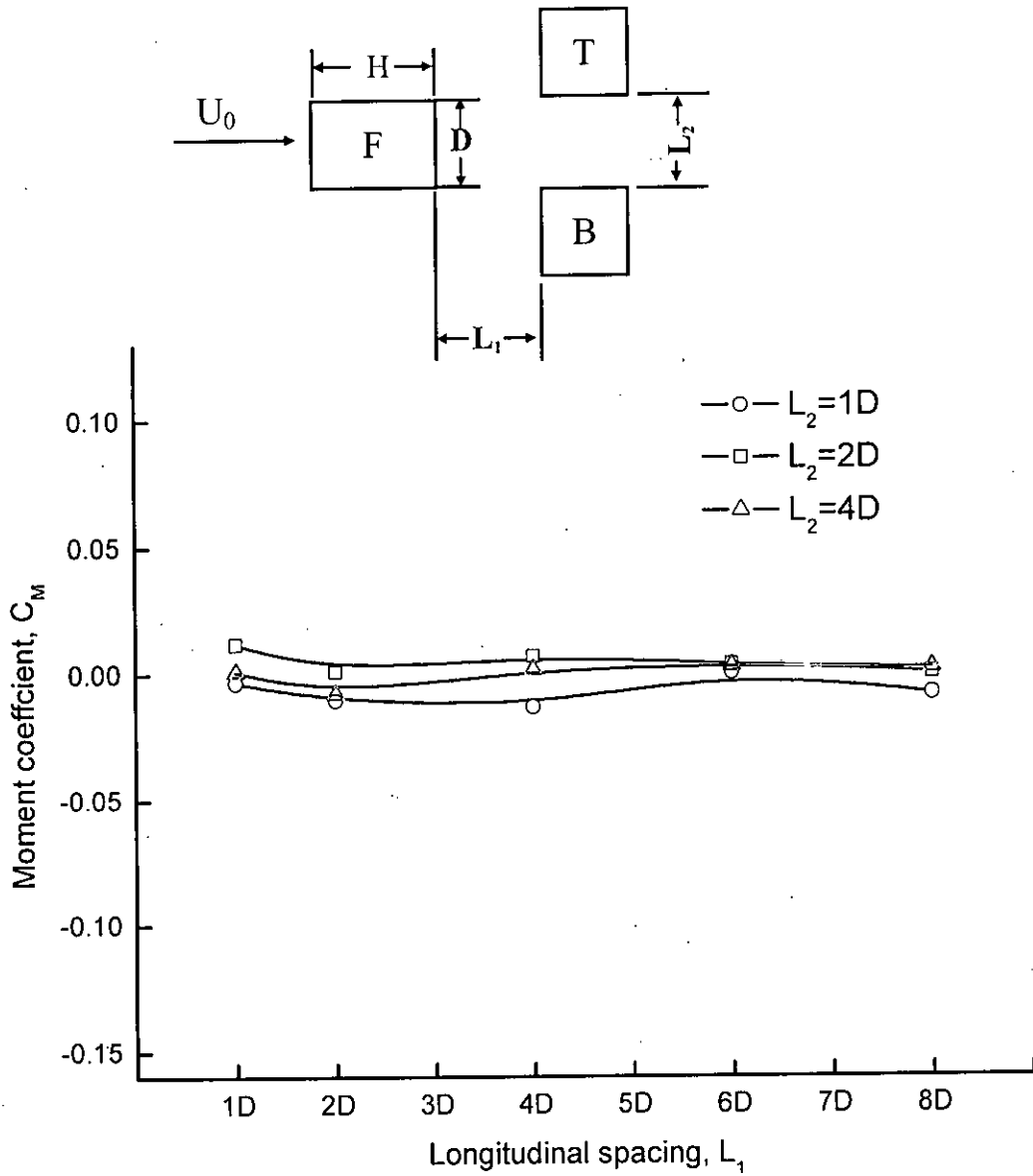


**Figure 5.20:** Variation of moment coefficients ( $C_M$ ) on upstream rectangular cylinder (F) with longitudinal spacing ( $L_1$ ) for different values of transverse spacing ( $L_2$ ).

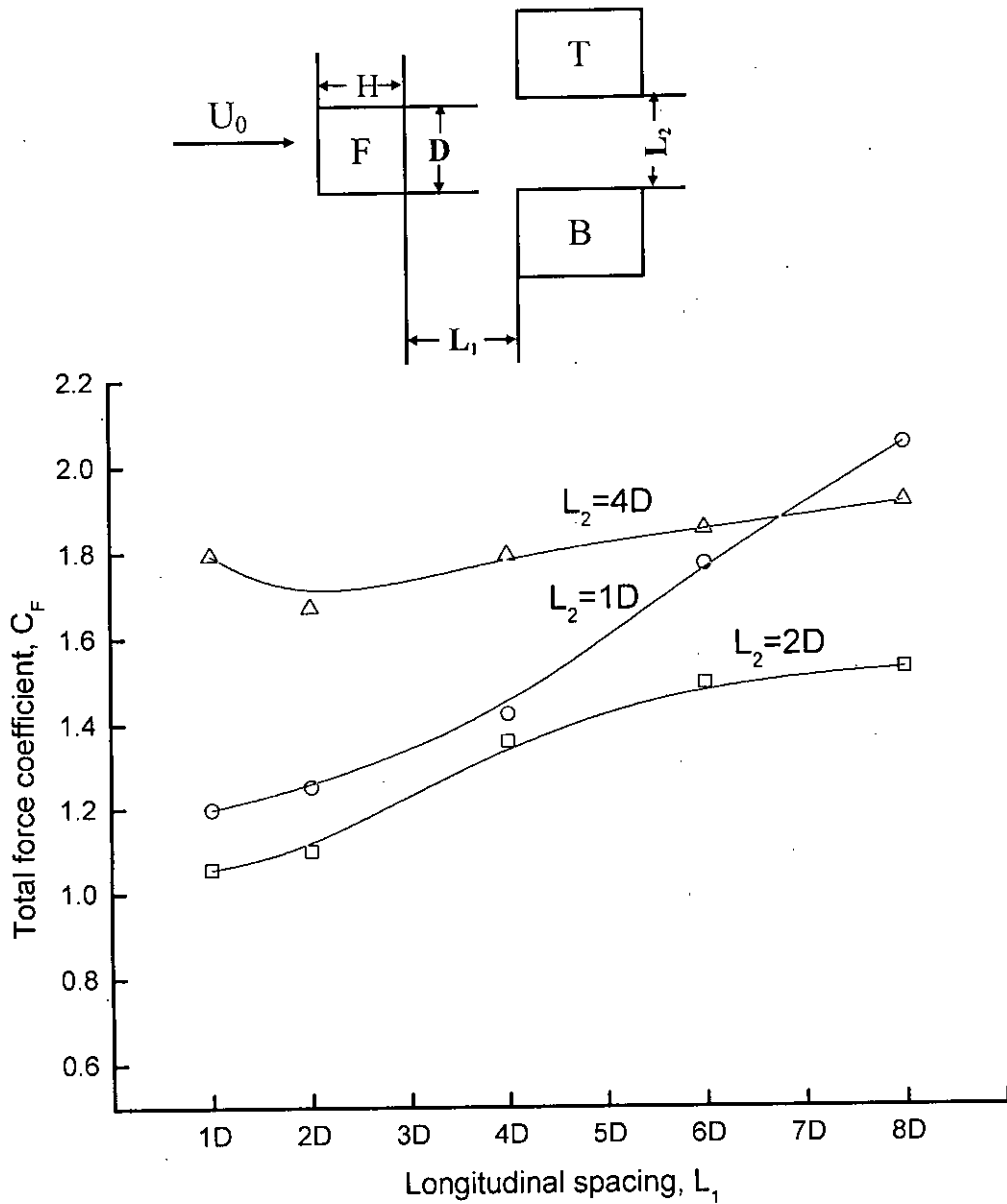


**Figure 5.21:** Variation of total force coefficients ( $C_F$ ) on upstream square cylinder (F) with longitudinal spacing ( $L_1$ ) for different values of transverse spacing ( $L_2$ ).

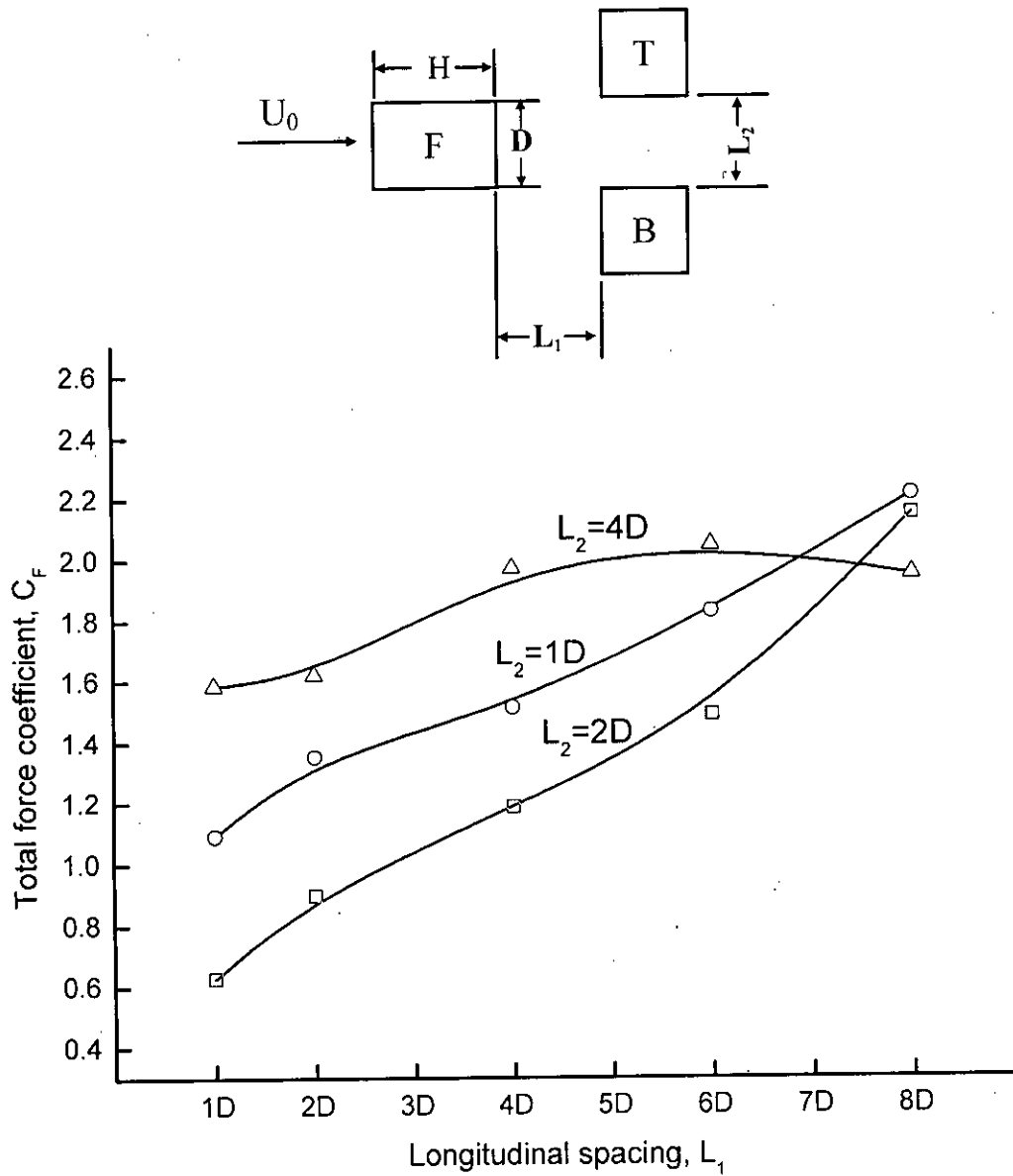


**Figure 5.22:** Variation of total force coefficients ( $C_F$ ) on upstream rectangular cylinder (F) with longitudinal spacing ( $L_1$ ) for different values of transverse spacing ( $L_2$ ).

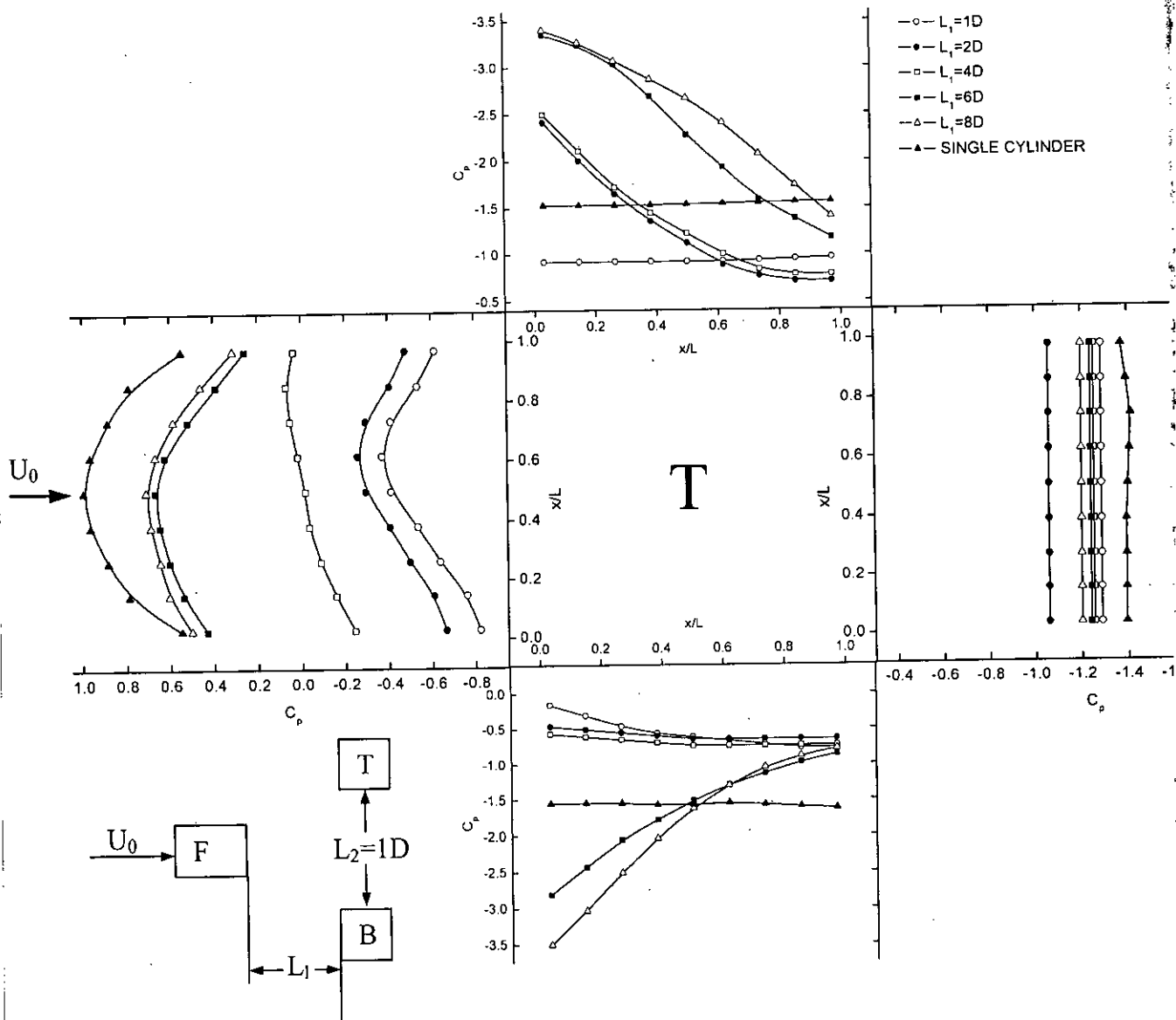


**Figure 5.23:** Effect of longitudinal spacing ( $L_1$ ) on  $C_p$  for downstream square cylinder (T or B) keeping transverse spacing ( $L_2$ ) constant at 1D.

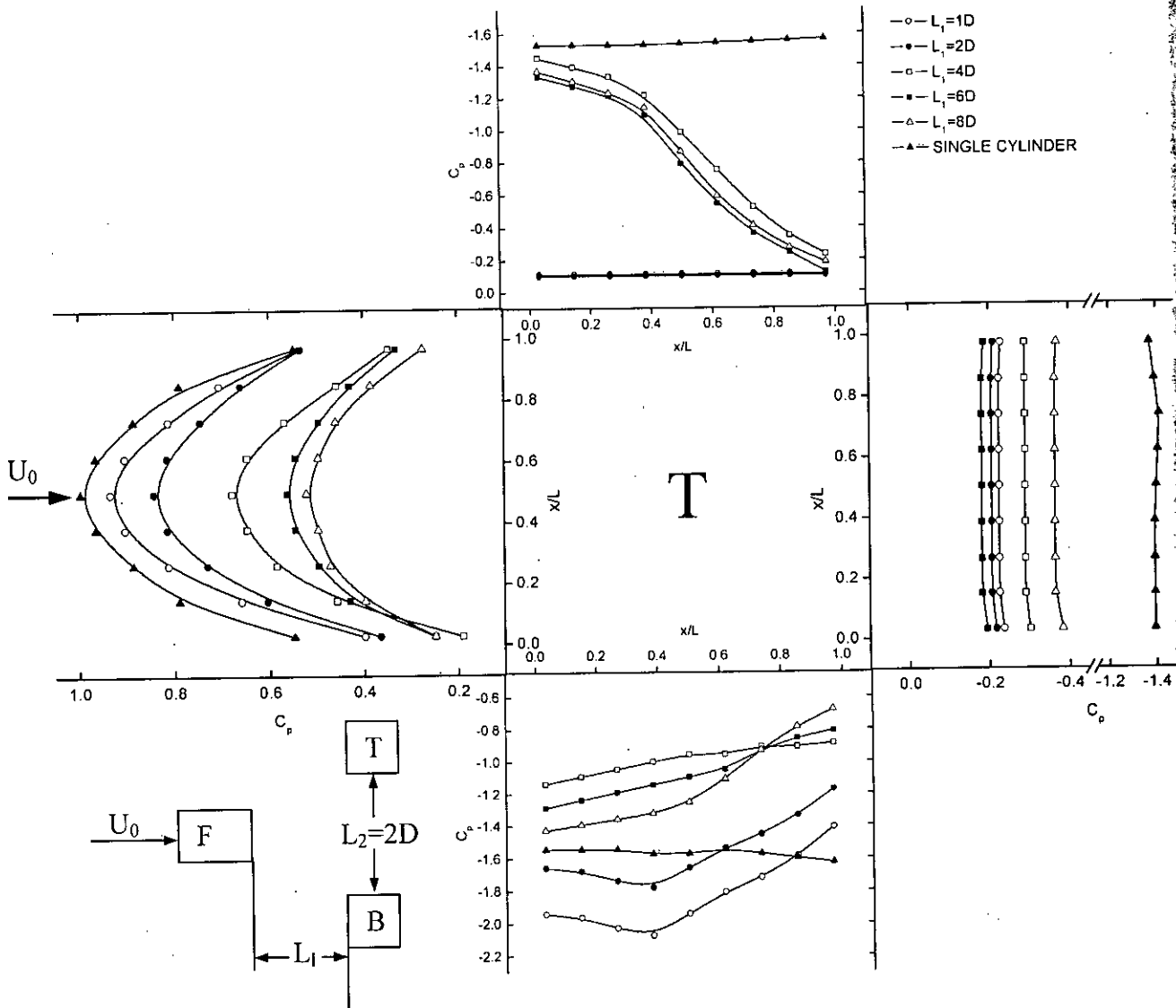


Figure 5.24: Effect of longitudinal spacing ( $L_1$ ) on  $C_p$  for downstream square cylinder (T or B) keeping transverse spacing ( $L_2$ ) constant at  $2D$ .

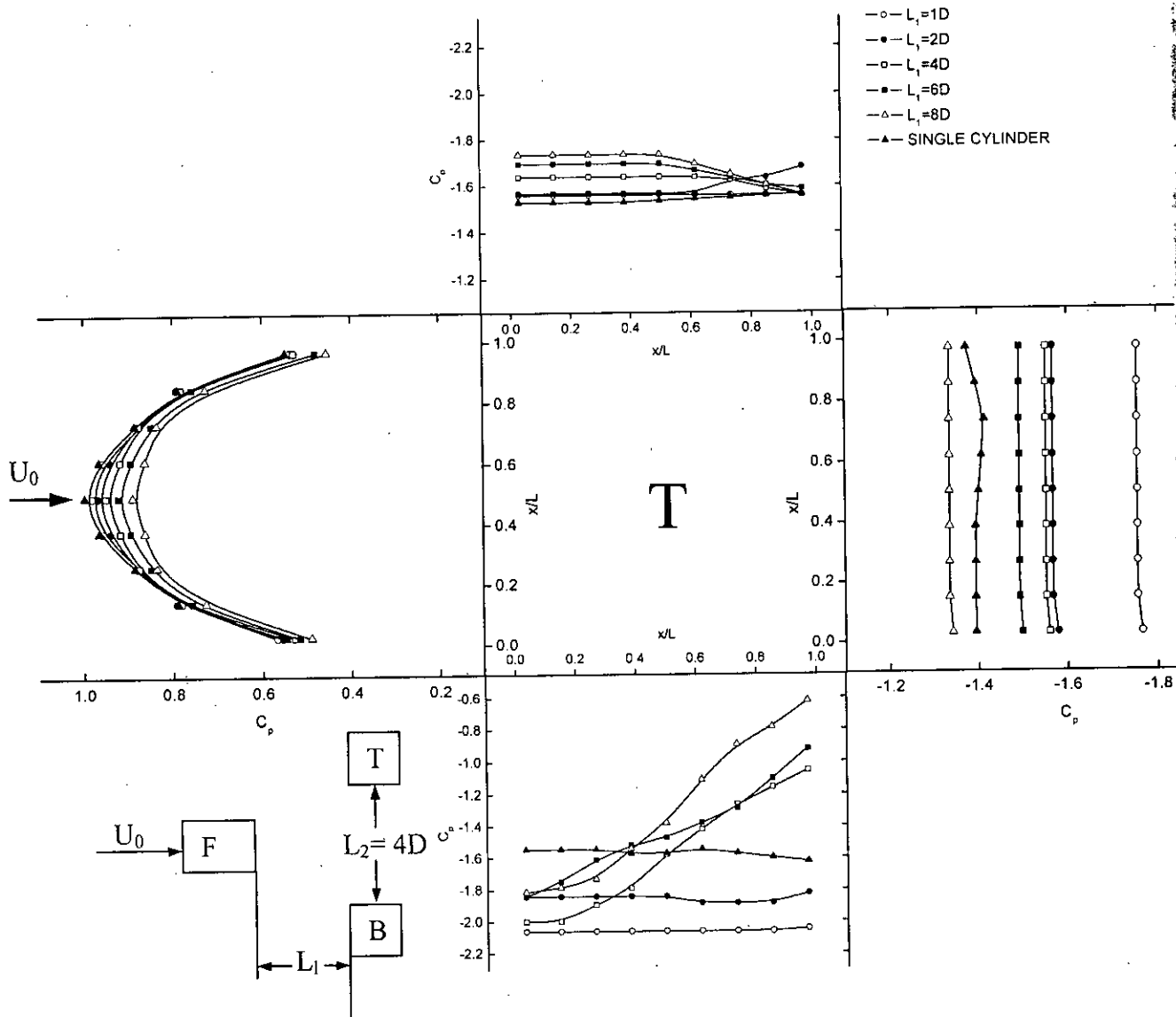


Figure 5.25: Effect of longitudinal spacing ( $L_1$ ) on  $C_p$  for downstream square cylinder (T or B) keeping transverse spacing ( $L_2$ ) constant at  $4D$ .

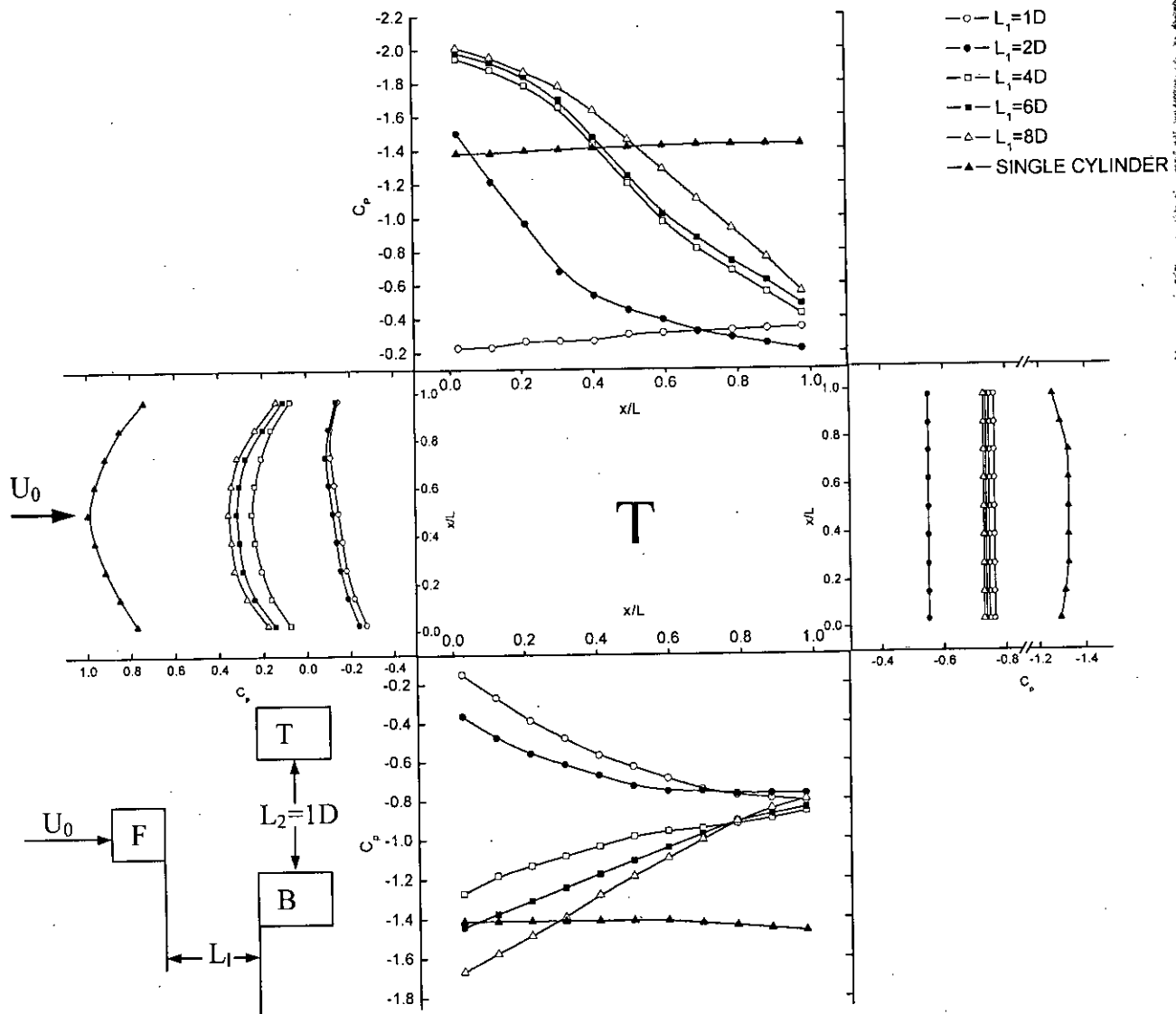


Figure 5.26: Effect of longitudinal spacing ( $L_1$ ) on  $C_p$  for downstream rectangular cylinder (T or B) keeping transverse spacing ( $L_2$ ) constant at  $1D$ .

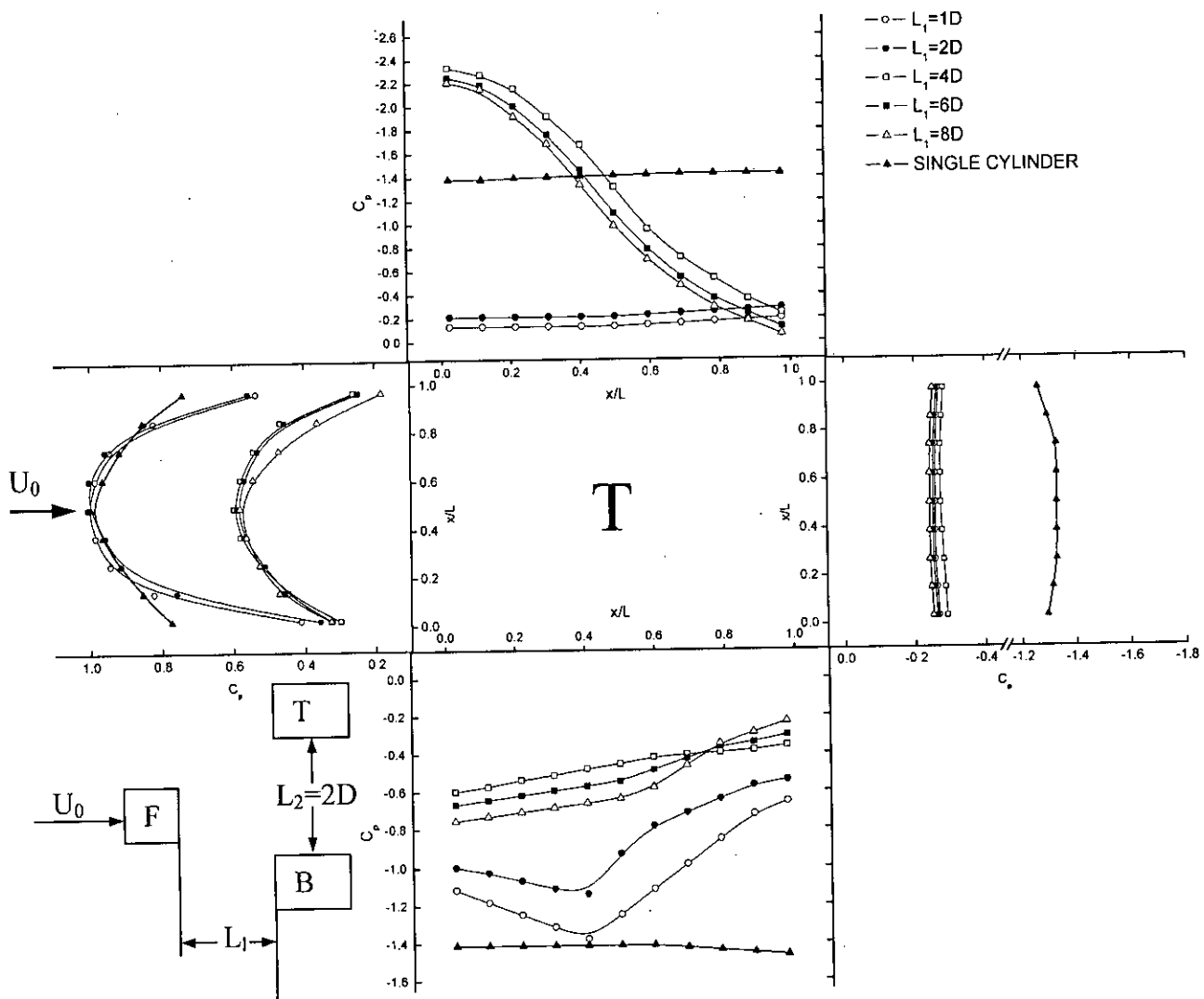


Figure 5.27: Effect of longitudinal spacing ( $L_1$ ) on  $C_p$  for downstream rectangular cylinder (T or B) keeping transverse spacing ( $L_2$ ) constant at  $2D$ .



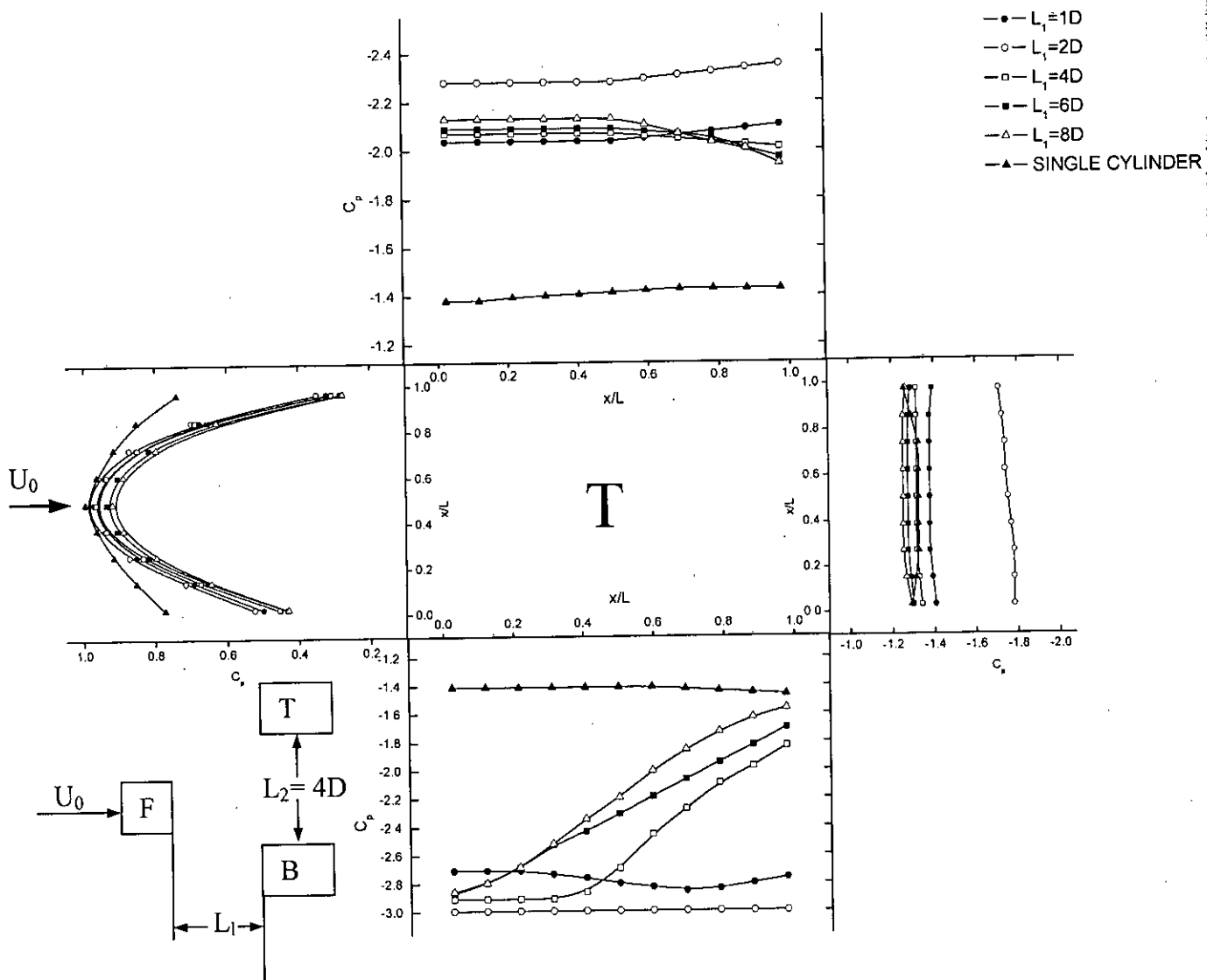
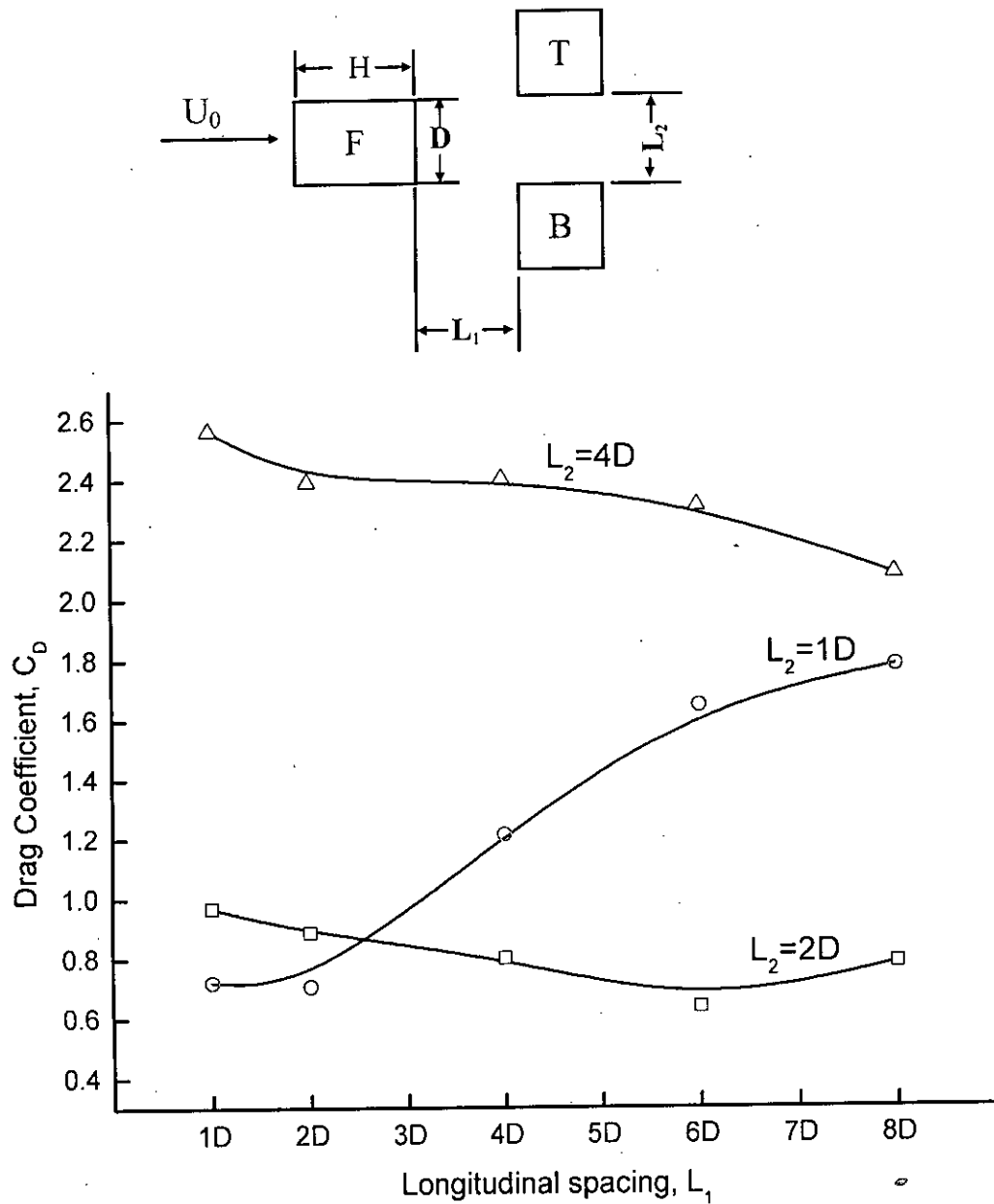
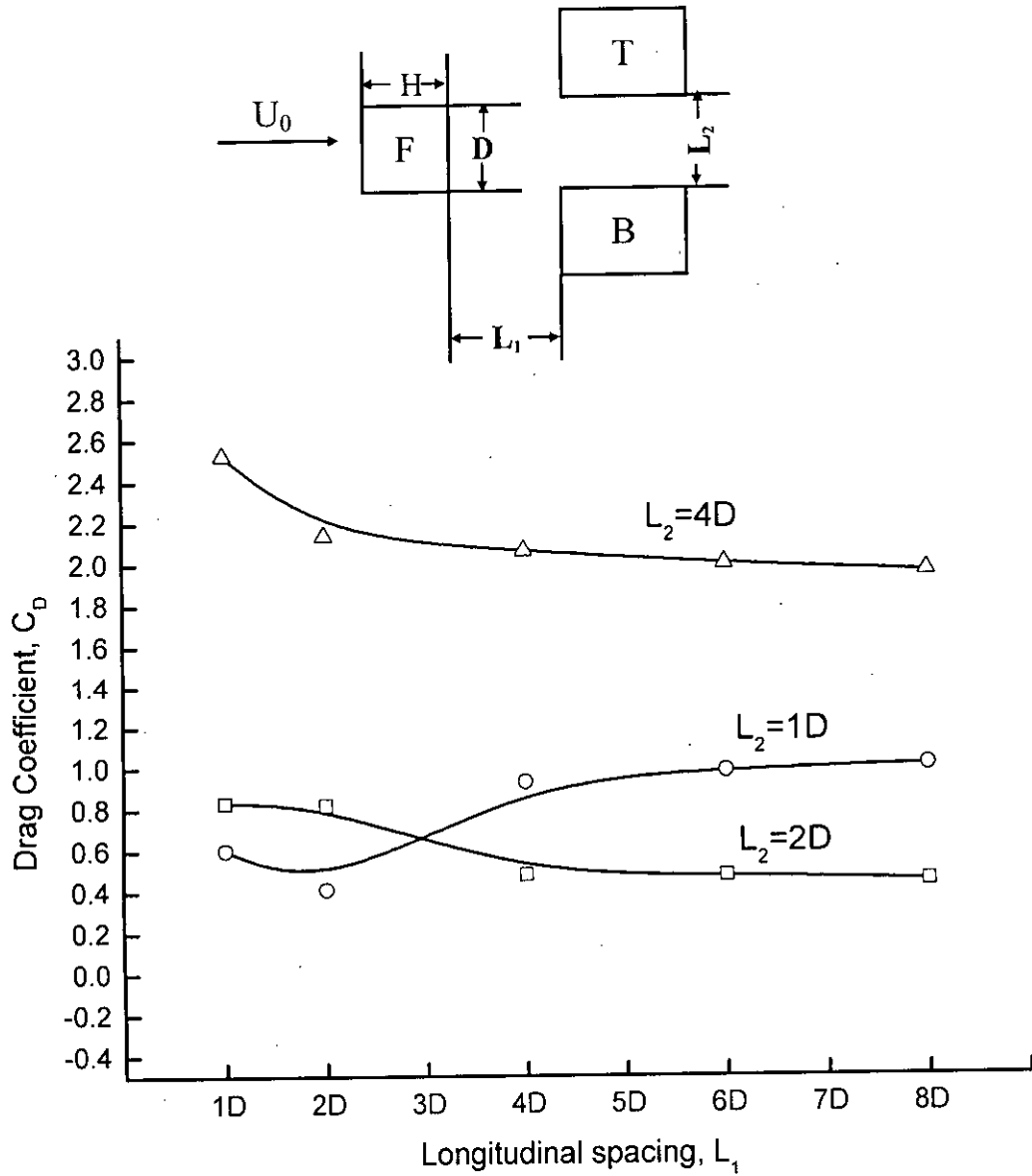


Figure 5.28: Effect of longitudinal spacing ( $L_1$ ) on  $C_p$  for downstream rectangular cylinder (T or B) keeping transverse spacing ( $L_2$ ) constant at  $4D$ .



**Figure 5.29:** Variation of drag coefficients ( $C_D$ ) on downstream square cylinder (T or B) with longitudinal spacing ( $L_1$ ) for different values of transverse spacing ( $L_2$ ).



**Figure 5.30:** Variation of drag coefficients ( $C_D$ ) on downstream rectangular cylinder (T or B) with longitudinal spacing ( $L_1$ ) for different values of transverse spacing ( $L_2$ ).

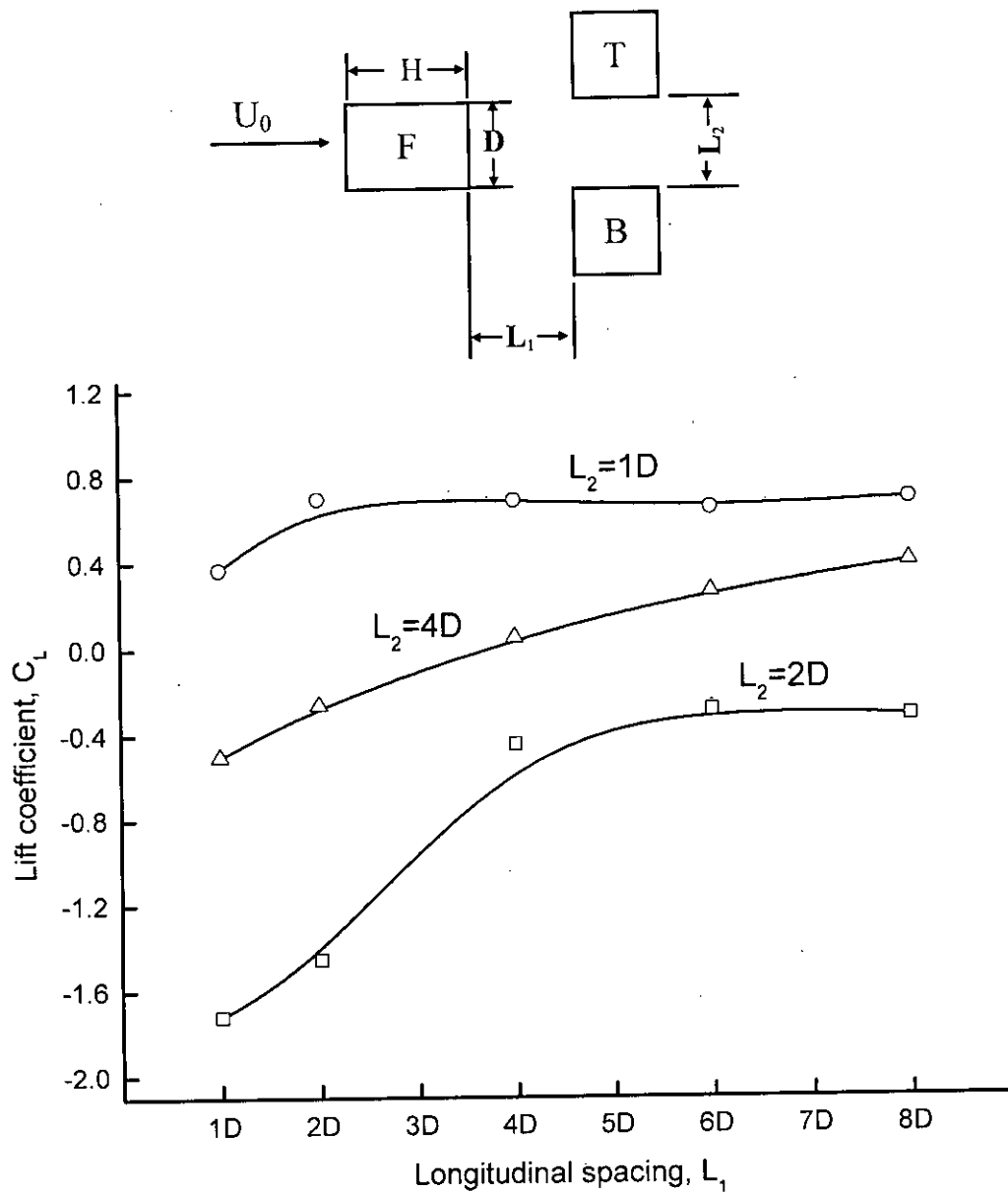


**Figure 5.31:** Variation of lift coefficients ( $C_L$ ) on downstream square cylinder (T or B) with longitudinal spacing ( $L_1$ ) for different values of transverse spacing ( $L_2$ ).

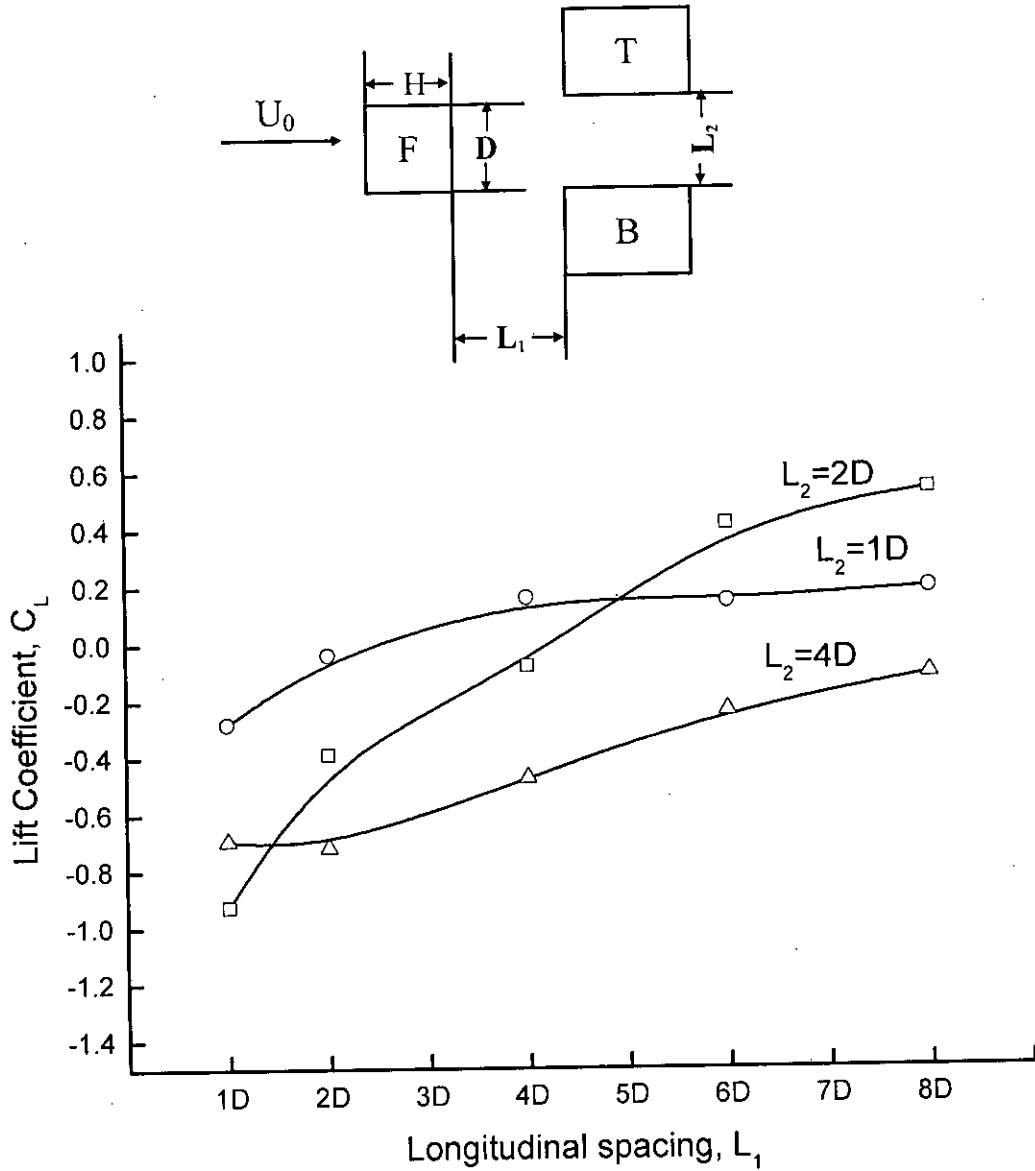


**Figure 5.32:** Variation of lift coefficients ( $C_L$ ) on downstream rectangular cylinder (T or B) with longitudinal spacing ( $L_1$ ) for different values of transverse spacing ( $L_2$ ).

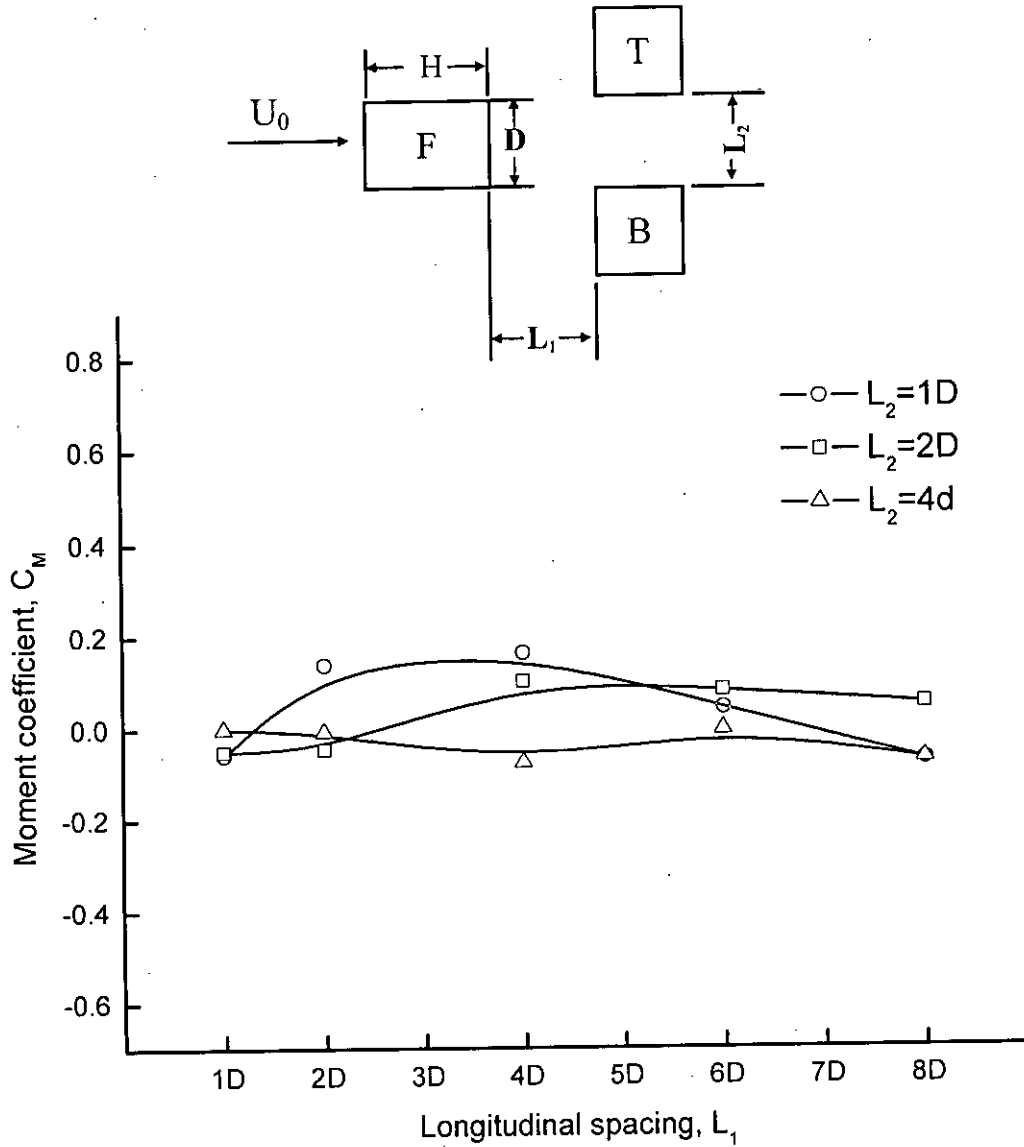


**Figure 5.33:** Variation of moment coefficients ( $C_M$ ) on down stream square cylinders (T or B) with longitudinal spacing ( $L_1$ ) for different values of transverse spacing ( $L_2$ ).

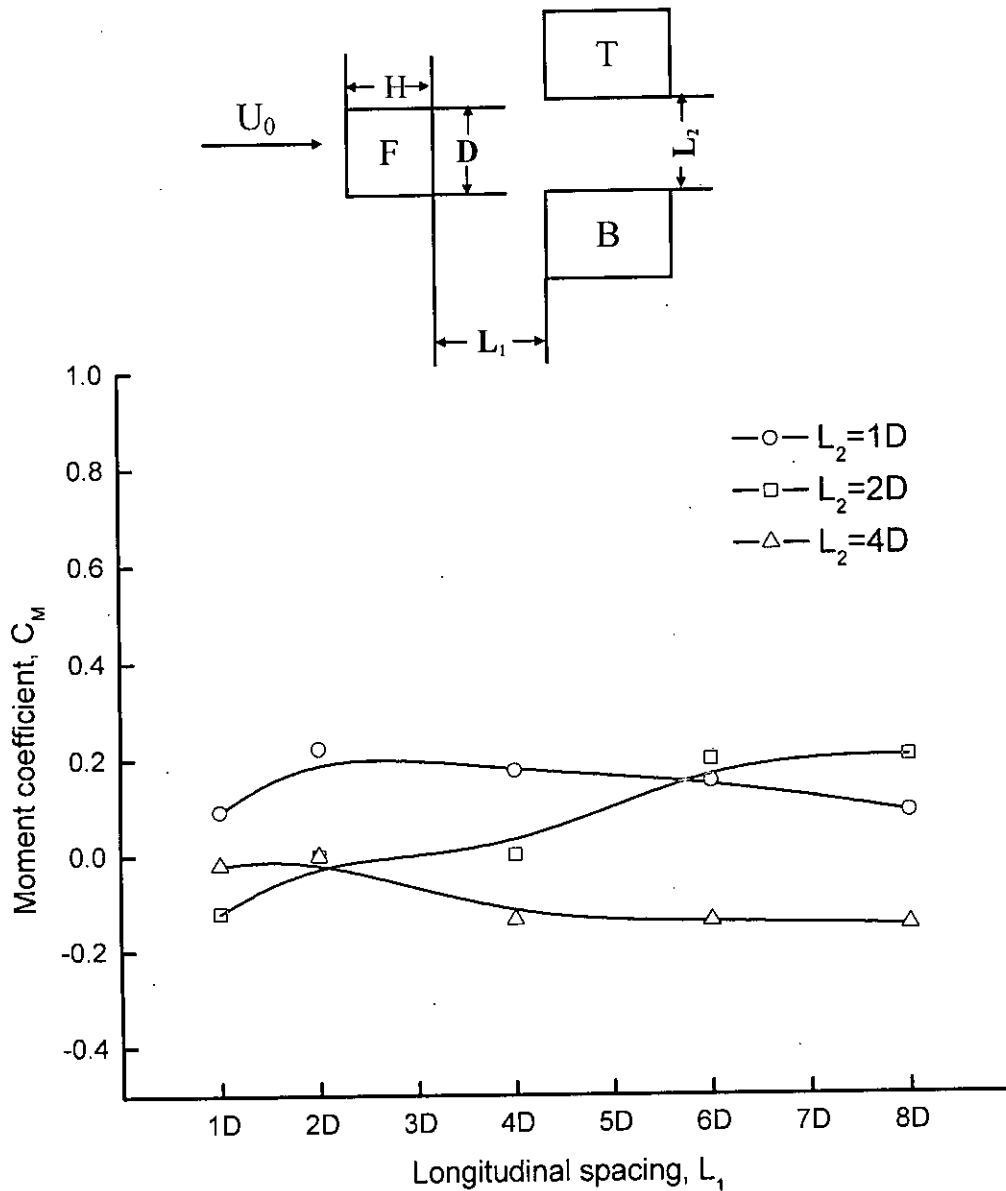


**Figure 5.34:** Variation of moment coefficients ( $C_M$ ) on down stream rectangular cylinders (T or B) with longitudinal spacing ( $L_1$ ) for different values of transverse spacing ( $L_2$ ).

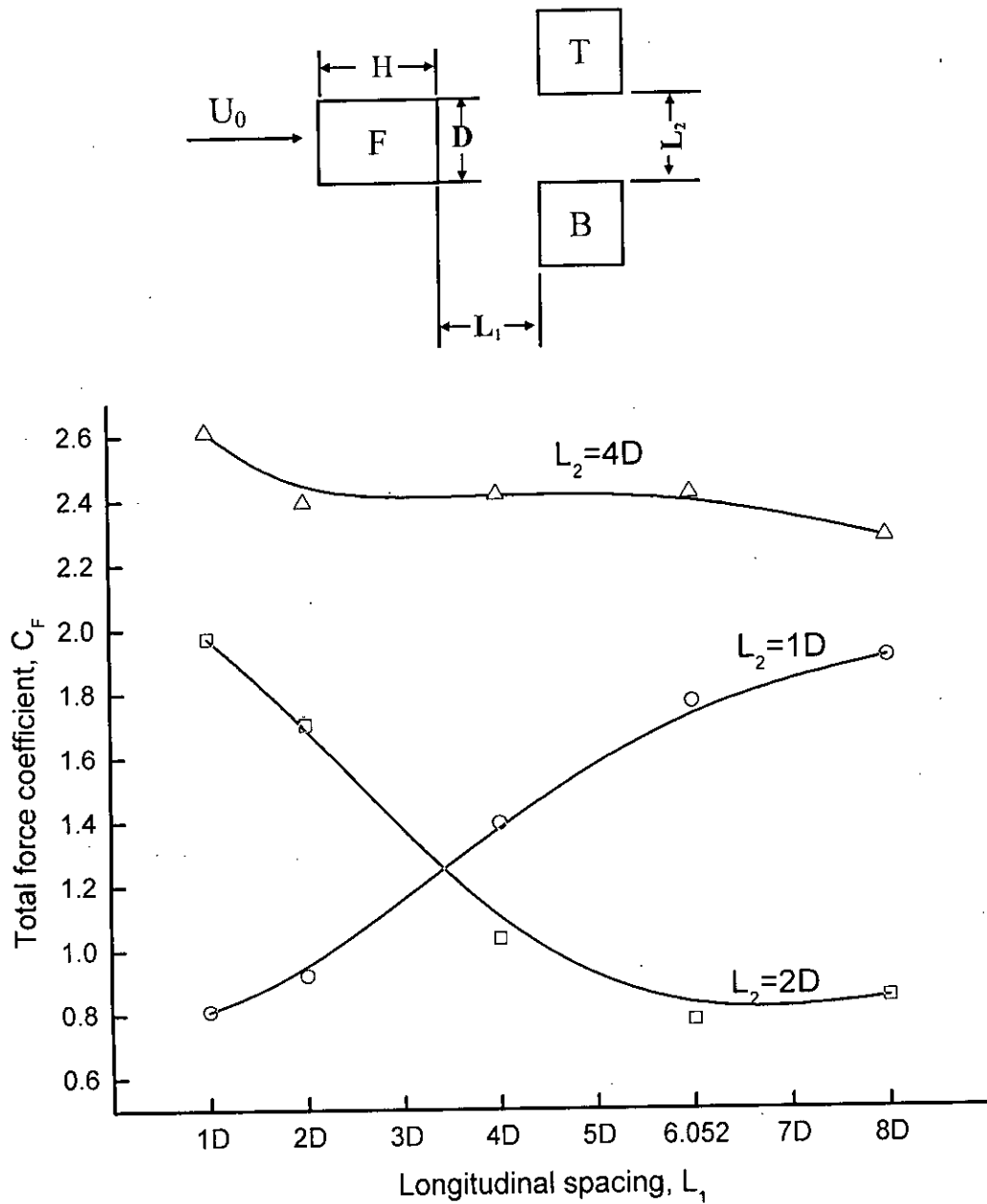


**Figure 5.35:** Variation of total force coefficients ( $C_F$ ) on downstream square cylinder (T or B) with longitudinal spacing ( $L_1$ ) for different values of transverse spacing ( $L_2$ ).



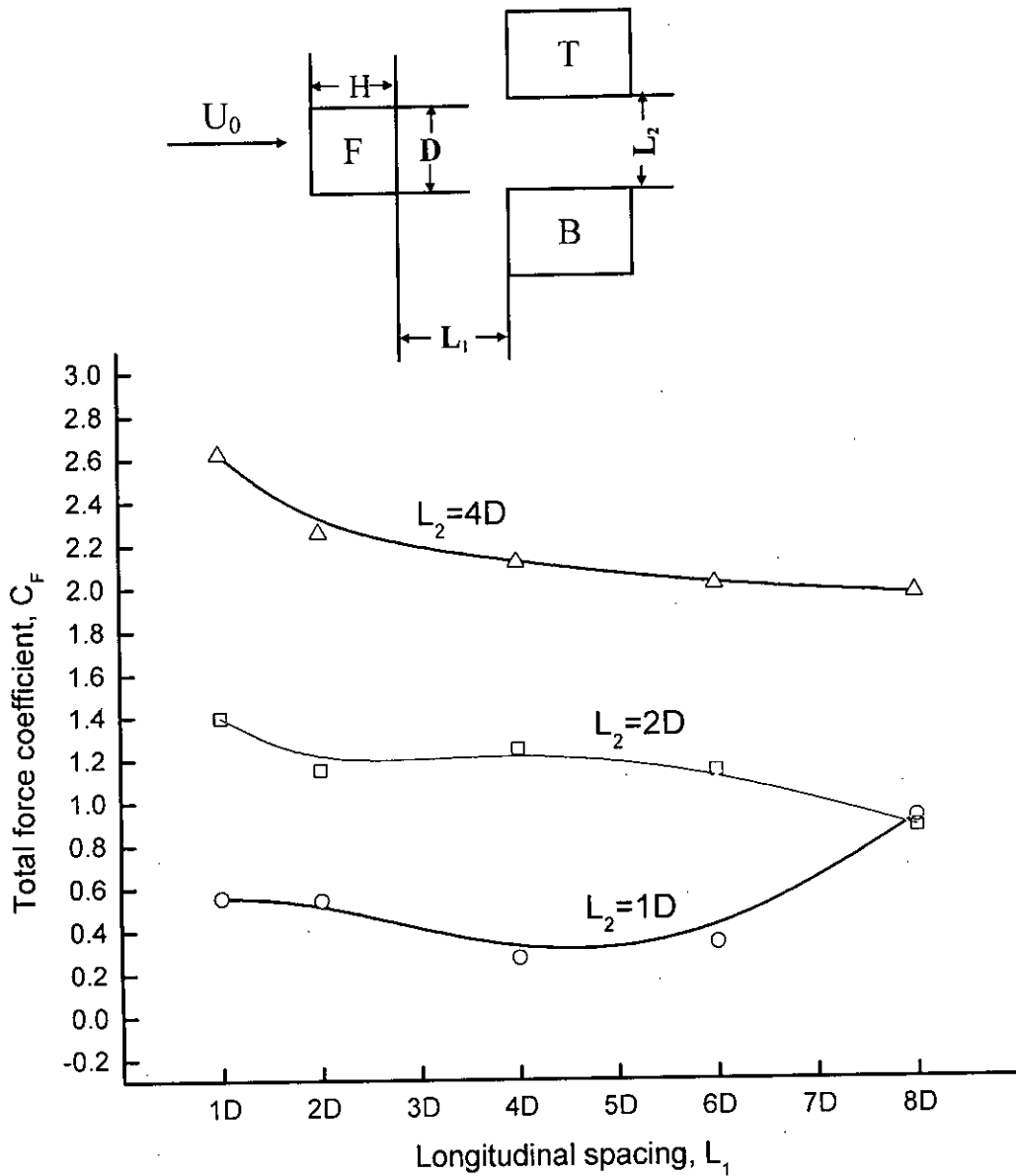


**Figure 5.36:** Variation of total force coefficients ( $C_F$ ) on downstream rectangular cylinder (T or B) with longitudinal spacing ( $L_1$ ) for different values of transverse spacing ( $L_2$ ).

## CHAPTER 6

### CONCLUSIONS AND RECOMMENDATIONS

The following conclusions can be drawn from the experimental investigation of flow around square and rectangular cylinders and this chapter also includes the scope of extension and development of the present study.

#### 6.1 Conclusions

1. At an angle of attack,  $\alpha = 0^\circ$ , no flow reattachment occurs on the surfaces of each isolated cylinder. However, the flow on the top, bottom and back surfaces is completely separated.
2. Flow reattachment occurs on the bottom surface of the single cylinder at small angle of attack and the location reattachment shifts from the rear corner towards the front corner of the bottom surface with increase in angle of attack.
3. At small angle of attack the  $C_p$ -value decreases considerably near the front corner of the bottom surface of each cylinder and the negative peak value of  $C_p$  is shifted towards the front edge with increase in the side ratio.
4. The minimum drag on the cylinders occur within  $8^\circ$  and  $12^\circ$  angle of attack for all side ratios. The total force coefficient is minimum at around the angle of attack  $8^\circ$  and  $12^\circ$ .
5. The  $C_p$ -values on the top, back and bottom surface of upstream cylinder are reduced due to the presence of downstream cylinders.
6. The  $C_p$ -distributions on the front surface of the downstream cylinders for transverse spacing,  $L_2 = 1D$  and longitudinal spacings,  $L_1 = 1D$  and  $2D$  are negative for both the two groups. Whereas, these are always positive in the case of single cylinder at any angle of attack (below  $35^\circ$ ).

7. At a transverse spacing,  $L_2 = 1D$ , the values of  $C_p$  is reduced due to the presence of upstream square cylinder on all the faces of downstream rectangular cylinder except near the front part of top surface, at longitudinal spacing ( $L_1$ ) of  $4D$  to  $8D$ .
8. Higher suction is developed near the frontal region of the bottom surface of the downstream cylinder in both groups at transverse spacing  $L_2 = 2D$  and Longitudinal spacing  $L_1 = 1D$ .
9. Very high negative pressure is developed on the bottom surface of the downstream square and rectangular cylinders at  $L_2 = 1D$  and  $L_1 = 8D$ . The maximum negative  $C_p$  occurs at square cylinder which is  $-3.50$ .
10. The variation of  $C_D$  of the front square and rectangular cylinder is appreciable upto the longitudinal spacing,  $L_1 = 4D$  and the value of  $C_D$  approach to that of the single cylinder at longitudinal spacing greater than  $4D$ .
11. The total force coefficient ( $C_F$ ) of an individual cylinder in the staggered form is always less than that of the single cylinder. The exception is that at transverse spacing,  $L_2 = 4D$  and longitudinal spacing,  $L_1 = 1D$  to  $4D$  for downstream rectangular cylinder and all the spacing  $L_1$  for downstream square cylinder.
12. Even though the net wind load on an individual cylinder in staggered form decreases; however, some portions of the surfaces experiences high local  $C_p$ .

## 6.2 Recommendations

1. The same experiment can be done with flow visualization technique to get a better understanding about the formation of wakes and vortex shedding pattern.
2. Further studies can be carried out by changing the formation of staggered cylinders i.e. two cylinders at upstream and one cylinder at downstream.
3. Investigation of flow around staggered square and rectangular cylinders at different angles of attack may be done.

4. The effect of surface roughness on the flow over isolated and group of square and rectangular cylinders can be investigated.
5. The effect of Reynolds number on staggered cylinders with varying side ratios may be investigated.
6. Building models of various other shapes and sizes can be brought under this kind of investigation.
7. The test can also be conducted with different spacings and more cylinders.

## **REFERENCES**

---

---

**REFERENCES**

- [1] Bearman, P.W. and Trueman, D.M., "An Investigation of the Flow Around Rectangular Cylinders" *The Aeronautical Quarterly*, Vol. 23, pp. 229-237, 1972.
- [2] Lee, B.E., "The Effect of Turbulence on the Surface Pressure Field of a Square Prism" *Journal of Fluid Mechanics*, Vol.69, pp.263-282, 1975.
- [3] Nakamura, Y. and Matsukawa, T., "Vortex Excitation of Rectangular Cylinders with a Long Side Normal to the Flow", *Journal of Fluid Mechanics*, Vol. 180, pp.263-282, 1987.
- [4] Vickery, B.J., "Fluctuating Lift and Drag on a Long cylinder of Square Cross-Section in a Smooth and in a Turbulent Stream", *Journal of Fluid Mechanics*, Vol. 25, part. 3, pp.481-491, 1966.
- [5] Parkinson, G.V. and Modi, V.J., "Recent Research on Wind Effects on Bluff Two-Dimensional Bodies", *Proceedings of International Research Seminar, Wind Effects on Building and Structures*, Ottawa, Canada, pp. 485-514, 1967.
- [6] Barriga, A.R., Crowe, C.T. and Roberson, J.A., "Pressure Distribution on Square Cylinder at a Small Angle of Attack in a Turbulent Cross Flow", *Proceedings of the 4<sup>th</sup> International Conference on Wind Effects on Buildings and Structures*, London, U.K., pp.89-93, 1975.
- [7] Robertson, J.M., "Pressure Field at Reattachment of Separated Flows", *Proceedings of the 2<sup>nd</sup> U.S. National Conference on Wind Engineering Research*, Colorado, June 22-25, 1975.
- [8] Castro, I.P.P. and Robins, A.G., "The Flow Around a Surface Mounted Cube Uniform and Turbulent Streams", *Journal of Fluid Mechanics*, Vol. 79, pp.307-335, 1977.
- [9] Roberson, J.A., Chi Yu Lin, Rutherford, G.S. and Stine, M.D., "Turbulence Effects on Drag of Sharp-edged Bodies" *Journal of Hydraulics Division*, Vol.98, No.HY7, pp.1187-1201.

- 
- [10] Nakamura, Y. and Yujiohya, "Vortex Shedding from Square Prisms in Smooth and Turbulent Flows", *Journal of Fluid Mechanics*, Vol.164, pp.77-89, 1986.
- [11] Davis, R.W. and Moore, E.F., "A Numerical Study of Vortex Shedding from Rectangulars", *Journal of Fluid Mechanics*, Vol.116, pp.475-506.
- [12] Okajima, A., "Strouhal Numbers of Rectangular Cylinders", *Journal of Fluid Mechanics*, Vol.123, pp.379-398, 1982.
- [13] Roberson, J.A., Crowe, C.T. and Tseng, R., "Pressure Distribution on Two and Three Dimensional Models at Small Angle of Attack in Turbulent Flow", *Proceedings of the 2<sup>nd</sup> U.S. National Conference on Wind Engineering Research*, Colorado, June 22-25, 1975.
- [14] Nakamura, Y. and Ohya, Y., "The Effects of Turbulence on the Mean Flow Past Square Rods", *Journal of Fluid Mechanics*, Vol.137, pp.331-345, 1983.
- [15] Bostock, B.R. and Mair, W.A., "Pressure Distributions and Forces on Rectangular and D-shaped Cylinders", *The Aeronautical Quarterly*, Vol. 23, pp.1-5, 1972.
- [16] Sakamoto, H. and Arie, M., "Vortex Shedding from a Rectangular Prism and a Circular Cylinder Placed Vertically in Turbulent Boundary Layer", *Journal of Fluid Mechanics*, Vol.126, pp.147-165, 1983.
- [17] Laneville, A., Gartshore, I.S. and Pakinson, G.V., "An Explanation of some Effects of Turbulence on Bluff Bodies", *Proceedings of the 4<sup>th</sup> International Conference on Wind Effects on Buildings and Structures*, London, U.K., pp.333-341, 1975.
- [18] Hua, C.K., "The Behaviour of Lift Fluctuations on the Square Cylinders in the Wind Tunnel Test", *Proceedings of 3<sup>rd</sup> International Conference on Wind Effects on Buildings and Structures*, Tokyo, Japan, pp.911-920, 1971.
- [19] Matsumoto, M., "The Dynamical Forces Acting on the Vibrating Square Prism in a Steady Flow", *Proceedings of 3<sup>rd</sup> International Conference on Wind Effects on Buildings and Structures*, Tokyo, Japan, pp.921-930, 1971.

- 
- [20] Parkinson, G.V. and Modi, V.J., "Recent Research on Wind Effects on Bluff Two Dimensional Bodies", Proceedings, International Research Seminar, Wind Effects on Buildings and Structures, Ottawa, Canada, pp.485-514, 1967.
- [21] Hussain, H.S. and Islam, O., "Study of Wind Load on Buildings and Structures", Journal of the Institution of Engineers, Bangladesh, Vol. 1, Nos. 2-3, July-October, 1973.
- [22] Keffer, J.F., "The Uniform Distribution of a Turbulent Wake", Journal of Fluid Mechanics, Vol.22, Part-1, pp.135, 1965.
- [23] Gatshore, I.S., "Two Dimensional Turbulent Wake", Journal of Fluid Mechanics, Vol.30, Part-iii, pp.533, 1930.
- [24] Pearlstein, A.J. and Mantle, W.J., "Stability and the Transition to the Three Dimensional in Flows Past Axisymmetric Bluff Bodies", National Science Foundation CTS 94-22770, The Summary of Engineering Research-2000, College of Engineering, University of Illinois at Urbana-Champaign, USA.
- [25] Pearlstein, A.J. and Petteni, F. and Wang L., "Stability of the Wake Behind a Rotating Circular Cylinder", The Summary of Engineering Research-2000, University of Illinois, USA.
- [26] Peris,R., Action Du Vont Sur Les cheminees De Grando Hantour, Proceedings International Research Seminar, Wind Effects on Buildings and Structures, Ottawa, Canada, Vol. II pp.243-282, 1967.
- [27] Senthoooran, S., Lee, Dong-Dae and Parameswaran, " A computational model to calculate the flow-induced pressure fluctuations on buildings" Journal of Wind Engineering and Industrial Aerodynamics , Vol. 92, pp. 1131-1145, 2004.
- [28] Li, Q.S., Xiao, Y. Q., Fu, J.Y. and Li, Z.N., " Full-scale measurements of wind effects on the Jin Mao building" Journal of Wind Engineering and Industrial Aerodynamics , Vol. 95, pp. 445-466, 2007.



- 
- [29] Gu, M. and Quan, Y., “ Across-wind loads of typical tall buildings” *Journal of Wind Engineering and Industrial Aerodynamics* , Vol. 92, pp. 1147-1165, 2004.
- [30] De Grenet, E.T. and Riccardelli, F., “ Spectral proper transformation of wind pressure fluctuations: application to a square cylinder and a bridge deck” *Journal of Wind Engineering and Industrial Aerodynamics* , Vol. 92, pp. 1281-1297, 2004.
- [31] Leutheusser, J., “Static Wind Loadings of Grouped Buildings”, *Proceedings of the 3<sup>rd</sup> International Conference on Wind Effects on Buildings and Structures*, Tokyo, Japan, pp.211-220, 1971.
- [32] Hayashi, M., Akirasakurai and Yujiohya, “Wake Interference of a Row of Normal Flat Plates Arranged side by side in a Uniform Flow”, *Journal of Fluid Mechanics*, Vol.164, pp.1-25, 1986.
- [33] Koenig, K. and Roshko, A., “An Experimental Study of Geometrical Effects on the Drag and Flow Field of Two Bluff Bodies Separated by a Gap”, *Journal of Fluid Mechanics*, Vol.156, pp.167-204, 1985.
- [34] Bearman, P.W. and Wadcock, A.J., “The Interaction Between a Pair of Circular Cylinders Normal to a Stream”, *Journal of Fluid Mechanics*, Vol.61, pp.499-511, 1973.
- [35] Baines, W.D., “Effects of Velocity Distribution on Wind Loads and Flow Patterns on Buildings”, *Proceeding of a Symposium on Wind Effect on Buildings and Structures*, U.K., pp.197-225, 1963.
- [36] Mandal, A.C., “A Study of Wind Effects on Square Cylinders”, M.Sc. Engg. Thesis, Department of Mechanical Engg., BUET, Dhaka, 1979.
- [37] Islam, T., “An Experimental Investigation of Wind Effect on Rectangular Cylinders”, M.Sc. Engg. Thesis, Department of Mechanical Engg., BUET, Dhaka, 1988.

- [38] Mandal, A.C., Islam, O., "Study of Wind Effect on a Group of Square Cylinders with Variable Longitudinal Spacings", Mechanical Engineering Research Bulletin, Vol. 3, No.1, 1980.
- [39] Whitbread, R.E., "Model Simulation of Wind Effects on Structures", Proceeding of a Symposium on Wind Effects on Buildings and Structures, Teddington, U.K., pp.283-301, 1963.
- [40] Pope, A. and Harper, J.J., "Low Speed Wind Tunnel Testing", John Willy and Sons, New York, 1966.

